Surface Functionalization of Cellulose Nanofiber for its Effective Use as Nanofiller in Fiber Reinforced Plastics

	Safarul bin Mustapha
year	2021-03
	2
	17104 397
URL	http://hdl.handle.net/10228/00008353

SURFACE FUNCTIONALIZATION OF CELLULOSE NANOFIBER FOR ITS EFFECTIVE USE AS NANOFILLER IN FIBER REINFORCED PLASTICS

SAFARUL BIN MUSTAPHA

GRADUATE SCHOOL OF LIFE SCIENCE AND SYSTEMS ENGINEERING KYUSHU INSTITUTE OF TECHNOLOGY

MARCH, 2021

SURFACE FUNCTIONALIZATION OF CELLULOSE NANOFIBER FOR ITS EFFECTIVE USE AS NANOFILLER IN FIBER REINFORCED PLASTICS

Name : Safarul Bin Mustapha

Student Number : 18899006

Supervisor : Assoc. Prof. Dr. Yoshito Andou

(Assoc. Prof. Dr. Toshinari Maeda)

Co-supervisors : Prof. Dr. Toshiki Miyazaki

: Assoc. Prof. Dr. Shyam S.Pandey

: Assoc. Prof. Dr. Tamaki Kato

External Co-supervisor : Prof. Dr. Hidayah Ariffin

Graduate School of Life Science and Systems Engineering

Department of Biological Functions and Engineering

Kyushu Institute of Technology

March, 2021

Preface

This thesis deals with the studies accomplished by the author under the guidance by Assoc. Prof. Dr Yoshito Andou, Graduate School of Life Science and Systems Engineering, Department of Biological Functions and Engineering, Kyushu Institute of Technology.

Safarul Bin Mustapha

18899006

Graduate School of Life Science and Systems Engineering,

Kyushu Institute of Technology,

2-4 Hibikino, Wakamatsu,

Kitakyushu 808-0196, Japan

ACKNOWLEDGEMENTS

ABSTRACT

Cellulose nanofibre (CNF), which is produced from lignocelluloses, has been growing exponentially as a low-carbon material because of its relative ease of high specific surface area, high strength and stiffness, lighter in weight and biodegradability. This cellulosic fibre has been studied intensively for fibre reinforced polymer composites as outstanding reinforcing potential instead of glass or carbon fibre. Due to hydrophilicity derived from hydroxyl groups in the structure and inherent tendency to form a strong network held through hydrogen-bonding, CNF is difficult to disperse in almost of the hydrophobic polymer matrix. Therefore, this study focused on surface modification strategies to expand the applications. The present work aimed to investigate the surface modification of CNF by new greener strategies and prepare environmentally friendly next-generation fibre reinforced plastics. The surface modification of CNF was easily performed by optimizing the modification method with acid. Surface modification using an acid treatment such as acetic acid, phosphoric acid, and sulfuric acid successfully converted from the hydroxyl group to the ester group in the CNF, confirmed by FT-IR and SEM-EDS. Moreover, the XRD analysis revealed that this treated CNF was the cellulose type I even after acid treatments. The acid treatment method could improve interface adhesion between CNF and polymer matrix. The dispersibility of CNF in the silicone elastomer as a polymer matrix could not see agglomerated CNF compare to unmodified CNF in the matrix, respectively. The mechanical properties of the silicone composite also improved. Therefore, acid treatments have the potential to be an effective method as a surface modification of CNF. In order to compare the performance of CNF dispersibility in the polymer matrix and mechanical properties, acetyl cellulose as a commercial product was investigated to prepare fibre reinforced plastics with polyurethanes (PUs). Thermoplastic resin as a polymer matrix for fibre reinforced plastics is major activities in this

research field. On the other hand, CNF can be worked as a network agent for thermoset resin such as PUs, polyurea, and epoxy resin. Therefore, acetyl cellulose was adopted due to less hydroxyl group as reactive sites to the isocyanate group in PUs because of suppression of networking. Though some remained hydroxyl groups in acetyl cellulose were reacted with isocyanate group in PUs monomer to make a network, molecular weight of PUs was hardly grown by networking. However, this issue could overcome after modification reaction conditions. These composites showed enhancement of mechanical properties and transparent film after hot-pressed moulding. Mechanical performance of PUs and transparency of moulding film to proof dispersibility of fibre in the PUs matrix was investigated by CNF, and phosphoric acid-treated CNF to compare with the acetyl cellulose PUs. Since agglomeration has occurred through hydrogen bonding between hydroxyl groups in cellulose structure, another material as an intercalator was mixed due to preventing hydrogen bonds between celluloses. Silica/CNF as a filler was successfully prepared using ethanol/water mixed solvents at room temperature without a catalyst. This method prevented the CNF from agglomeration when drying and enhanced the dispersion of CNF in the hydrophobic polymer. Polypropylene (PP) as a polymer matrix was melt blending with silica/CNF filler. It significantly increased the mechanical properties of the composite. In conclusion, this study provided to overcome in greater depth bothersome of CNF to prepare fibre reinforced plastics which can be shown to enhance mechanical performance due to prevent agglomeration of CNF from a hydrophobic matrix. The resulting products and method can expand and contribute to an application to replace existing materials.

<h1 style="text-align:center">TABLE OF CONTENTS</h1>

CONTENTS

CHAPTER 1: INTRODUCTION AND LITERATURE REVIEW

CHAPTER 2: TAILORED HIGHER PERFORMANCE SILICONE ELASTOMER WITH CELLULOSE NANOFIBRE (CNF) THROUGH ACIDIC TREATMENT

CHAPTER 3: ENHANCING MECHANICAL PROPERTIES OF POLYURETHANE WITH CELLULOSE ACETATE AS CHAIN EXTENDER

CHAPTER 4: COVALENT INCORPORATION OF CELLULOSE NANOFIBRE (CNF) INTO POLYURETHANE ELASTOMER AND THE EFFECT ON MECHANICAL PROPERTIES

CHAPTER 5: THE DESIGN OF DRY CNF FILLER BY HYBRIDIZATION WITH SILICA PARTICLE FOR MOULDED POLYPROPYLENE COMPOSITE

CHAPTER 6: CONCLUSION AND RECOMMENDATIONS

LIST OF FIGURE

LIST OF TABLE

LIST OF ABBREVIATIONS

BC	Bacterial cellulose
BD	1,4 butanediol
CNC	Cellulose nanocrystals
CNF	Cellulose nanofiber
CA	Cellulose acetate
DLS	Dynamic laser scattering
DMF	Dimethylformamide
DMSO	Dimethyl sulfoxide
DP	Degree of polymerization
DTBL	Dibutyltin (IV) dilaurate
DTG	Differential thermogravimetry
FRP	Fibre reinforced plastic
FT-IR	Fourier Transform Infrared spectroscope
GPa	Gigapascals
HDI	Hexamethylene diisocyanate
$H_{12}MDI$	Dicyclohexylmethane 4,4'-diisocyanate
HPAs	Heteropoly acids
HQEE	Hydroquinone bis(2-hydroxyethyl)ether
IPDI	Isophorone diisocyanate
ISO	Isosorbide
LSCM	3D laser scanning confocal microscope
MTMS	Mmethoxytrimethylsilane
MPa	Megapascals
MDI	Methylene diphenyl diisocyanate
MCA	Monochloroacetic acid
NC	Nanocellulose
NFC	Nanofibrillated cellulose
PDMS	Polydimethylsiloxane
PEG	Poly(ethylene) glycol

PPG	Poly(propylene oxide) glycol
PP	Polypropylene
PTMO	Poly(tetramethylene) glycol
PUs	Polyurethanes
PTMG	Poly(tetramethylene ether) glycol
PSD	Particle size distributions
SEM	Scanning electron microscopy
SiOH	Hydrophilic silanol groups
SiP	Silica particles
SEM-EDS	Energy dispersive X-ray spectroscopy
TEMPO	Oxidation mediated by 2,2,6,6-Tetramethylpiperidine-1-oxyl
TEOS	Tetraethyl orthosilicate
TDI	Toluene diisocyanate
TGA	Thermogravimetric analysis
UHMWPE	Ultrahigh molecular weight polyethylene
WAXD	Wide Angle X-ray Diffraction

CHAPTER 1

Introduction and Literature Review

1.0   Introduction

The growing demand for environmental sustainability has led to research on various cellulose-based materials to minimize the environmental impact of conventional hazardous materials. Cellulose fibre has unique properties such as renewability, biocompatibility, excellent mechanical properties, and tailorable surface chemistry. By comparing to cellulose, cellulose nanofibre (CNF) is lighter in weight with high surface area to volume ratio, higher strength, stiffness and it can act as a superb reinforcing agent for developing green bio-nano composites. CNF can be used in many different applications, including energy production, polymer composite, environmental improvement, food, pharmaceuticals, and tissue engineering. However, CNF is naturally poor-dispersed in low-polar materials due to its hydrogen bonding. To overcome the agglomeration of CNF in low-polar materials, the surface modification for CNF is the main step to interfere with the hydrogen bond between CNFs. It has a reactive surface of hydroxyl groups which can be functionalized to various surface properties.

In this study, we focus on surface modification treatment on the CNF and develop a simple method with a greener process for fabrication polymer composite with CNF. The Treated CNF can be used as a filler and expected enhanced mechanical properties of the polymer. Surface modification strategies on CNF specifically using carboxymethylation, TEMPO oxidation, acetylation, isocyanate grafting and silylation has been studied extensively. These techniques were successfully developed and introduce different functional group on the CNF surface. However,

some of this method is not environmentally friendly, as they usually require a catalyst, high energy and harsh chemical, besides complicated reaction processes. Therefore we introduce a simple and greener method as a surface modification.

The second part of this study investigates the performance of treated CNF dispersibility in the polyurethanes (PUs) matrix by understanding the PUs mechanism by using cellulose derivatives, which is cellulose acetate as a chain extender in PUs polymerization. The PUs was prepared by pre-polymer methods and are formed by a chemical reaction between an isocyanate and a hydroxyl group. Throughout the study, cellulose derivatives as chain extender are discussed.

Without surface modification and high CNF content in the PUs polymer will cause a slightly poor adhesion between the fibre and matrix interface. The PUs/cellulose composites are usually prepared by solvent casting and *in situ* polymerization technique using dimethylformamide (DMF) as a solvent. However, due to the high boiling point (153°C), nanocomposite entails difficulties for solvent removal later, time-consuming and hazardous effects of DMF solvent. Therefore, we improve the process by using acetone as a polymerization solvent. The treated CNF was used to develop high mechanical and thermal properties PUs with good biocompatibility by introducing a much stronger chemical bond between CNF and PUs. The enhancement of the physical and mechanical properties from incorporating CNF in aliphatic isocyanates-based PUs has been thoroughly investigated.

Last part of this study is to control hydrogen bonding between cellulose chains through physical interaction with another material for polymer composites. Generally, surface modification was

done to improve the CNF dispersibility. However, the chemical modification method involves many processes and chemicals involved, time-consuming and not eco-friendly. Therefore, we attempted a new approach using ethanol/water mixed solvent applied to fine particles and CNF to prevent the agglomeration of CNF when drying. This hybrid filler can obtain nanocomposite materials by an accessible, without chemical modification, fast, and low-cost method.

1.1 Objectives

Cellulose nanofibre (CNF) has a high number of hydroxyl groups, which lead to inter-intra-interaction through hydrogen bonding between cellulose chains and high hydrophilicity which limits its uses in several applications. Each CNF unit monomer contains three hydroxyl functions which enable to chemical modification. This study provides an overview of surface modification of CNF as a nanofiller in the composite polymer.

The objectives of this study include:

1. To control hydrogen bonding between cellulose chains through modification of functional groups based on greener process.

2. To investigate performance of CNF as filler and/or chain-extender in polyurethane.

3. To control hydrogen bonding between cellulose chains through physical control with another materials for polymer composites.

1.2 Cellulose

Cellulose is the most abundant biopolymer available in nature, and it is one of the major components in the plants. Cell wall of plant cell is attributed their mechanical performances to cellulose. This polymeric material synthesised by a wide variety of living species such as plants,

animals, bacteria, and some amoebas. Structural properties of cellulose can retain a semi-crystalline state of aggregation even in an aqueous environment. Cellulose is a natural linear polymer of anhydroglucose units linked at the one and four carbon atoms by ß-glycosidic bonds [1]. It consists of repeating monomer units of β-D- anhydroglucopyranose rings linked by β-1, 4-linkages forming a linear chain [2][3]. Each monomer unit contains three hydroxyl functions which allow for chemical modification. The microfibrils of cellulose are particularly harsh and inflexible due to the presence of hydrogen bonds. Figure 1.1 shows a single cellulose macro fibril is composed of tiny bands of cellulose microfibrils and generate cellulose filaments, which imparts intrinsic strength to plant-based materials [4].

While cellulose is a fundamental structural material of most plants, bacterial cellulose (BC) is also known as microbial cellulose. It is biodegradable and also natural cellulose which is produced by bacteria. The diameter of the BC fibres is 20–100 nm. The high purity in the structure gives the material high water-holding capacity, high tensile strength and flexibility [5]. Moreover, BC formed a strong gel film of crystalline microfibrils and also free of lignin, hemicelluloses, and pectin, which are typically present in plant-derived celluloses. Therefore, making the BC purification easy, low energy process, whereas purification of plant celluloses usually requires harsh chemicals [6][7].

Cellulose is a polysaccharide compound and the homopolymer of glucose. A large number of glucose units combines to form a cellulose polymer molecule, which depends on their chain length and rate of polymerisation [8]. The degree of polymerisation (DP) is a measure of how many D-anhydroglucopyranose units there is in the polymer. Since no polymer is homogenous in length,

the molecular weight distribution will have an important influence on the properties of the fibres [9].
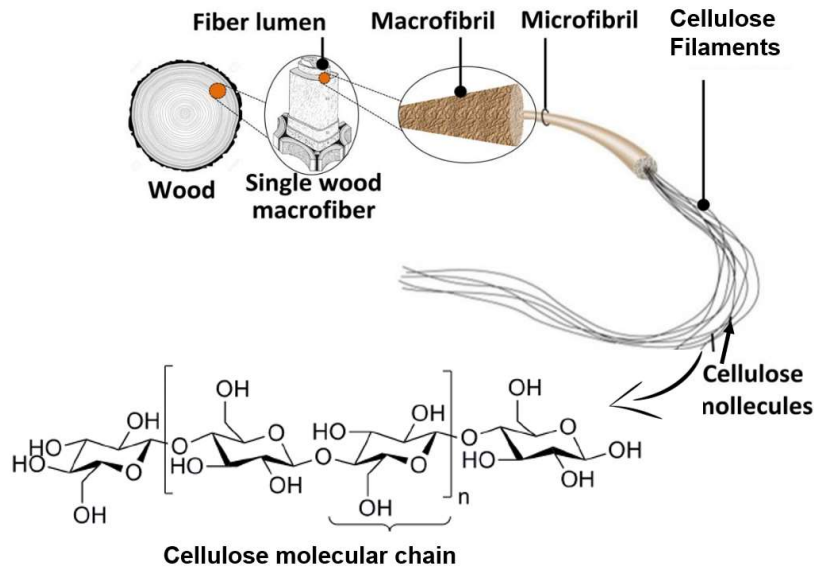
Figure 1.1: Schematic of the hierarchical structure of cellulose filaments [4]

The DP of cellulose is varying between 10,000 and 15,000, where DP is dependent on the cellulosic source material. The hydrogen bonding between hydroxyl groups and oxygen atoms of the adjoining ring molecules stabilises the linkage, resulting in the linear configuration of the cellulose chain [10].

1.2.1   Types of Cellulose

Polymorphs of cellulose are based on a wide variety of molecular orientation and hydrogen bonding network in the crystalline region [11] which can characterised as cellulose I, cellulose II, cellulose III and cellulose IV. Figure 1.2 shows the transformation of cellulose into its various polymorphs. Cellulose I is a crystalline biopolymer naturally produced by a variety of organisms such as trees, plants, tunicates, algae, and bacteria. Furthermore, cellulose I comprise two slightly

different forms which are cellulose Iα and cellulose Iβ. The crystal phase forms of cellulose I depends on sample origins. Although Cellulose Iα has been found in the cell wall of some algae and bacterial cellulose, cellulose Iβ is associated with cotton, plant and ramie fibres [12]. Cellulose I have been widely used in several applications such as preparing hydrogel for wound dressing and reinforcer as nanofiller into other polymers to improve mechanical properties [11]. Cellulose II is a crystalline form that is formed from cellulose I, and it has structural changes in the molecule and the most stable structure. Cellulose II can be produced by two processes which are from regeneration (solubilisation and recrystallisation) and mercerisation (aqueous alkali treatment, followed by washing) [13]. However, it has been found that cellulose II cannot be converted back to cellulose I [14]. Cellophane and rayon are regenerated cellulose product which are cellulose II [15]. Cellulose III is formed when cellulose I or cellulose II is treated with amines or liquid ammonia, followed by the removal of these reagents. Cellulose III is a reversible reaction; it can be achieved by thermal treatment and restored to cellulose I and II [16].
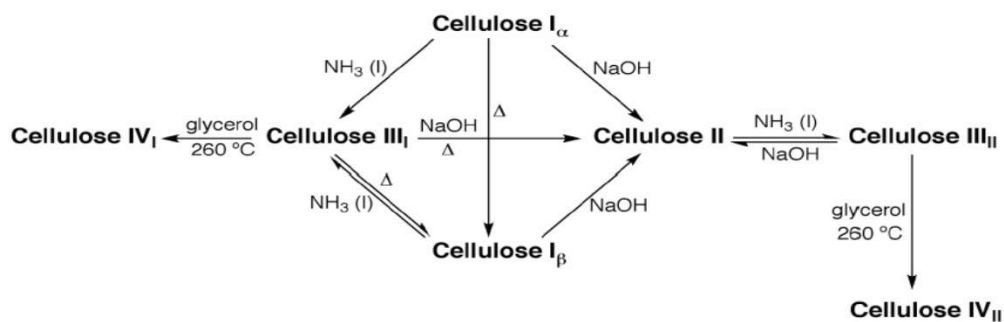
Figure 1.2: Possible interconversions of cellulose polymorphs [14]

Additionally, cellulose III is much easier for celullase to digest due to its significantly high amorphous content [17][18]. Polymorph cellulose IV can be obtained by heating cellulose III up to 260ºC in glycerol and cellulose I cannot be directly transformed into cellulose IV. According to

a study reported by Wada *et al.* [19] , cellulose IV also detectable in the primary cell wall and similar structure to cellulose I. This cellulose I is referring to low crystalline cellulose which can be found in fungal cell walls.

1.2.2   Nanocellulose

Nanocellulose (NC) is a term referring to nano-structured cellulose, is a natural nanofiber that can be obtained via fibrillated by cellulose extracted from biomass resources such as wood, herbs, plants, and organisms. It is biodegradable, lightweight, and holds reactive hydroxyl groups which makes it suitable for surface functionalisation for use in a variety of applications [20]. There are different techniques used to produce NC (Figure 1.3), including acid hydrolysis, mechanical process, and enzymatic hydrolysis. The acid hydrolysis method is considered to be the simpler and fast process for processing NC. Furthermore, NC is roughly classified into cellulose nanocrystals (CNC), cellulose nanofiber (CNF), also called nano-fibrillated cellulose (NFC), and bacterial cellulose (BC).
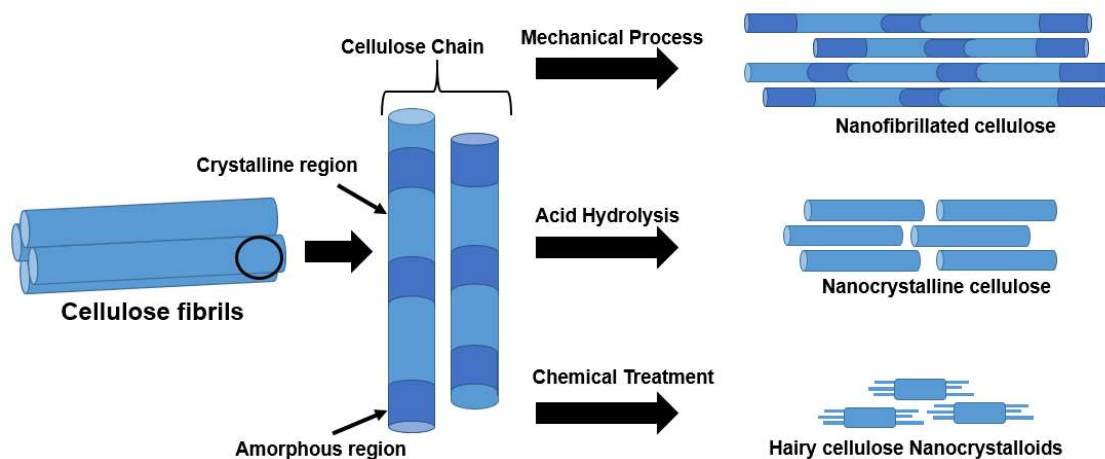
Figure 1.3: Schematic representation of the extraction of NC from cellulose [20]

Acid hydrolysis is commonly used for prepared CNC, where H_2SO_4 and HCl the most used acid. These strong acids used to break the glycoside bond in cellulose and remove amorphous regions leaving highly crystalline particles that vary in size, but it depending on cellulose source. This acid hydrolysis usually produces CNC a rod-like structure with about 90% crystallinity. Besides, acid hydrolysis by H_2SO_4 has negatively charged half-ester sulphate groups onto the CNC surface, allowing the CNC particles to repel each other through electrostatic repulsion and preventing aggregation in aqueous suspensions[21].

Different methods of the mechanical process have been developed to produce CNF from cellulose such as high-pressure homogenisation, ball milling, microfluidization, ultrasonication, and water jet system [22][23]. In general, this mechanical process preserves both the crystalline and amorphous phases. CNF has not high crystallinity comparing with CNC but consists of both crystalline and more amorphous domains instead. This method also produces long-entangled fibrils of CNF, which may be micrometres long. Comparing to CNC, CNF has a large surface to volume ratio, high tensile strength and stiffness, high flexibility, good electrical and thermal properties [9].

Moreover, NC derivatives are a promising material and have broad applications as functional paper, optoelectronics, catalysis, energy storage, environmental remediation and packaging. Recent developments in biomedicine and biotechnology, NC derivatives also uses as tissue scaffolds, drug delivery, antibacterial coatings and biosensors application. Phosphorylated NC derivatives are a particularly interesting material, covering most of the applications in various dimensions, including bone scaffolds, adsorbents, and as flame retardants because of high thermal properties

[24][25]. Polymer nanocomposites using NC derivatives has a great interest due to the unique characteristics of those nanomaterials. Current problematic of NC derivatives is the hydrophilicity, making it incompatible with the hydrophobic polymer matrix. Therefore, surface modification of NC derivatives has to be performed to improve its dispersibility in the polymer matrix [26].

1.3   Surface modification of nanocellulose

One of the challenges in preparing composites with NC and a hydrophobic polymer matrix is the low compatibility. Besides, NC possesses a high hydrogen bond that makes it have hydrophilic properties in nature [27]. Without surface modification on NC surface, NC tendency to agglomeration in a polymer matrix and decreases the mechanical properties of composites material. The surface modification of NC is an effective method for improving the interface compatibility between composites material [28]. Surface modification of NC can be divide into introduced functional group and generation of hydrophobic into NC surface.

1.3.1   Functional group

Carboxymethylation, oxidation, phosphorylation, and sulfonation is a process introduced a functional group on the NC surface (Figure 1.4). The carboxymethylation process introduces carboxymethyl groups onto the NC surface, making the surface negatively charged [29][30]. This process is conducted by etherification of the hydroxyl groups with monochloroacetic acid (MCA) in the presence of alkali, which increases the water retention value and significantly decreases the ratio of crystalline to amorphous cellulose [31]. Oxidation mediated by 2,2,6,6-Tetramethylpiperidine-1-oxyl (TEMPO) can be used as a pre-treatment to promote NC separation. Surface treatment by TEMPO oxidation can selectively oxidise hydroxyl groups at the C_6 position

on the NC surface and create carboxylate groups, which promote dispersion of NC in an aqueous environment [32]. Moreover, this treatment maintained the crystallinity of NC [33]. The phosphate groups were introduced onto the NC surface by phosphorylation using phosphoric acid. This chemical modification also introduces negatively charged groups to the NC surface in different forms such as phosphate, or phosphite esters. These groups stabilise nanoparticle suspensions through electrostatic interactions [24]. Sulfonation is a technique for imparting a low anionic charge and introduce a sulphate group to the surface of NC materials and provides a stable colloidal suspension [34][35]. Furthermore, the introduction of sulphate groups into the NC surface compromises the thermo-stability of NC [30].
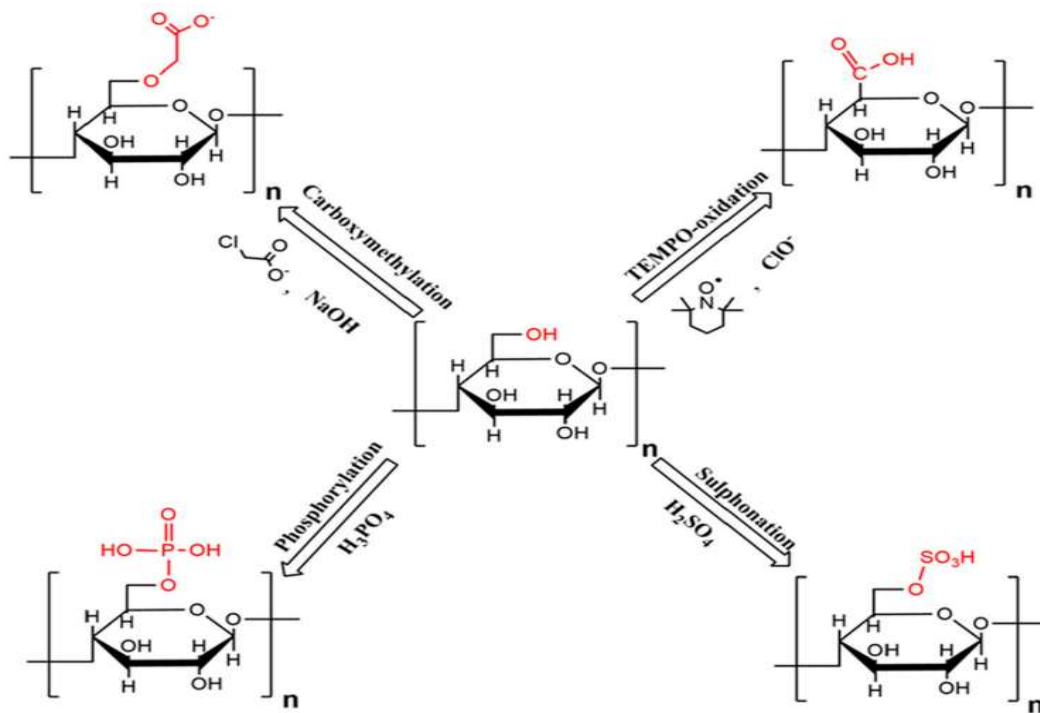
Figure 1.4: Different surface modification techniques through which ionic charges are introduced to the NC surface [24]

1.3.2 Generation of hydrophobic on NC surfaces

Presence of three hydroxyl groups per anhydroglucose unit within cellulose chains and on the surface of NC, allowing the chemical modifications to introduce functional groups using various techniques [36]. Chemical modification techniques such as acetylation, silylation, and urethanization, making the NC surface hydrophobic. Acetylation method reduces the number of hydroxyl groups in NC, which increases hydrophobicity and weakens hydrogen bonding [37]. Acetic anhydride is commonly used as an acetylating agent reacting with free hydroxyl groups in NC. Silylation introduces hydrophobic alkyl moieties onto the NC surface; this technique is a simple way to increase the hydrophobicity on the NC surface. Various silylating reagents can be used, such as chlorosilanes and hexamethyldisilazane [38]. Zhang *et al.* [39] demonstrated surface silylation on NFC surface using methyltrimethoxysilane and polydimethylsiloxane (PDMS) as a model network (Figure 1.5). Resulting, highly hydrophobic NFC was obtained and improvement in both the static and dynamic mechanical properties in polydimethylsiloxane polymer.
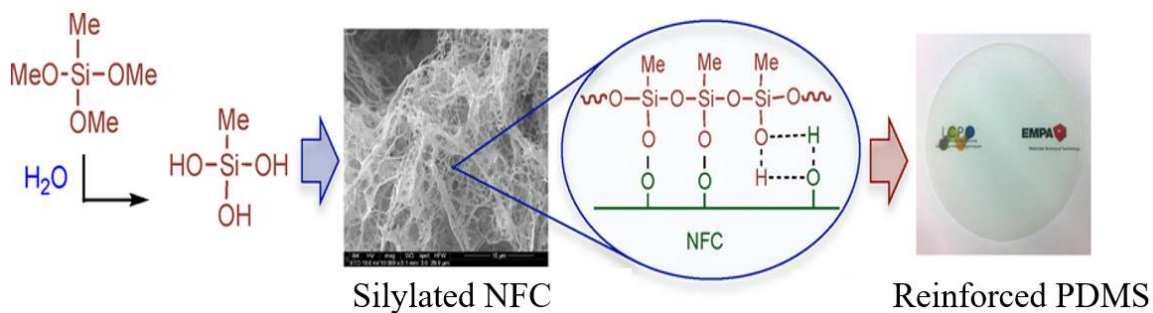
Figure 1.5: Surface silylation on NFC and polydimethylsiloxane as a model network [39].

1.4 Hydrophobic Polymer

Hydrophobic polymers included materials such as polypropylene, polystyrene, polyvinylchloride, polytetrafluoroethylene, polydimethylsiloxane, polyesters, and polyurethanes. Some of these

polymers are frequently poor in mechanical properties, and fillers can provide overcoming of this limitation. An example, silica nanoparticles were introduced into polypropylene polymer to enhance the mechanical properties and thermal stability [40]. Furthermore, incorporation of hydrophilic cellulose suspension to a nonpolar hydrophobic polymer matrix can be improved by interacting cellulose with a surfactant or surface-active agents [41].

1.5   Nanofiller in Nanocomposites

Polymer nanocomposites are comprised of a polymer or copolymer with nanoparticles or nanofillers mixed or dispersed in the polymer matrix [42]. The reinforcement of nanofiller in polymeric systems depends on the filler type, the type of functional group on the filler, the aspect ratio of the filler, the amount of filler, the type of polymer, and the method of processing. Homogeneous dispersion of the nanofiller in the polymeric matrix and interaction between the filler and the polymer is necessary for good reinforcement [43]. Reinforcement of nanofillers into the polymer can lead to improvements in their mechanical strength, thermal stability, barrier and flammability properties, without affecting their processability [44]. The reinforcing effect of nanofiller is attributed to several factors, such as polymer matrix properties, type of nanofiller, the concentration of polymer and filler, particle aspect ratio, particle size, particle orientation and particle distribution [45]. There is various type of nanofillers has been studied recently such as silica [46][47], carbon nanotubes [43][48], graphene [49][50][51], and nanocellulose [52][53][54][55], to obtain a nanocomposite polymers and with different application.

Incorporation of nanofiller into polymer nanocomposites can be done by *in situ* polymerisations, solution method and melt extrusion [56]. These method is depending on the type of polymeric

matrix, nanofiller and desired properties for the final products. In polymer chemistry, *in situ* polymerisation methods is a mixing of nanomaterial in a solution monomer, followed by polymerisation in the presence of the dispersed nanomaterial [57]. This polymerisation requires the utilisation of monomers, an initiator, and a high-temperature reactor. Rueda *et al.* [58] prepared PUs/CNC nanocomposites using *in situ* polymerisation method and CNCs as precursors of polyurethane chains. Moreover, polymer nanocomposite and nanofiller can be prepared by dispersed in an appropriate solvent by ultrasonication, magnetic stirring and high-speed shear mixing. After the evaporation process through dispersion of nanofiller in a polymer solution after homogenisation even though polymer chains may reassemble, the composite polymer can be produced. This method has been extensively used due to its efficiency in dispersing nanofillers regardless of the polymer polarity. Nevertheless, it depends on the solvent compatibility between the polymer and the fillers [59].

The melt extrusion process consists of melting the polymer pellets through a combination of applied heat and friction. This molten polymer then forced under high pressure through a small outlet [60]. Figure 1.6 shows the twin-screw extruder and hot melt processing. It is one of the most widely applied processing technologies used to prepare plastic products, including bags, films, sheets, tubes, fibres, and pipes [61]. Reinforcement of CNF as nanofiller in polypropylene (PP) could be done using a twin-screw extruder to achieve uniform dispersion in the polymer matrix. This extruder method allows for the processing and fibrillation of cellulose at solid content [62]. Combination of different types of nanofiller and polymer to produce polymer nanocomposites show the unique design possibilities and creating functional materials with desired

properties for specific applications. The possibility of using natural resources and environmentally friendly offered new opportunities for future applications.
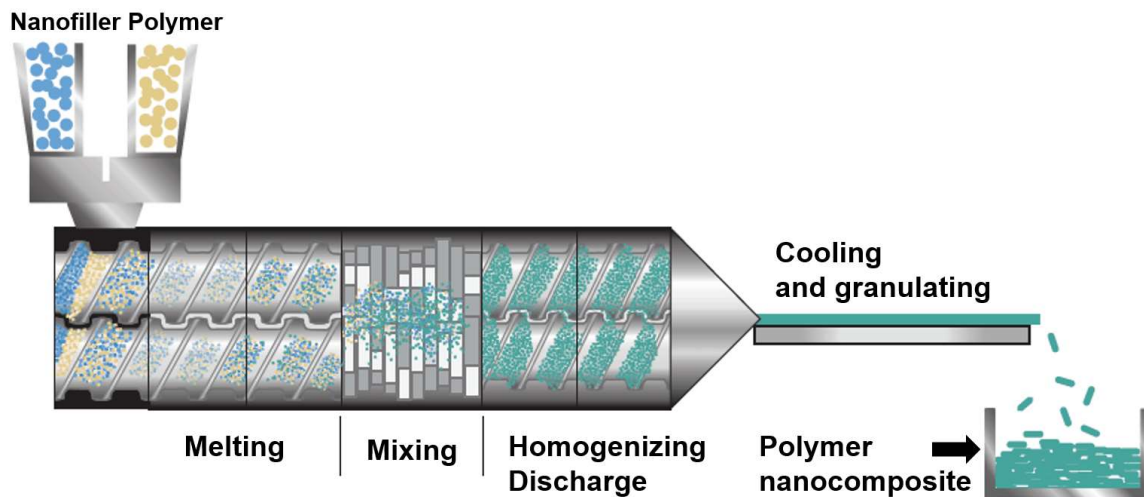
Figure 1.6: Schematic representation of twin-screw extruder and processing of hot melt extrusion

1.6 Polyurethanes

Polyurethanes (PUs) are versatile material and most popular type of polymers in nowadays because of their physicochemical properties based on the chemical composition. This material was discovered by Otto Bayer and co-workers while searching for alternatives to natural rubber. This unique material was patented in Germany in 1937. The chemistry of PUs is synthesised from polyisocyanate (OCN-R-NCO) and polyhydroxy compound (HO-R-OH) and chain extender, which is -NHCOO- repeating macromolecular compounds [63]. The versatility of PUs chemistry enables the chemist to engineer polyurethane ingredients to achieve the desired properties.

Furthermore, synthesis of PUs using pre-polymer technique also has been studied intensively [64][65]. This pre-polymer technique mechanism is as shown in Figure 1.7. The synthesis involves two main steps. First step synthesis, polyol will react with a diisocyanate generate a PUs pre-

polymer, and the pre-polymer still has open diisocyanate group, which will be reacted with a chain extender to complete the polymerisation. This pre-polymer technique allows the modification of PUs using cellulose as a chain extender.
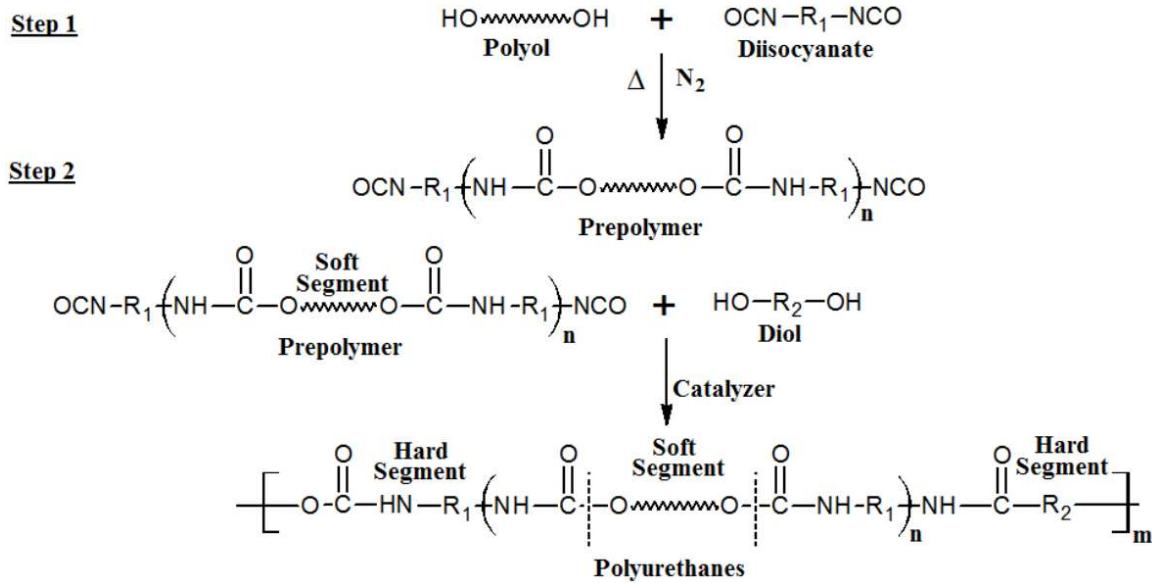
Figure 1.7: Schematic representation of the PUs synthesis mechanism [65]

The broad applicability of polyurethane is due to functionality in a selection of monomeric materials from a wide variety of macro diols, diisocyanates and chain extender. Nowadays, PUs is used in multipurpose applications such as coatings, paints, elastomers, textiles, insulators, elastic fibre, foams, and footwear. During the early stages of discovery, most of the PUs were synthesis by using toxic solvents and monomers. Recently, monomers from natural sources were introduced, making the PUs attractive in the industry due to the green nature of PUs materials [66].

1.6.1 Polyol

One of the significant monomers in PU synthesis is a polyol, which usually termed as a soft segment. They can be categorised as polyether, polyester, or polycarbonate-based polyols. Polyether polyols are made by the reaction of epoxides with compounds having an active hydrogen atom. Moreover, polyester polyols are made by the polycondensation reaction of multifunctional carboxylic acids and polyhydroxyl compounds [67]. Polycarbonate-based polyols are produced on the ground of alkylene oxides and CO_2 [68]. Polycarbonate-based polyol provides significantly enhanced hydrolytic stability, chemical resistance, high modulus and strength [69]. It is crucial to choose suitable polyol as the properties highly depend on polyol and its contents. Low molecular weight polyol controls rigidity, whereas high molecular weight polyol contributes to elastomeric properties.

Common polyether polyols include poly(tetramethylene) glycol (PTMO), poly(propylene oxide) glycol (PPG), and poly(ethylene) glycol (PEG). The PTMO is one of the most industrially important class of materials, which are widely being studied in recent years. The PTMO or poly(tetramethylene ether) glycol (PTMG) is prepared through polymerisation of tetrahydrofuran with different molecular weights [70]. Besides, PPG and PEG can be prepared using a different weight of ethylene oxide/propylene oxide. By changing the total hydroxyl group and polymer chain, the polyol properties such as reactivity, compatibility, and solubility also can be changed.

1.6.2 Isocyanate

Isocyanate is the functional group with the formula $R-N=C=O$, which are reactive towards active hydrogen groups such as an amine (-NH), hydroxyl (-OH), the carboxylic acid (-COOH), urea, and

amide [71]. This chemical reacts with active hydrogen groups to produce urethane (carbamate) linkages. The isocyanates building block can be either aromatic isocyanates or aliphatic isocyanates in segmented polyurethane elastomers. Figure 1.8 shows the chemical structure of aromatic isocyanate and aliphatic isocyanates. The aromatic isocyanates are more reactive than the aliphatic isocyanates and generally develop better mechanical strength, thermal and flame retardant properties and also give more rigid PUs [72][71]. Toluene diisocyanate (TDI) and methylene diphenyl diisocyanate (MDI) are some of the common aromatic isocyanates used in the industry [73]. These aromatic isocyanates oxidize when exposed to UV-light, therefore not suitable to be used for outdoor coatings application [74].

Moreover, potentially to form aromatic amines after degradation, aromatic isocyanate-based PUs are also considered to have higher toxicity than aliphatic isocyanate-based PUs [75]. Aliphatic isocyanate most frequently used in coating applications because they produce PUs with excellent UV resistance, transparent and exterior durability [76]. This isocyanates-based PUs also produce rubbery materials with high elongation but low in tensile strength [77]. The most common types of aliphatic isocyanates are hexamethylene diisocyanate (HDI), dicyclohexylmethane 4,4'-diisocyanate (H_{12}MDI), and isophorone diisocyanate (IPDI). Additionally, aliphatic isocyanates are used to produce degradable PUs [73] and as a surface modification of cellulose and nanocellulose to promote dispersion in PUs matrix [78][79].
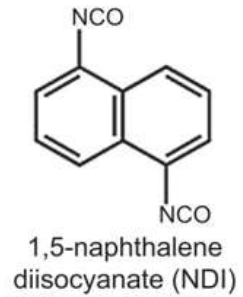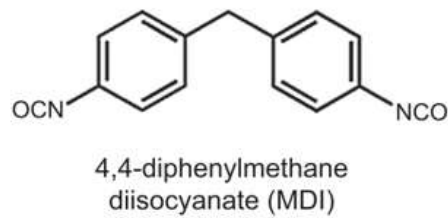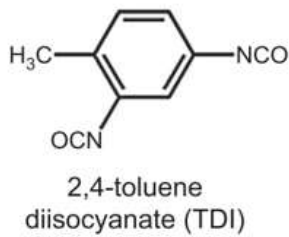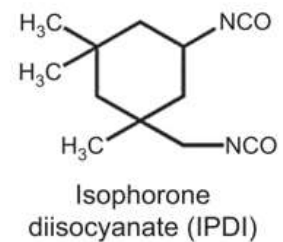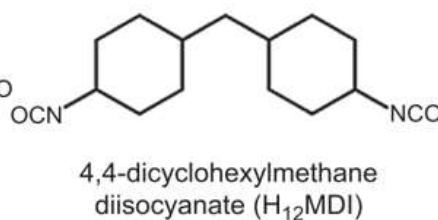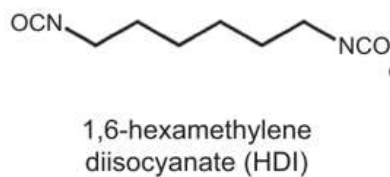
Figure 1.8: Chemical structure of aromatic isocyanate and aliphatic isocyanates [75]

Girouard *et al.* [80] reported that the chemical modification of cellulose nanocrystals (CNC) with IPDI had enhanced the dispersion in PUs composite, which increased the tensile strength and work of fracture more than 200% as compared to the neat PUs with high elongation. Figure 1.9 show CNC modified by isophorone diisocyanate (IPDI), this modification was having two monomers (primary and secondary) –NCO groups with both urethane and isocyanate functionality.
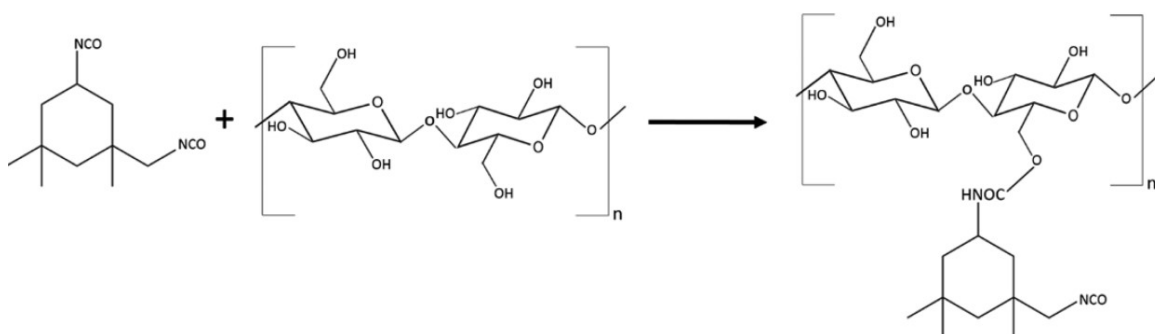
Figure 1.9: Illustration of IPDI/CNC reaction with the secondary NCO group on IPDI [80].

The pendant primary isocyanate group at the CNC surface were used as a route to facilitate covalent bond formation with a polyurethanes (PUs) elastomer, resulting in a significant improvement in the tensile properties of PUs polymer compared to the neat PUs. Polyurethane materials attract much attention due to their versatile applications with a wide variety of polyols and isocyanates market ready to synthesise PUs.

1.6.3 Chain extender

Chain extenders are reactive low molecular weight compounds such as hydroxylamines, glycols, or diamines and are used to increase the block length of the hard segment in PUs synthesis [73] [81]. Chain extender also shorter chain length as compared to polyols. The structure of the chain extenders determines the rigidity of the hard blocks and the density of hydrogen bonds [82]. The most common chain extender used in PUs synthesis is 1,4 butanediol (BD), 1,6 hexanediol, cyclohexane dimethanol, ethylene glycol, hydroquinone bis(2-hydroxyethyl)ether (HQEE) [69].

Cellulose is composed of repeating glucose units connected by 1,4-glycosidic linkages; the abundant free hydroxyl groups can be used to crosslink with PUs. The hydrophilicity of cellulose should be reduced before cellulose is used in PU synthesis [83]. Cellulose and cellulose acetate (CA) used as a chain extender in PUs polymerisation has been done by Ikhwan *et al.* [64] and Chung *et al.* [83].

CHAPTER 2

Tailored higher performance silicone elastomer with cellulose nanofiber (CNF) through acidic treatment

Abstract

Cellulose nanofiber (CNF) can be used for reinforcer to silicone polymer to expect enhancement of its mechanical strength. However, CNF is a hydrophilic material, which typically poor-dispersed characteristic in non-polar polymer matrices.   To overcome this bothersome, surface modification of CNF has been studied to tailor the interfacial interactions between CNF and matrices for fibre dispersibility in matrices. In this work, CNF was treated with some acids to modify a functional group on CNF. The acid treatment approaches successfully introduced the functional groups onto CNF surface, which confirmed by FT-IR, TGA and SEM-EDS analyses. Moreover, the XRD analysis revealed that this treated CNF was the cellulose type I and acid treatments did not vary it. The TGA results showed lower thermal degradation of all treated CNF as compared to control CNF. Additionally, the effects of treated CNF as nanofiller in the silicone elastomer were evaluated the mechanical properties. The treated CNF also showed a good dispersibility in silicone composite, and no agglomeration was observed.   And also, the tensile strength and elongation of silicone composite with treated CNF as nanofiller showed high performance compare to silicone composite with pristine CNF. The highest tensile value was recorded at 3.4 MPa in silicone/CNF-P samples using phosphoric acid-treated CNF. Therefore, a low concentration of acid treatments has the potential to be an effective method as a surface modification of CNF.

Keywords: Cellulose Nanofibre, composite polymer, acid treatment, Sylgard, elastomer

2.1   Introduction

Cellulose fibre can be derived from renewable resources, eco-friendly, has excellent mechanical properties, good biocompatibility, and tailorable surface chemistry [84]. By comparing to cellulose fibre, cellulose nanofibre (CNF) is lighter in weight with high surface area to volume ratio, higher strength, stiffness and it can act as a superb reinforcing agent for developing green bio-nano composites [20]. The CNF can be produced and extracted from cellulose by applying a mechanical treatment such as high-pressure homogenisation, microfluidization, ultrasonication, and water jet system [23][85].

CNF can be reinforced to polymer composite which will make a lightweight compared to other fibre reinforced plastic (FRP) such as glass fibre reinforced plastic and carbon fibre reinforced plastic. Polymer composites with CNF can be enhanced by well-dispersed CNF into the polymer matrices. However, nanocellulose is naturally poor-dispersed in low-polar materials due to its hydrogen bonding. To overcome the agglomeration of CNF in low-polar materials, the surface modification for CNF is the main step to interfere the hydrogen bond between CNFs. It has a reactive surface of hydroxyl groups which can be functionalised to various surface properties [86]. Surface modification strategies on CNF specifically using carboxymethylation, TEMPO oxidation, acetylation, isocyanate grafting and silylation has been discussed by Abdul Khalil *et al*. [87]. Some of these strategies introduced the ionic groups on CNF surface to change its characteristic from hydrophilic to hydrophobic. On the other hand, the esterification reaction of CNF with acetic anhydride, butyric anhydride, and caproic anhydride has been studied to overcome the agglomeration [88] [89].

The size and distribution of nanofibre are important for FRP because the defect due to an agglomeration can be reduced by the mechanical properties of the hybrid composite polymer [90]. The CNF has been extensively used in the production of nanocomposites using phenolic resin, styrene butyl acrylate, amylopectin, polyurethane, and melamine formaldehyde [91].

Silicones are synthetic polymers with organic groups attached to an inorganic backbone giving a combination of unique properties such as high flexibility, low surface energy, high thermal stability, high gas permeability, and low biological activity [92]. With these unique properties, silicones particularly polydimethylsiloxanes (PDMS) have been used in a wide range of applications including coatings, painting, construction industry, medical applications, cosmetics, sensors, and optical materials [93][94]. The current problem with silicone is it has low mechanical properties but can be improved by the addition of fillers, for example, natural fibre or inorganic filler materials such as glass fibre [95], SiO_2 [96][97], Al_2O_3 [97], and $CaCO_3$ [98][99]. The strength of silicone polymers without filler is substandard for most applications, thus the addition of reinforcing fillers increase its hardness and enhance its mechanical strength [100].

A study by Jankauskaitė *et al.* [101] mentioned that the cellulose which was used as nanofiller in silicone without surface modification has caused the aggregation. Despite the clear polarity difference between the CNF and the siloxane derivatives, the coexistence of these two types of chemical compounds in the same material can induce a new combination of properties to the material. Silicone is a well applied and common materials in our life. The disadvantages of silicone materials are on their mechanical performances, specifically low tensile strength and tear strength. The combination of silicone and CNF may be expected to overcome their low

performance. However, both of these materials have different chemical structures which makes the difference in their properties.

In this study, CNF produced by a waterjet system was treated with several acid solutions and was used as a nanofiller in silicone to improve the tensile strength of the composite polymer. The successful of acid treatments on CNF surface were evaluated based on their chemical structures, crystallinity, and dispersibility in solvents. Moreover, the silicone/CNF composites were assessed on their transparency and mechanical properties by comparing with the original silicone.

2.2 Experimental

2.2.1 Materials

Commercial CNF (5 wt % in water, DP 650) was kindly provided by Sugino Machine Limited, Toyama Prefecture, Japan. This CNF was produced by a super high-pressure water jet system. Phosphoric acid (85%), acetic acid (99%), sulfuric acid (95%), and hydrochloric acid (35-37%) were purchased from Wako Pure Chemical Industries Ltd, Japan. All chemicals were used as it is without further purification and reverse osmosis (RO) water was used throughout the experiments. Silicone used was Sylgard 184 (Dow Corning Toray Co., Ltd).

2.2.2 Acid treatment

Commercial CNF was treated through acids as listed in Table 2.1. The CNF mixture solution was sonicated under 40 Hz for 3 hours and continuously stirred for 4 hours at room temperature. Then, the product was washed with RO water and centrifuged at 8000 rpm for 10 minutes until it reached pH 6−7. The treated CNF was solvent exchanged to ethanol and stirred for 24 hours and then it

was centrifuged at 8000 rpm for 10 minutes and sediment was collected. This process were repeated 3 times to ensure water is removed.

Table 2.1: Percentage and volume of acids in the acid treatment of CNF

Sample Code Name	CNF aq. (5 wt %)	Acids	Acid volume (Total 100 mL)
CNF-P	10 g	Phosphoric acid (85% w/w)	30 mL
CNF-A	10 g	Acetic acid (99% w/w)	30 mL
CNF-S	10 g	Sulphuric acid (95% w/w) and hydrochloric acid (37% w/w)	30 mL and 10 mL

2.2.3 Preparation of silicone/CNF composite

The treated CNF (0.6% w/w) was added into Sylgard 184 using a mixing ratio of 10:1 (base polymer: curing agent). The blend compound was mixed through planetary centrifugal mixer AR-100 (Thinky U.S.A., Inc) for 2.5 minutes successively. Then, the mixture was slowly poured into a glass petri dish (9 cm diameter) and degassed under vacuum for 2 hours to eliminate air bubbles, and the mixture was cured at 80 °C for 2 hours and demoulding a silicone/CNF composite which was prepared with average 0.8 mm thickness for mechanical testing. Silicone polymer was used as a control.

2.3   Characterization

2.3.1   Functional groups analysis

Functional groups of treated CNF were analysed with a microscopic Fourier Transform Infrared (FT-IR) spectroscope Nicolet iS5 using iD7 ATR (Thermo Fisher Scientific, Japan). Prior to analysis, samples were dried at room temperature for 24 hours. The spectrum was recorded over the wavenumber ranging between 400 and 4,000 cm^{-1}. The spectra were the average of 16 scans at a spectral resolution of 4 cm^{-1}.

2.3.2   Morphological analysis

The surface morphologies of CNF and treated CNF were observed under a 3D laser scanning confocal microscope (LSCM) model VK-X 100 (KEYENCE Corporation, Osaka, Japan) under prescribed conditions of laser: red semiconductor laser, λ=658 nm, 0.95 mW, and pulse width of 1 ns using a depth composition procedure.

2.3.3   SEM-EDS analysis

SEM-EDS images were observed using a scanning electron microscopy equipped with energy dispersive X-ray spectroscopy (SEM-EDS) (JCM 6000, JEOL Ltd. Tokyo, Japan). All CNF samples were dried at 24 hours in room temperature prior to analysis. The samples were coated with carbon using a vacuum sputter coater before observation by SEM-EDS.

2.3.4   Dynamic laser scattering (DLS)

Dynamic laser scattering (DLS) measurements were done to determine the size distributions by intensities and numbers for CNF after acid treatments. A DelsaMAx Pro was used (Beckman

Coulter, Inc), and analyses were carried out at room temperature, scattering angle of 163.5° using disposable sizing cuvettes fill with 100% ethanol solvent to reduce the agglomeration. The intensity of size distributions was obtained from the analysis of the correlation function using the Rayleigh Spheres model in the DelsaMax software.

2.3.5 Wide Angle X-ray Diffraction (WAXD)

The WAXD measurements were performed using a X-ray diffractometer (MiniFlex 600, Rigaku Co., Japan) at 30 kV and 15 mA at room temperature. Cu Kα radiation ($\lambda = 1.54$ Å) was used as the X-ray source. The diffraction angle was scanned from 3° to 70° at a rate of 1.4°/min. The crystallinity index (I_c) was determined using the height of 200 peaks (I_{002}, $2\theta = 23.5°$) and the minimum intensity between 200 and 110 peaks (I_{AM}, $2\theta = 18°$) which can be expressed as:

$$I_c(\%) = \frac{I_{002} - I_{AM}}{I_{002}} \times 100 \qquad (1)$$

where I_{002} represents both crystalline and amorphous material while I_{AM} represents amorphous material.

2.3.6 Thermogravimetric analysis (TGA)

TGA was carried out on EXSTAR TG/DTA 7200 (SII Nanotechnology Inc., Japan). The samples were scanned form 30 to 550 °C with the heating rate of 10 °C/min under the protection of nitrogen flow at 100 mL/min.

2.3.7   Mechanical properties

The silicone/CNF composite was shaped into rectangular films with a size of $40 \times 5 \times 0.8$ mm. The mechanical properties of silicone/CNF were determined by an IMC-18E0 model machine (Imoto Machinery Co. Ltd, Kyoto, Japan) at a rate of 10 mm/min crosshead speed at 23 °C. The measurement was carried out using five replicates.

2.3.8   Optical property

Optical property of the composite films was determined by UV–Vis spectra. A rectangular piece of each film sample (4 cm × 4 cm) was directly mounted between the two spectrophotometer magnetic cell holders. The transmittance spectra of the composite films were measured at selected wavelength ranges from 190 to 1000 nm using a UV–Vis spectrophotometer (GENESYS 50, Thermo Fisher Scientific, USA). The optical properties of silicone and silicone composite films were characterized by the transmittance of visible (660 nm) regions.

2.4   Result and Discussion

2.4.1   Acid treatment and functional group analysis

In this study, low concentration of acids were used in the treatment of CNF. The surface of CNF holds an abundance of hydroxyl groups, allowing the possibility of extensive chemical modifications. Surface modification on CNF was done in order to achieve good compatibility with a polymer matrix. Carboxymethyl etherification, C6-carboxylation, phosphorylation, phosphite esterification, and sulfate esterification, are the common method use as surface modification and lead to their better compatibility in the hydrophobic polymer matrix [102]. However, some of this method required high concentration acid with combination high temperature, using harsh

chemical, and catalysts [25][88]. Therefore, the idea of using the low concentration acid treatment is to reduce the hydroxyl group in CNF by introducing another functional group. The reduction of hydroxyl groups caused the improvement in the dispersion of CNF in non-polar polymers matrices [53][103]. The sonification process during acid treatment would facilitate the physical swelling of CNF and more surface areas would be exposed [104] [105]. This will allow the acid group to attack the hydroxyl group in CNF. The hydrochloric acid was added in CNF-S sample as a catalyst for swelling the cellulose and promote the sulfate group to attach to the CNF surface, which occurred after the esterification reaction of CNF with sulphuric acid [106] [9]. The modified CNF was washed repeatedly with RO water to remove unreacted acid. By using chemical modification on CNF, the properties of the CNF could be changed and controlled in specific ways.

The FT-IR analysis was carried out to study the functional groups present in treated CNF and to examine the changes of chemical structure that occurred due to the acid treatments as shown in Figure 2.1. The broad peak was observed at 3400-3300 cm^{-1} was attributed to the stretching vibration of O-H bonding from absorbed water molecules of the cellulose chains. This peak also includes inter- and intra-molecular hydrogen bond vibrations in hydroxyl groups in cellulose I [107][108]. The peak at 2895 cm^{-1} was attributed to the CH stretching vibration of all hydrocarbon constituent in polysaccharides and the peak at 894 cm^{-1} attributed to the ß-glycosidic linkages of the cellulose chain [109]. The peak at 1647 cm^{-1} may be attributed to the bending mode due to the absorbed water. In the treated CNF-P, new peaks of a phosphate group were observed at 980 and 480 cm^{-1}, which was assigned as the $P(OH)_3$ stretch and OPO bending of H_3PO_4, respectively [110].

Besides, the weak absorption of the carboxyl group in the treated CNF-A was observed at the peak of 1740 and 1260 cm^{-1} which were assigned to C=O ester and C-O, respectively, indicating the occurrence of acetylation during the acetic acid treatment. On the other hand, for the treated CNF-S, the peak at 1050 and 1002 cm^{-1} were observed by the shifted group of O=S=O [111], suggesting that the introduction of sulfate group into CNF surface was successful. Based on the FT-IR spectra, this method was shown to successfully obtain surface modified CNF through this low concentration of acid treatment combined with sonification process.
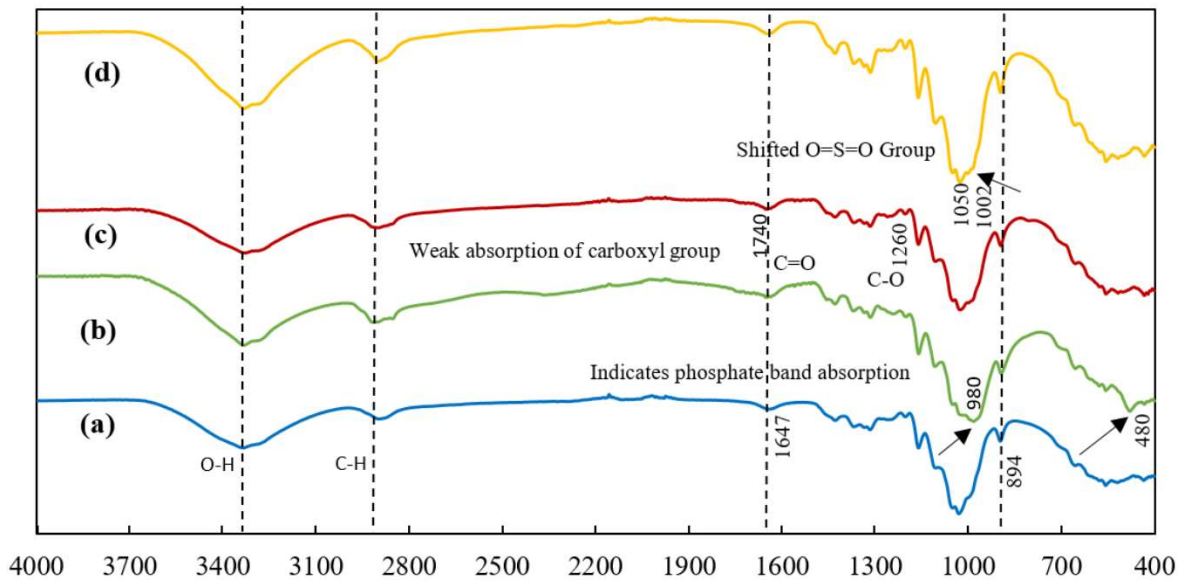
Figure 2.1: FT-IR spectrum of CNF treated with different acid solutions; (a) CNF, (b) CNF-P, (c) CNF-A, and (d) CNF-S

2.4.2   Scanning electron microscopy energy dispersive X-ray spectroscopy (SEM-EDS) analysis

The elemental analysis obtained via energy dispersive X-ray spectroscopy (EDS) is shown in Table 2.2, indicating that the functional group was successfully introduced in CNF through acid

treatment. EDS is an analytical technique used for the elemental compositions and chemical characterisations, by emitting specific wavelengths of X-rays demonstrating the atomic structure characteristic of various elements [112]. Based on Table 2.2, the treated CNF-P sample showed a significant percentage of phosphorus (P) element at 3.42% after acid treatment. Besides, there was also a 14.03% increase of element O due to the substitution of OH groups by the phosphate groups containing additional O atoms [113]. In treated CNF-A, element C was reduced to more than 5% comparing to control CNF and increased element O was observed in treated CNF-A, indicating that the successful acid treatment [114]. Meanwhile, the treated CNF-S has shown the presence of sulphur element at 3.23% as compared to control CNF.

Table 2.2: Elements analysis of CNF and treated CNF.

Element	CNF (%)	CNF-P (%)	CNF-A (%)	CNF-S (%)
C	92.51	82.55	87.29	88.12
O	7.45	14.03	12.71	8.55
P	0.03	3.42	-	-
S	0.01	-	-	3.23
Total	100	100	100	100

2.4.3 Dynamic light scattering (DLS) and morphological of treated CNF

Dynamic light scattering was performed to analyse the size of the length of CNF samples after acid treatment. The size distribution and the average length size of each sample were depicted in Figure 2.2a and 2.2b, respectively. DLS method also was done by Gamelas *et al.* [115] to study

cellulose nanofibrils length distribution obtained by TEMPO-mediated oxidation and mechanical treatment. The result obtained by DLS for treated CNF is the average size distribution curves, including the presence of a small number of particle and fibrils aggregates. Therefore, the values obtained from DLS is for comparison between treated samples and not as a direct measure of the real size of the CNF. In Figure 2a, the treated CNF-S showed the smallest size distribution at an average of 278 nm in comparison to treated CNF-P and CNF-A which showed broad size distribution with an average of 413 nm and 324 nm, respectively. Since electrostatic repulsion prevents from aggregation on the acidic treated CNF, the size distribution of both samples of CNF-P and CNF-A were expected to be of broad size distribution. On the other hand, CNF-S exhibited narrow size distribution, suggesting that prior hydrolysis occurred on CNF-S contrary to the treated CNF-P and CNF-A.

Size distribution is an important aspect to access the distribution of CNF as nanofiller to prevent the agglomeration in the silicone hybrid composite. The average size was taken into account due to the inability to discriminate the aggregation between fibrillated material and particles. The size distribution of treated CNF samples was reduced by acid treatment. Before the acid treatment procedure, the CNF sample showed a broad size distribution range of 537 nm. Consequently, after the treatment, the average size distributions of treated CNF samples were reduced, as shown in Figure 2.2b. The previous study reported that CNF produced by mechanical methods have long fibril shapes with 1–100 nm in diameter and 500–2000 nm in length [116]. This result may also indicate that CNF-S was preferentially hydrolysed.
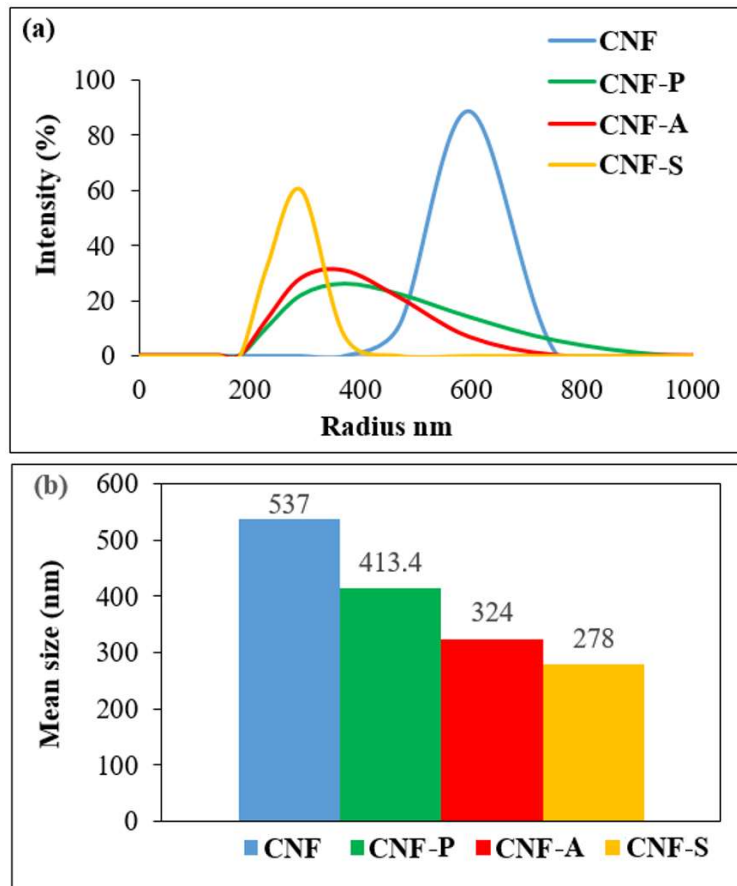
Figure 2.2: Size distributions of control CNF and acid-treated CNF; (a) Range of intensity distributions and (b) Mean size of particle-size distributions.

Figure 2.3 shows the surface image of CNF and treated CNF under a 3D laser microscope. Measurements of all samples were taken after the acid treatment process without drying to prevent self-agglomeration and to preserve the native state of the CNF samples. Smaller particles size of CNF was difficult to be observed under optical microscope [117]. High dynamic range (HDR) processing technique was applied to enhance the CNF images. This high-level gradation technique can be obtained by capturing several images with different brightness levels and will reproduce a clear image. This technique can reveal that the pristine CNF sample shows a large and long fibre as compared to CNF-P and CNF-A. After acid treatment, the reduction of fibre size were revealed

from CNF-P and CNF-A samples, these results are similar to the DLS results. Number of long fibres in CNF-S image (**Figure 2.3d**) is significantly less than that of CNF-A and CNF-P. These results also reflect their DLS observations.
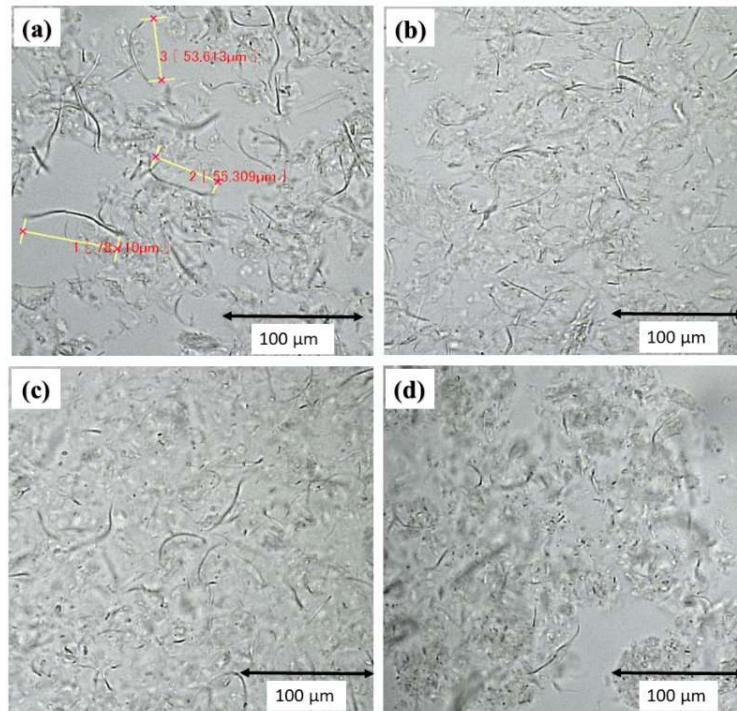
Figure 2.3: Microscope images of CNF before and after acid treatment under a laser microscope at 20 × magnification without staining but placed in water; (a) CNF, (b) CNF-P, (c) CNF-A, and (d) CNF-S

2.4.4 Wide-angle X-ray diffraction (WAXD) analysis of treated CNF

The crystalline structure of CNF and treated CNF was investigated by WAXD to provide the data on the cellulose crystallinity and the influence of the acid treatments. Figure 2.4 shows the diffracted peaks at 2θ around 16. 5° (110), 23. 5° (200), and 35° (040) which represent the typical structure of cellulose I [22][85] and the structure of the crystalline region were remained and not

disrupted by acid treatments. This finding was in agreement with the FT-IR analysis. Tang *et al.* [118] reported that cellulose treated with NaOH/urea causing the cellulose I crystals to be dissolved into NaOH/urea solution and broke its hydrogen bonds. Part of the hydrogen bonds were reformed and cellulose was recrystallized into cellulose II during the precipitation step. In order to maintain the crystallinity of cellulose I to prevent from recrystallization of cellulose II, the acid treatment used in our study was done without the neutralisation using NaOH.

The crystallinity of the control CNF was 78% and after acid treatments, the crystallinity of treated CNF samples were decreased to 73%, 65%, and 65% for CNF-P, CNF-A, and CNF-S, respectively. Interestingly, the crystallinity of CNF was decreased to 19% from original CNF after sonication for 3 hours even though crystallinity of CNF is generally increased due to preferentially hydrolysis occur to amorphous phase with acid. The introduction of functional groups onto the cellulose backbone by acid treatment has disrupted the crystalline structure by decreasing the number of inter and intra-molecular hydrogen bonding, hence reducing the crystallinity of the CNF structure [113]. The WAXD data also indicated that the CNF after acid treatments was able to sustain at high degree of crystallinity in the CNF structure.
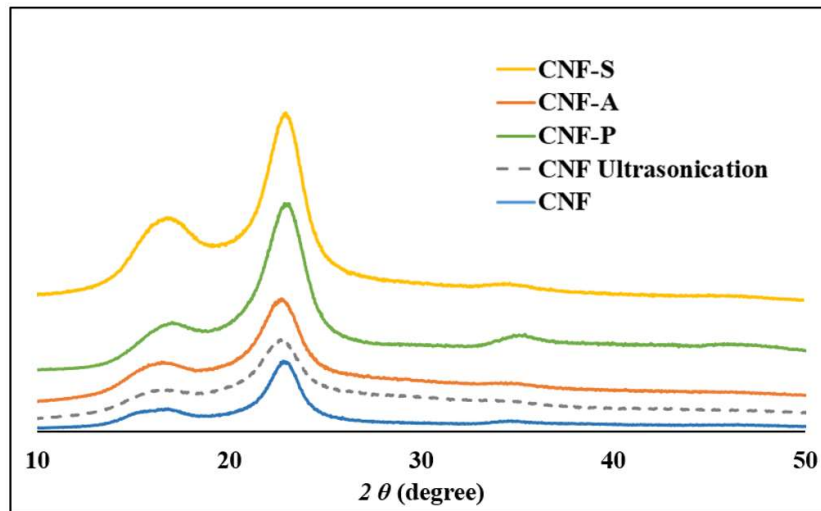
Figure 2.4: X-ray diffraction spectra of CNF and treated CNF

2.4.5 Dispersibility of CNF on different solvents

Due to the hydrophilic nature of cellulose, CNF cannot be uniformly dispersed in most non-polar polymer matrices and polar and non-polar solvents. After acid treatments, the treated CNF was washed with RO water until it reached pH 7 and then freeze-dried. For the dispersion study, each sample was sonicated for 1 hour until dispersed in the dedicated solvents. It is important to understand that even under sonication in organic solvent, it was difficult to achieve individual CNF without surface modification. The dispersibility of CNF and treated CNF samples were determined by dispersing the samples in acetone (ACt), ethanol (EtOH), methanol (MeOH), chloroform (CHCI$_3$), RO water (H$_2$O RO), dimethyl sulfoxide (DMSO), dimethylformamide (DMF), hexane (Hex), and toluene (TOL) as shown in Figure 2.5. The dispersity of the samples were accessed after sonication and left for 3 days under ambient temperature.
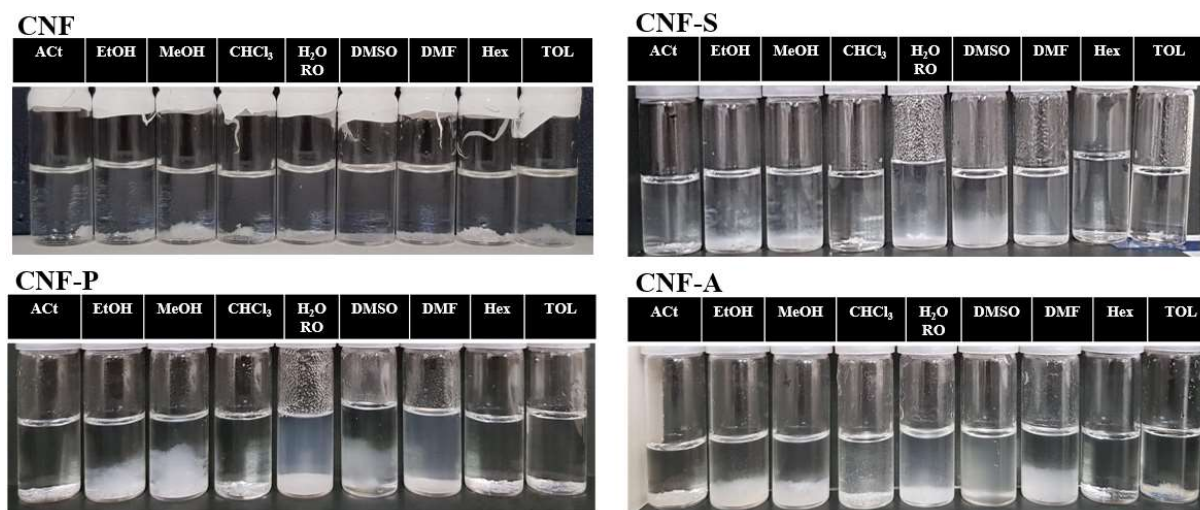
Figure 2.5: Dispersibility of control CNF and acid-treated CNF in polar and non-polar solvents.

Hydrogen bonding is formed during freeze-drying of CNF which led to a more stable structure due to irreversible hornification, making CNF difficult to redispersed in the solvent [119]. From the digital image in Figure 2.5, sediments can be observed in all the tested solvents indicating that the poor dispersion due to the formation of hydrogen bonding during freeze-drying. The presence of anion groups such as sulfate, carboxyl and phosphate groups on the surface CNF via acid treatment improved the charge repulsion, hence providing improved dispersibility of CNF in some solvents [120][121][26]. Treated CNF-S and CNF-P samples were well dispersed in H_2O RO, DMF and partially dispersed in DMSO, EtOH and MeOH. Meanwhile for CNF-A samples, they dispersed well in H_2O RO, DMSO and partially dispersed in DMF and sedimented in EtOH and MeOH after 3 days observation. On the other hand, the CNF and treated CNF sample did not have good dispersibility in ACt, TOL, and Hex solvents, either before or after acid treatment.

2.4.6　　　　Thermal degradation behaviour of CNF and treated CNF

The thermal stability of the CNF and treated CNF was investigated by TGA, as shown in Figure 2.6. The TGA curves revealed the weight loss percentage of materials with regards to the thermal degradation temperature. All CNF samples displayed a slight weight loss below 100°C due to the presence of residual adsorbed moisture. All treated CNF showed lower thermal degradation compared to control CNF (270°C), the reason may decrease the degree of polymerization of CNF after acid treatment [122]. Among them, the lowest thermal degradation was for treated CNF-S, which was at 220°C. The decrease in the thermal stability can be attributed to the presence of sulphate group in cellulose, which reduced the thermal degradation temperature of CNF [116] [123][21]. Contrary to our findings, one study reported that the cellulose treated with phosphoric acid enhanced the thermal degradation of cellulose [124]. However, in our study, the treated CNF-P exhibited low thermal degradation at 233°C, which was similar to a study by Daud *et al.* [113]. The treated CNF-A had slightly higher thermal degradation as compared to other treated CNF samples which were at 248°C. The presence of carboxyl groups on the CNF-A surface is responsible for the lower thermal stability [125]. Therefore, the acidity of CNF may be a key factor to accelerate thermal degradation reaction since acidic functional groups may act as self-catalyst to the degradations. All treated CNF samples had weight loss average at 24-34% as compared to control CNF at 9.5% of weight loss. The residual weight of the acid-treated CNF from TGA was higher than that of control CNF. From these profiles, the thermal degradation reaction showed different behaviors between the acid-treated CNF and control CNF. Therefore, the acid-treated NFC may occur carbonization via any side reactions.
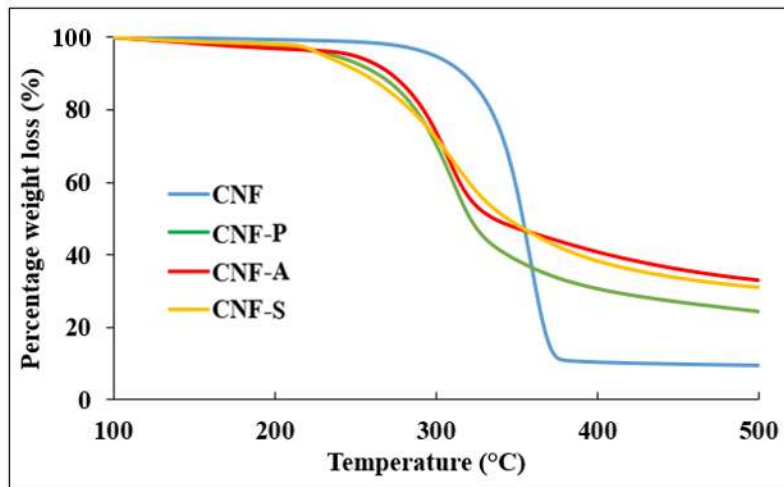
Figure 2.6: Thermal degradation characteristic of CNF and treated CNF

2.4.7 Silicone composite with treated CNF

The treated CNF used for silicone composite production was exchanged solvent to ethanol prior to silicone/CNF composite preparation. This process aimed to reduce the self-aggregation (hornification) and promoted the efficient dispersion of CNF in a silicone polymer. Study form Cichosz *et al.* [126] reported that the undried cellulose modified with maleic anhydride after a solvent exchange with ethanol gives the highest performance at tensile strength and elongation at break of ethylene–norbornene copolymer-based composites. The efficiency of nanofiller dispersion in the matrices and the capability of nanofiller interfacial interactions were critically affected by the physical and mechanical properties. The filler as a reinforcer in polymer matrices is often agglomerated in the polymer matrices due to their high surface areas [127]. To reinforce non-polar polymers such as silicone with CNF, surface modification using acid treatment was conducted to introduce the functional groups onto the CNF. This treatment is expected to increase polymer compatibility.
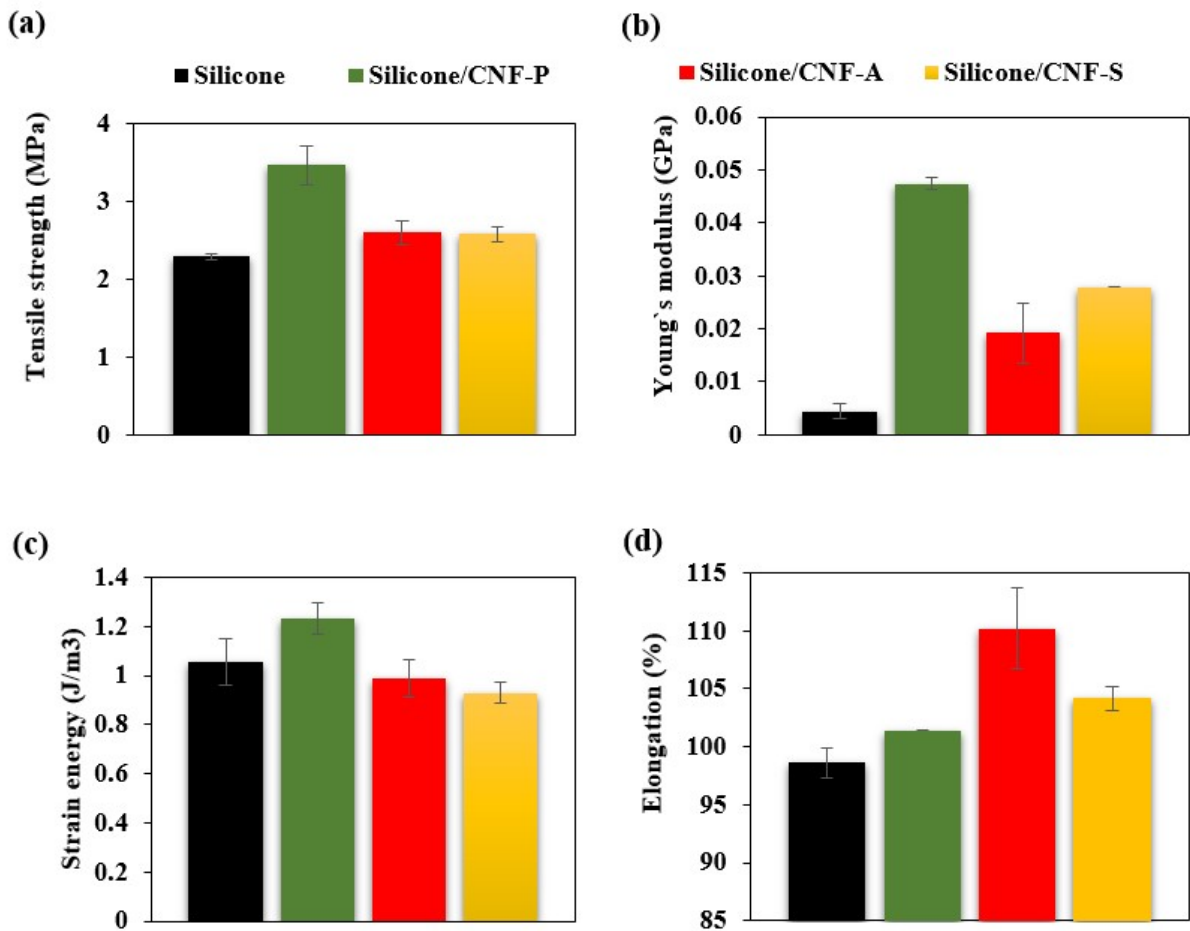
Figure 2.7: Mechanical properties of silicone and silicone composite with treated CNF; (a)

Tensile strength, (b) Young`s modulus (c) Strain energy, and (d) Elongation

The silicone/CNF composites were characterised according to the mechanical properties, as shown

in Figure 2.7. The treated CNF reinforcements enhanced the mechanical properties of the silicone

composite. The highest tensile values were recorded at 3.47 MPa in silicone/CNF-P, followed by

silicone/CNF-A and silicone/CNF-S, as shown in Figure 7a. There was 51.5% improvement in

the tensile strength of the silicone/CNF-P as compared to silicone polymer. Besides, the treated

silicone/CNF-P had a higher value in Young's modulus (Figure 7b) and strain energy (Figure 7c)

as compared to others. The Young's modulus of the silicone composite is significantly improved

with the treated CNF content embedded in the composite [128]. The improvement in tensile strength and Young's modulus is indicative of strong interfacial adhesion between filler and matrices. These also lead to a better filler dispersion, efficient stress transfer and elongation at break [129]. The elongation in Figure 2.7d showed an improvement of 11% for silicone/CNF-A, followed by silicone/CNF-S at 5.5%. This improvement was due to the good adhesion property of the treated CNF to silicone, which resulted in a higher elongation at break than the pure silicone. The mechanical properties of the composite polymer were dependent on the distribution and size of nanofiller particles in the matrices [89] and chemical bonding between the polymer and nanofiller [88]. These characteristics are very important because agglomeration might reduce the mechanical properties of the composites and load transfer between reinforcement and polymer.

The transparency of treated CNF in silicone composites were observed for dispersibility of untreated and treated CNF in silicone composite as a shown in Figure 2.8. The silicone composite with treated CNF-P (Figure 2.8b) showed homogeneously white cloudy as compared with original silicone polymer as shown in Figure 2.8 (a). As a result, silicone composite with treated CNF showed the nanofiller effect demonstrated the synergistic enhancement in both tensile strength and elongation as compared to silicone polymer (Figure 2.8a). This is because the treated CNF was homogeneously dispersed in silicone polymer. Figure 2.8c shows the CNF agglomeration occurred in silicone polymer when use in dry form. The transmittance properties of silicone and silicone composite are shown in Figure 2.9, and Table 2.3 show the optical properties at transmittance at 660 nm. Incorporating treated CNF in the silicone matrix greatly reduced the transmittance of the composite compared to silicone. The higher the transmittance value of the composite, the better the transparency, because more visible light (660 nm) can pass through the

composite [130]. Therefore, silicone composite with treated CNF-P shows higher transmittance value comparison with other composites since CNF-P in silicone showed good dispersibility. Surface modification with acid treatment shows a great potential as a low-cost and environmental-friendly method to improve the surface properties of CNF to be used as nanofiller for a non-polar polymer.

(a)	(b)	(c)
(2.0mm Thickness)	(1.0mm Thickness)	(1.0mm Thickness)
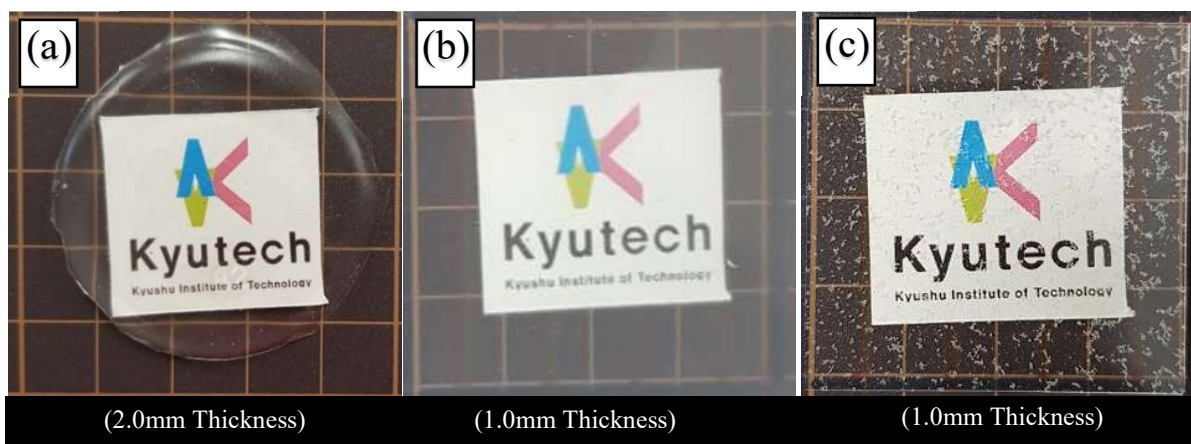
Figure 2.8: Image of silicone and silicone composite with treated CNF. (a) Silicone, (b) Silicone/treated CNF-P, and (c) Silicone/CNF composite (dried CNF)
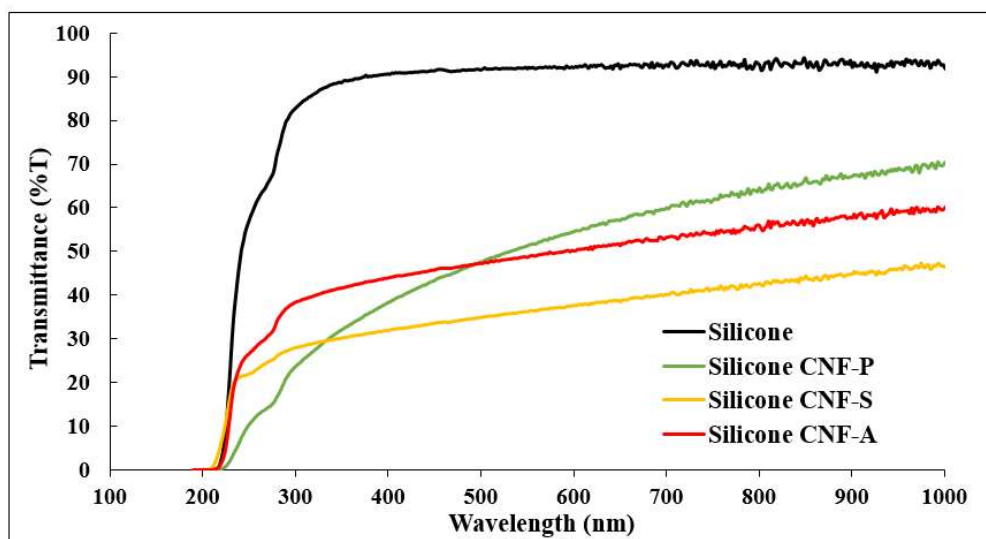
Figure 2.9: UV–Vis transmittance spectra for silicone and silicone composite

Table 2.3: Optical properties of silicone and silicone composite

Sample	Thickness (mm)	%Transmittance (660 nm)
Silicone	0.846	92.8
Silicone NFC-P	0.889	58.1
Silicone NFC-A	0.865	52.3
Silicone NFC-S	0.814	39.1

2.5 Conclusion

CNF treatment with acid has confirmed to modify surface property through FT-IR, XRD, SEM-EDS, and TGA. Their results showed to obtain modified CNF with acid as a simple method. In this method, the WAXD showed the crystalline structure of cellulose I before and after treatment with acid, and degree of crystallinity showed decreasing after acid treatment which may proof the conversion of the hydroxy group in CNF. The shift of thermal degradability also showed the modification of CNF surface comparison with that of pristine CNF. Especially, a phosphoric acid treatment for CNF could disperse well in silicone matrices and its mechanical properties were enhanced to compare with original silicone. Therefore, this study could be a platform to design renewable nanocomposites and provide high-quality materials with improved properties and various polymer matrices in the future.

CHAPTER 3

Enhancing Mechanical Properties of Polyurethane with Cellulose Acetate as Chain Extender

Abstract

Polyurethanes (PUs) are a class of versatile engineering materials synthesized by the reaction between polyol, isocyanate, and chain extender as the hardener. Among various cellulose derivatives, cellulose acetate (CA) possessed unique features such as excellent mechanical properties, good thermal stability, tailorable surface chemistry, and can be used as hydroxyl providers to enhance the properties of PUs. Our goal is to develop a simple method to prepare PUs by using varying weight ratio of CA as the chain extender or crosslinking agent. PUs modified with varying weight percentage of CA (5%, 10%, and 30%) (based on total parts per weight of poly(tetramethylene oxide) (PTMO) and isocyanate) were compared with PUs modified with 1, 4-butanediol (BD), acting as the control. The morphological, chemical structural, thermal stability, and mechanical properties of the modified PU CA polymer were investigated thoroughly. The findings from this study found that modified PUs with CA possessed higher thermal stability. The PUs with 10% of CA as chain extender was found to be the optimal percentage for the preparation of PUs with the highest tensile strength and elongation properties. However, the utilisation of higher weight percentage of CA reduced the elongation property of the modified PUs due to excessive crosslinking effect.

3.1 Introduction

Polyurethanes (PUs) is one of the most versatile and unique polymers which are formed by chemical reaction between an isocyanate and a hydroxyl group. The growth in the polyols and polyurethane market is expanding due to their multi-functionalities in many applications. PUs can been applied in furniture coatings, adhesives, construction materials [131], various biomedical applications such as artificial skin, pericardial patches, soft-tissue adhesive, drug delivery devices, and scaffolds for tissue engineering [132], [133]. PUs are formed from urethane linkage, a carbamate ester linkage synthesised by the reaction between an isocyanate group and hydroxyl group [134]. The terminal hydroxyl group allows for alternating blocks, called "segments" to be inserted into PUs chain [135]. Soft segments are derived from polyols such as polyester, while the hard segments are formed from the combination of a diisocyanate and a chain extender [136]. The chain extender is usually a small molecule containing hydroxyl or amine functional groups [137]. The isocyanate groups are reactive towards active hydrogen groups such as amine (-NH), hydroxyl (-OH), carboxylic acid (-COOH), urea, and amide. The isocyanates building block can be either aromatic isocyanates or aliphatic isocyanates in segmented polyurethane elastomers.

Aromatic isocyanates are more reactive than the aliphatic isocyanates in PUs polymerization and generally contributed to better mechanical strength, thermal and flame retardant properties [71], [72]. Toluene diisocyanate (TDI) and methylene diphenyl diisocyanate (MDI) are some of the typical aromatic isocyanates used in the industry to enhance the mechanical performances of the polymer [73]. However, aromatic PUs is not suitable for outdoor coatings application due to degradation and/or metamorphose under exposure of UV-light [74]. Moreover, aromatic isocyanate-based PUs are more likely to form aromatic amines after degradation which have higher

toxicity in comparison to aliphatic-based PUs [75]. To overcome the setbacks, aliphatic isocyanate-based PUs are often considered as they possessed excellent UV resistance, high transparency, and good outdoor durability as required in coating applications [76]. The most common aliphatic isocyanates are hexamethylene diisocyanate (HDI), dicyclohexylmethane 4,4'-diisocyanate (H_{12}MDI), and isophorone diisocyanate (IPDI). Some researchers focused on PUs polymerization using aliphatic isocyanates to produce degradable PUs with the inclusion of biodegradable fillers in the matrix.

Cellulose fibre is derived from renewable resources which is eco-friendly. It has excellent mechanical properties, good biocompatibility, and also tailorable surface chemistry [84]. The enhancement of the physical and mechanical properties from the incorporation of cellulose-based materials in aliphatic isocyanates-based PUs have been thoroughly investigated [138][139][140]. Girouard et al.[80] reported that the site-selective modification of cellulose nanocrystals with IPDI enhanced the dispersion in PUs composite that increased the tensile strength, elongation and work of fracture more than 200% as compared to the neat PUs. Similar study also reported on the enhancement in tensile strength (287%) and Young`s modulus (900%) with the inclusion of 1 wt % cellulose in the PUs matrix as compared to neat PUs [141]. However, high content of cellulose fibre in PUs often led to poor adhesion between the fibre and matrix interface [142]. Furthermore, the hydrophilic properties of cellulose diminish the dispersion in PUs matrix without surfactant or surface modification [143]. To overcome this problem, thermoplastic cellulose acetate (CA), a derivative of cellulose was found to be a suitable substitute as chain extender in PU polymerisation which have been previously reported [83].

CA is synthesised via esterification of cellulose and widely used as biodegradable plastics, modern coatings, optical films, composites, and laminates [144]. Due to their interesting chemical functionalities, CA has the potential to be also used as hydroxyl providers in the modification of PUs. Their ability to be incorporated readily in PUs matrix can be achieved using the blending method [145][146][147] and electrospinning [148]. PUs prepared via these methods are usually used for ultrafiltration, scaffold in tissue engineering, air filter, biomedical, and pharmaceutical materials for wound healing and drug delivery [149].

Herein, this study reports on the preparation and characterization of modified PUs with varying weight percentage of CA (5%, 10% and 30%) as the chain extender. In comparison to previous studies, our approach to prepare modified PU based on aliphatic diisocyanate minimized the utilization of harmful and toxic chemicals. This facile and simple method of modified PUs preparation should provide pertinent knowledge in future studies pertaining to the incorporation of CA in polymer matrix.

3.2 Experimental

3.2.1 Material

Cellulose acetate L-30 (CA, acetyl content 55%) was kindly obtained from Daicel Corporation, Japan. Poly(tetramethylene oxide) 2,000 (PTMO) and dibutyltin (IV) dilaurate (DTBL) were purchased from Wako Pure Chemical Industries Ltd, Japan. Dicyclohexylmethane 4,4'-diisocyanate ($H_{12}MDI$) and 1,4-Butanediol (BD) were obtained from Tokyo Chemical Industry Co., Ltd. All other reagent-grade chemicals were purchased from Wako Pure Chemical Industries Ltd, Japan and were used without further purification.

3.2.2 Synthesis of PUs/ CA

The PUs were prepared using PTMO and $H_{12}MDI$ using the prepolymer method in the presence of DTBL as catalyst. Table 3.1 depicts the prepolymer production composition. The prepolymer was prepared in super dehydrated DMF solvent under vacuum condition with constant nitrogen gas flow at 80 °C for one hour. DTBL was then added to the prepolymer as the catalyst. After the prepolymer reaction is completed, degassing is conducted using a vacuum chamber. Varying weight percentage of CA (5%, 10% and 30%) was then added to the prepolymer and was agitated for one hour under constant stream of nitrogen gas flow and vacuum condition. The polymer was then precipitated in acetone and filtered through a filter paper. Finally, the polymer was post-cured in vacuum oven at 70 °C for 24 h to remove any remaining solvent. The samples were denoted as PU CA 5%, PU CA 10% and PU CA 30%. As for the control sample, BD was used as the chain extender and the obtained sample is denoted as PU BD.

Table 3.1: Composition of modified PUs and PU BD polymer

	PU CA	PU BD
Prepolymer		
PTMO (M_w:1900-2120 g/mol)	0.23 mmol	0.23 mmol
H_{12}MDI (M_w:262.35 g/mol) /DBTL	0.69 mmol/0.05 mmol	0.69 mmol/0.05 mmol
Chain Extender		
CA (L-30)	5%, 10%, 30% (w/w)	-
1,4-Butanediol (M_w:90.12 g/mol)	-	0.46 mmol

3.2.3 Preparation of PUs film

PUs films were formed using a hydraulic hot-press (IMC-180C, Imoto Machinery Co., Japan) at 110 °C for 15 min under a pressure of 20 MPa, and then the cold press was performed at 30 °C for 30 minutes.

3.2.4 Characterisation of PUs film

3.2.4.1 Optical property

The optical property of the composite films was determined by UV–Vis spectra. A rectangular piece of each film sample (4 cm × 4 cm) was directly mounted between the two spectrophotometer magnetic cell holders. The transmittance spectra of the PUs films were measured at selected wavelength ranges from 190 to 1000 nm using a UV–Vis spectrophotometer (GENESYS 50, Thermo Fisher Scientific, USA). The optical properties of PU BD and modified PUs films were characterized by the transmittance of visible (660 nm) regions.

3.2.4.2   Chemical analysis

The chemical analysis was carried out using the Fourier Transform Infrared (FT-IR) spectroscope Nicolet iD7 ATR (Thermo Fisher Scientific, Japan). Each sample recording consisted of 16 scans recorded from 400 to 4000 cm^{-1}.

3.2.4.3   Thermogravimetric analysis (TGA)

TGA and DTG were carried out using EXSTAR TG/DTA 7200 (SII Nanotechnology Inc., Japan) with scan range from 30 to 550 °C at a constant heating rate of 10 °C /min under continuous nitrogen flow rate of 100 mL/min. Initial degradation temperatures (T_{onset}) were determined at 5% stage of mass loss while the maximum degradation temperatures (T_{max}) were calculated from the first derivative of the TGA curves (DTG).

3.2.4.4   Wide Angle X-ray Diffraction (WAXD)

The WAXD measurement was performed using X-ray diffractometer (MiniFlex 600, Rigaku Co., Japan) at 30 kV and 15 mA operated at room temperature. The X-ray source used was Cu Kα radiation ($\lambda = 1.54$ Å). The diffraction angle was scanned from 3° to 70° at a rate of 1.4°/min.

3.2.4.5   Mechanical properties

The test films were cut into a rectangular shape with a size of 40 × 5 × 0.5 mm. The mechanical properties of PUs were determined by an IMC-18E0 model machine (Imoto Machinery Co. Ltd, Kyoto, Japan) at a rate of 10 mm/min crosshead speed at 23 °C. The measurement was carried out with five replicates.

3.3   **Results and Discussion**

3.3.1   **Synthesis and morphological characteristics of the modified PUs**

During prepolymer synthesis, isocyanate group from $H_{12}MDI$ reacted with the hydroxyl groups from PTMO to form urethane chains in the presence of DTBL as the catalyst. The continued formation of urethane chain is further driven with the addition of CA, in which the remaining isocyanate (N=C=O) groups reacted with the abundant free hydroxyl groups. The precipitation in acetone further increased the size of the white precipitate (polymer) indicating the feasibility of acetone to remove unreacted diisocyanate, CA, and DMF. In addition, the usage of acetone not only completely removed the unreacted reactants but also shortens the drying time of the polymer which is a convenient process.

From Figure 3.1, there were no significant differences in the transparency of the modified PUs with CA (Figure 3.1b – 3.1d) and PU BD (Figure 3.1a) after the hot press method indicating good dispersion rate of the CAs in the PUs. Moreover, this also agrees with the value of the transmittance of PU BD and modified PUs (Figure 3.2) and visible light at 660 nm (Table 3.2). In terms of textural properties, PU CA 5% possessed smooth surface with soft plastic like properties. Meanwhile, PU CA 10% possessed rougher surface texture, soft and flexible akin to a rubber like material. The polymer becomes more rigid due to higher NCO/OH ratio from the increase in cross-linking [150]. Attributed to the excessive cross-linking, PU CA 30% possessed thermoplastic-like properties; high stiffness and brittleness.

Figure 3.1: Morphological of (a) control PU BD and modified PUs with different weight percentage of cellulose acetate; (b) PU CA 5%, (c) PU CA 10%, and (d) PU CA 30%
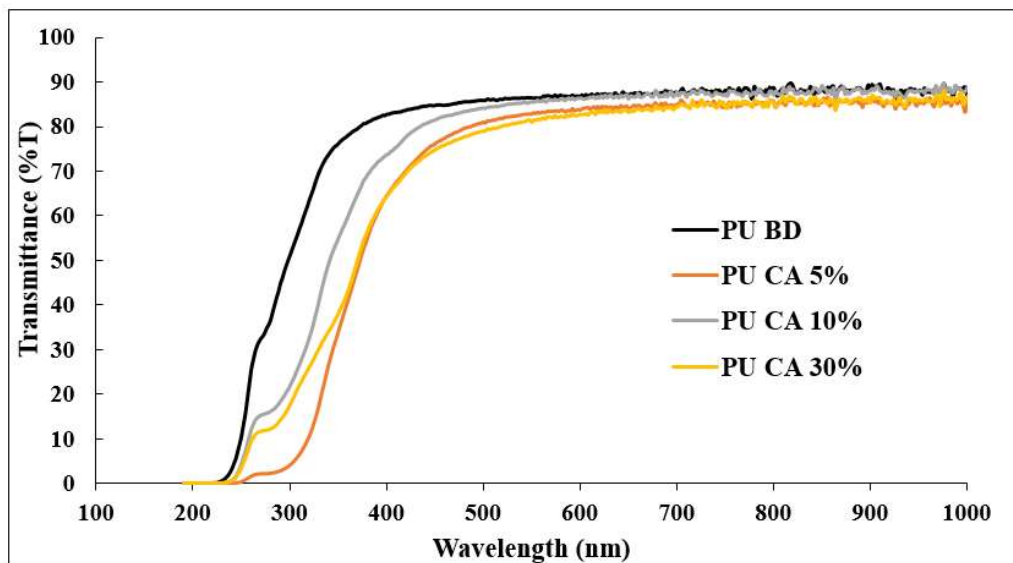
Figure 3.2: UV–vis transmittance spectra for PU BD and modified PUs

Table 3.2: Optical properties of PU BD and modified PUs

Sample	Thickness (mm)	%Transmittance (660 nm)
PU BD	0.434	87.4
PU CA 5%	0.448	84.7
PU CA 10%	0.436	87.3
PU CA 30%	0.453	84

3.3.2 Chemical structures of the modified PUs

As shown in Figure 3.3, the chemical structures of modified PUs with different amounts of CA and PU BD were investigated using FT-IR spectroscopy. The presence of urethane linkage was evident from the band observed at 3315 cm^{-1} attributed to the N-H stretching and bending vibration bands. The absence of the band at 2250 cm^{-1} attributed to isocyanate group (-NCO) demonstrated that diisocyanate did not remained in the PUs [151]. The characteristic peaks of the PUs were observed at 2925-2850 cm^{-1} for CH$_2$ and CH$_3$ stretching, respectively [152], [153]. The peak at 1100 cm^{-1} corresponds to C-O-C stretching vibration of PTMO [153]. The slight red shift in the C-H bond is observed in PU CA 5%, 10%, and 30% upon comparing to PU BD at 1524 cm^{-1}. The carbonyl C=O stretching peak of urethane appeared at approximately 1713 cm^{-1} for PU BD. The new C=O stretch peak arose from the urethane bonding was observed at 1627 cm^{-1} for both PU CA 5% and PU CA 10%. Meanwhile, for PU CA 30%, the C=O peak was shifted to 1667 cm^{-1}. This peak indicated the strong hydrogen bonding between the soft segments and hard segment of PUs [154]. This C=O peak could also be contributed from CA, indicating that CA can be effectively used as a chain extender [83]. The peak appearing around 600 cm^{-1} in PU CA 30%, but absent in PU CA 5% and PU CA 10% may be contributed from the unreacted CA.
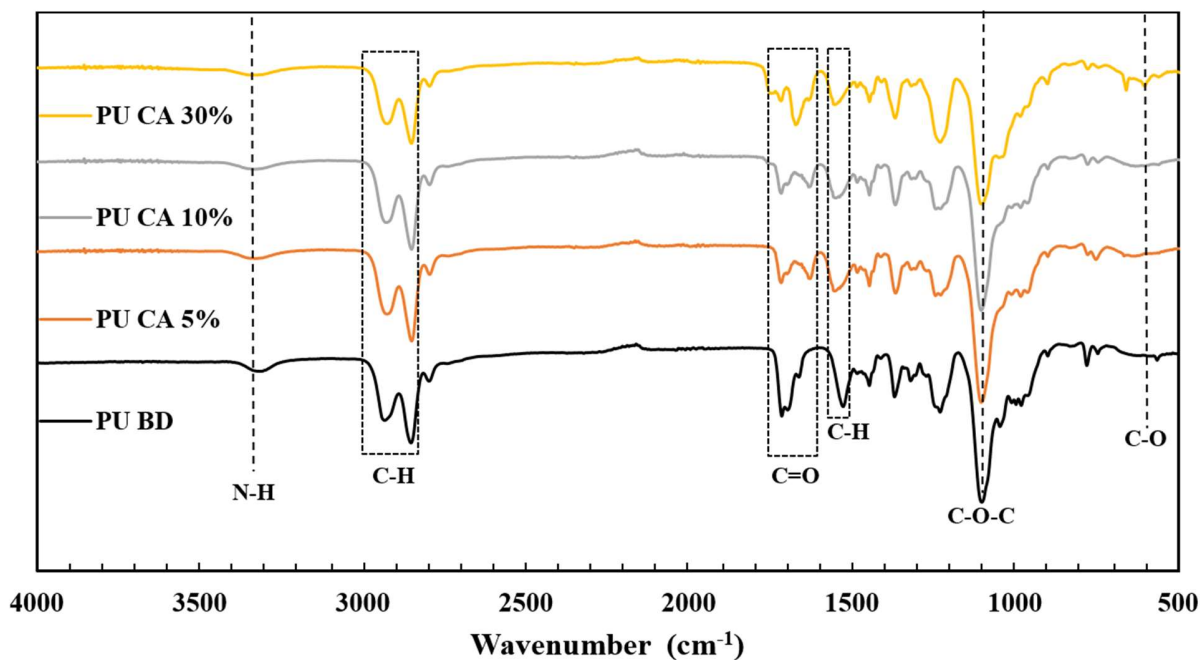
Figure 3.3: FT-IR spectra of PU BD and modified PUs with different weight percentage of cellulose acetate; PU CA 5%, PU CA 10%, and PU CA 30%

3.3.3 Thermal decomposition of the modified PUs

To probe the thermal behaviour, TGA and DTG analysis were carried out and their thermograms were shown in Figure 3.4a and 3.4b, respectively. The thermal decomposition parameters determined from the thermograms were further summarised in Table 3.3. As shown in Figure 3.4a, CA possessed a single stage thermal decomposition and highest thermal stability due to the propionyl groups from the cellulose backbone [155], in which at higher temperature, the glycosidic bonds of cellulose structure will breakdown [156]. The PU BD and the modified PU CA samples showed similar thermal degradation behaviour exhibiting two decomposition stages, indicating the successful polymerization with CA as the chain extender. The first degradation stage is attributed to the severance of the urethane bonds in which the decomposition leads to the formation of primary amine and olefin or the formation of secondary amine and carbon dioxide [157]. The

second stage of the degradation curve is attributed to the decomposition of ester groups [158]. The addition of CA as chain extender in PU further improved the thermal stability as compared to the PU BD, specifically the PU CA 10% attributed from the strong chemical bonding formation between the hydroxyl group of the CA and modified PUs [159], [160]. Additionally, the weight residue at 500°C of the modified PU CA 10% showed 12.22% followed by 6.9% residue of PU CA 5% and 4.37% residue of PU CA 30%.

The initial temperature (T_{onset}) was calculated from DTG curves in Figure 3.4b to access the decomposition temperature and degradation dynamics. The decomposition process of PU BD occurred at 302.5 °C while the modified PU CA 5% and PU CA 10% decomposition occurred at 314.2 °C and 317.7 °C, respectively. For PU CA 30%, it was observed that the decomposition process occurred at a lower temperature, 295.9 °C. The rate of weight loss was further analysed from the DTG curves to obtain the T_{max} values. The T_{max1} and T_{max2} of the PUs can be defined as the maximum temperature rate for decomposition of polyurethane rigid segments and soft segments [161]. The T_{max1} value for CA is the highest (366.6 °C) followed by PU BD (347.9 °C). The increase in the weight percentage of CA as chain extender further decreases the T_{max1} values ranging from 334-346 °C. The disruption of crosslinked network in the hard segment of the PUs with high concentrations of CA was observed. It might prevents the motion of the chains during relaxation process resulting in less soft segment-ordered structures or crystallisation [162], [163]. However, the higher density of urethane linkages leads to a more thermally stable PUs [164]. The T_{max2} values for all the modified PUs were found to possess almost similar decomposition temperature ranging from 413.0 °C to 419.6 °C as compared to PU BD (404.6 °C).

Table 3.3: The decomposition temperature of PU BD, CA (L-30) and modified PUs at 10 °C min^{-1} in nitrogen

Samples				Residue at 500 °C
	T_{onset} (°C)	T_{max1} (°C)	T_{max2} (°C)	(wt%)
CA L-30	298.5	366.56	-	13.91
PU BD	302.5	347.9	404.6	2.42
PU CA 5%	314.2	346.4	413.0	6.9
PU CA 10%	317.7	343.7	419.6	12.22
PU CA 30%	295.9	334.6	419.0	4.37
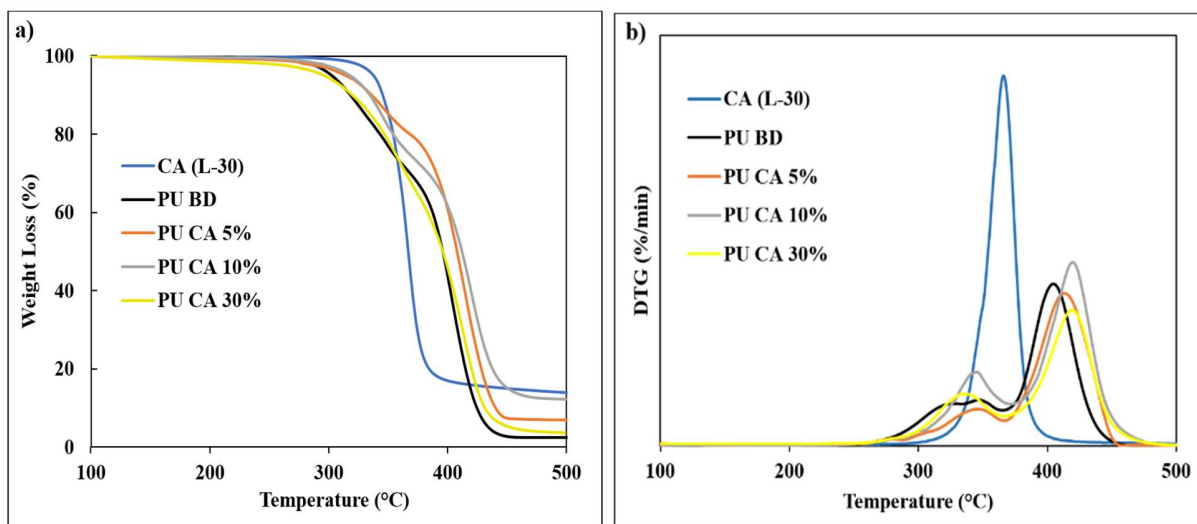
Figure 3.4: TGA (a) and DTG (b) curves for PU BD, CA (L-30), and modified PUs with different weight percentage of cellulose acetate; PU CA 5%, PU CA 10%, PU CA 30%

3.3.4 Wide-angle X-ray diffraction (WAXD) analysis of the modified PUs

Wide-angle X-ray diffraction was carried out to identify the crystalline structure of PU BD and modified PU CA samples. In segmented PUs, the phase separation between soft segments and

hard segments occurred due to their relative material, structural regularity, and thermodynamic incompatibility [165], [166]. Figure 3.5 shows the WAXD profiles of PU BD and modified PU CA. The crystallinity of each PUs to reveal the interaction between PUs chains and structures can appear from WAXD profiles. The PU BD showed a sharp diffraction peak appearing at $2\theta = 19.4°$. Meanwhile, the peak for modified PU CA 5% and 10% were observed at $2\theta = 20.0°$ and 20.4°, respectively. Particularly in comparison to PU CA 5 % and 10%, the 2θ degree of PU CA 30% shifted to 21.2°.
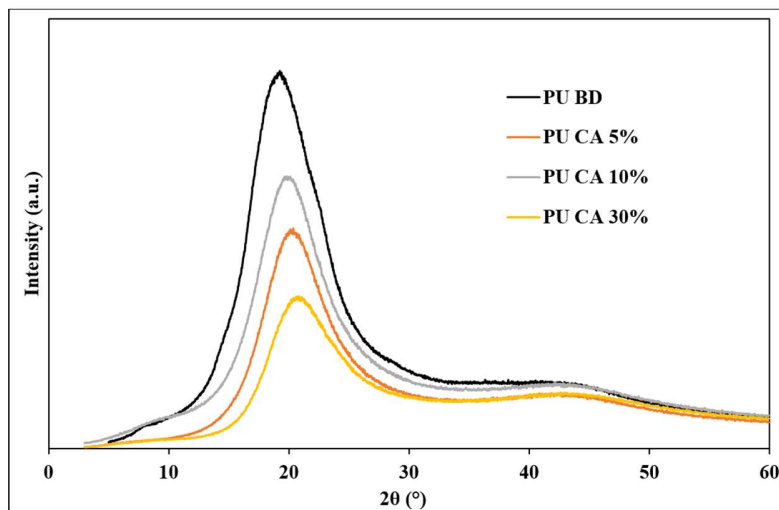
Figure 3.5: WAXD patterns of the PU BD and modified PUs with different weight percentage of cellulose acetate; PU CA 5%, PU CA 10%, and PU CA 30%

Based on the peak profiles, the reduce of crystalline structure is due to the short range ordering in the hard segment domains of PUs [167]–[169]. Density of cross-linkage in PUs cause a reduction of hydrogen bonding in hard segments and chemical crosslinking in soft segments, as well as annealing process [170]. Generally, the higher the intensity of the diffraction peaks, the higher the crystallinity in the polyurethane [171]. The WAXD spectra profiles also corroborated the findings

by Trovati *et al.* [158] which indicated that the PU BD and modified PUs samples with CA were soft PUs [172].

3.3.5 Mechanical properties of the modified PUs

Tensile test was carried out on the modified PUs with CA and PU BD to access their tensile strength and elongation behaviour. The mechanical properties of PUs are often related to their molecular masses and the ratio of soft and hard segment. As shown in Figure 3.6a, the enhancement in the tensile strength were apparent in the PUs modified with CA. The highest tensile value was obtained at 17 MPa for PU CA 10% followed by PU CA 30% at 16.9 MPa. There was a 354% improvement in the tensile strength in comparing PU CA 10% with PU BD, which was 4.8 MPa. The findings indicated that the tensile strength of PUs are affected by the amount of CA in the PU chains [83].

However, there was a huge difference in the tensile strength for PU CA 5% in comparison to other modified PUs which can be attributed to the insufficient isocyanate groups to crosslink with the hydroxyl group in CA. In addition, the elongation properties for the modified PU CA were shown in Figure 3.6b. The control PU BD sample exhibited the highest elongation percentage. Among the modified PUs with CA, PU CA 10% exhibited the highest elongation percentage followed by PU CA 5% and PU CA 30%. In comparison to PU BD, the elongation percentage decreased at a rate of 21.92 %, 5.10 %, and 76.60 % for PU CA 5%, PU CA 10% and PU CA 30%, respectively. The minimal decrease in the elongation percentage PU CA 10% indicated that CA as chain extender is comparable to BD. As higher weight percentage of CA is introduced as chain extender, the rigidity of the polymer will increase due to the excess urethane formation which is evident in

PU CA 30%. The increase in the content of hard segment led to rigid material with high modulus and tensile strength, but low in elongation [82].
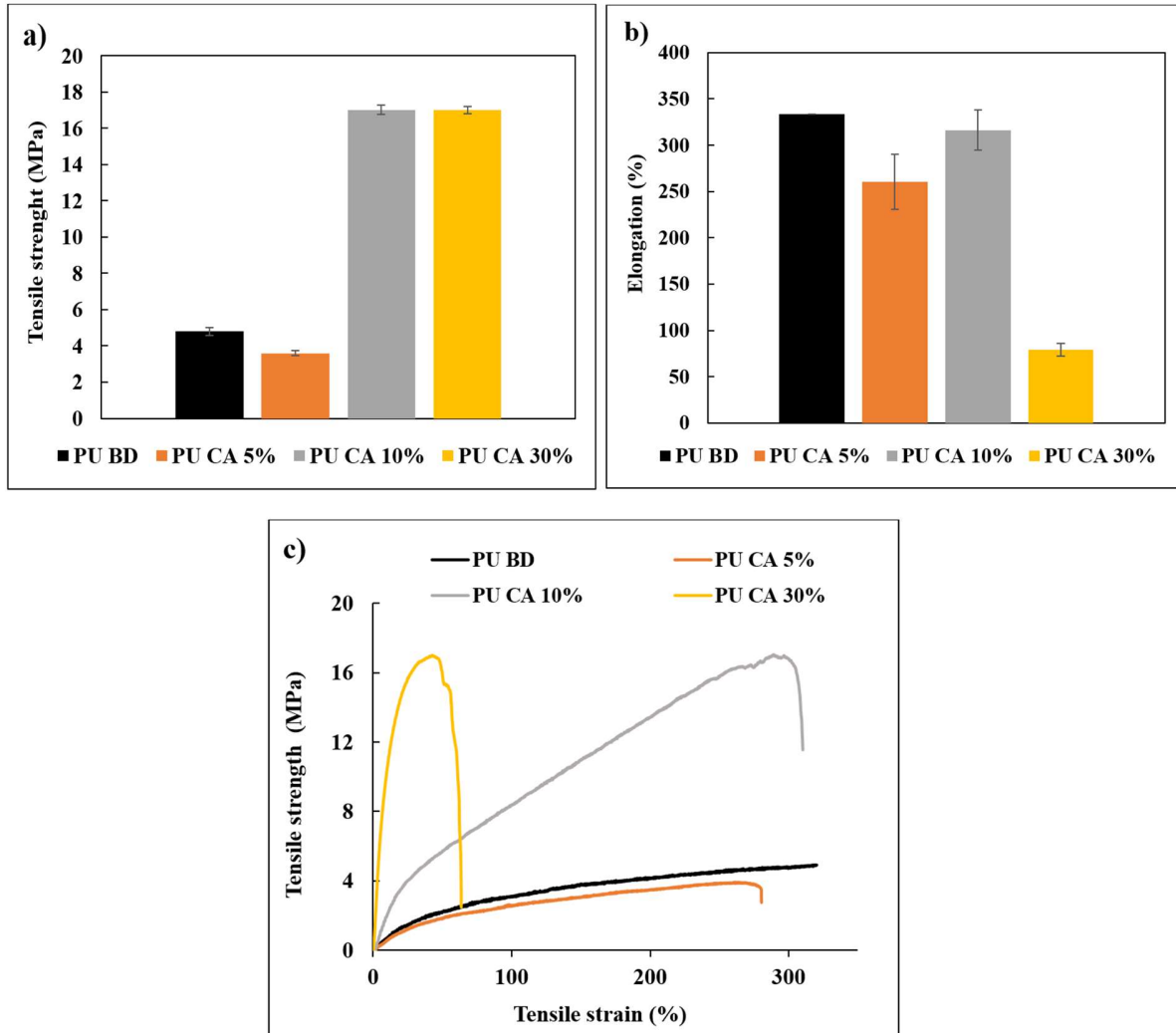
Figure 3.6: Tensile strength (a), elongation (b) and tensile strength curves (c) of PU BD and modified PUs with different weight percentage of cellulose acetate; PU CA 5%, PU CA 10%, and PU CA 30%

Figure 3.6c shows the tensile strength of the modified PUs. PU CA 30% exhibited the highest tensile strength at lower strain percentage due to the rigidity of the sample. The plausible

explanation can be attributed to the excess unreacted CA which does not have good affinity with the PU, as proved in the FTIR result. Meanwhile, for PU CA 5%, PU CA 10%, and PU BD, the tensile strength increased with elongation. Therefore, modified PUs with 10% of CA is the best mixing polymerization ratio to acquire polymer with high tensile strength and elongation properties.

3.4   Conclusion

Various weight percentage of CA was successfully used as chain extender in the polymerisation of PUs. The good transparency of the film formed in the modified PUs with CA (up to 30%) showed that CA dispersed homogenously within the PU matrix. In comparison to PU BD as the control, PU CA 10% was found to be the optimal mixing ratio to obtain a modified PUs with enhanced mechanical properties. The higher amount of CA used in the polymerisation led to the increase in the tensile strength but with reduced elongation properties. From their thermal behaviour, modified PUs with CA showed higher thermal stability in comparison to PU BD. Hence, CA can be used to replace BD as the chain extender to further enhance the PUs performance in terms of their transparency, thermal stability, and mechanical properties. Owing to these properties, the modified PU prepared using this simple process is a promising substitute as a new generation material for weather and waterproof coating, thermal insulation film for glass windows, powder coatings, and biomedical applications. The findings of this study also opened up avenue for the exploration of other modified cellulose to be used as chain extender in the preparation of fibre reinforced PUs.

CHAPTER 4

Covalent Incorporation of Cellulose Nanofibre (CNF) Into Polyurethanes Elastomer and the Effect on Mechanical Properties

Polyurethanes (PUs) is one of the most versatile and unique polymers which are formed by a chemical reaction between an isocyanate and a hydroxyl group. The present study investigates the PUs composite properties of aliphatic-based PUs prepared from a poly(tetramethylene oxide) (PTMO) and dicyclohexylmethane 4,4'-diisocyanate ($H_{12}MDI$) with different degree of polymerisation (DP) of cellulose nanofibre (CNF). Different DP of CNF was treated with phosphoric acid and been used in synthesis PUs via *in situ* polymerisation. Controls PUs with the conventional chain extender 1,4-butanediol was prepared as a reference. The morphology, chemical structure, mechanical, and thermal properties of the resultant PUs composite were investigated by scanning electron microscopy (SEM), Fourier transform infrared analysis (FT-IR), tensile test, wide angle X-ray diffraction (WAXD) and thermogravimetric analysis (TGA). Modified CNF shows a good dispersion rate in the PUs composite, and FT-IR result confirms a chemical bonding reaction between the hydroxyl group of modified CNF and isocyanate group in composite PUs. PUs composite with 20% of modified CNF, DP 650 archived the highest tensile strength, which is 51.5 Mpa. Besides, PUs composite with all modified CNF possessed higher thermal stability as compared to control PUs.

Keywords: cellulose nanofibre, *in situ* polymerisation, polyurethanes, aliphatic isocyanate, acetone solvent

4.1 Introduction

Polyurethanes (PUs) are unique polymers with a wide variety of applications in the form of rigid and flexible foams, coatings, adhesives and elastomers, such as heat insulation, building, automotive components, seating materials and medical devices. Building blocks of PUs, containing two or more functional groups, can be divided into polyisocyanates, polyols and chain extender [134]. Polyols typically consist of polyesters, polyethers or polycarbonates, whereas isocyanates can be eventually classified into aromatic and aliphatic [136]. The chain extender is usually a small molecule with either hydroxyl or amine groups [137]. Isocyanate will attack the hydroxyl group, and this reaction will structurise the urethane group in PUs polymerisation. The chemical structure and properties of PUs can be tailored over a wide range by using various isocyanate/polyol ratio and various amounts of chain extenders or additives [173]. Several types of PUs have been developed and used in various industries due to their superior properties. Beside, PUs has some disadvantages, that is, low thermal resistance, low adhesion and mechanical properties [174]. However, nanomaterials have been widely used to improve the properties of PUs due to their small size effect and surface effect, such as nano-silica, nano-zinc oxide, nano-titanium dioxide, clay, and cellulose nanocrystals [175].

The aromatic isocyanates are more reactive than the aliphatic isocyanates and generally develop better mechanical strength, thermal and flame retardant properties and rigid PUs [72][71]. Moreover, aromatic isocyanate-based PUs has lower UV light stability, leading to yellowish over the time and potential to form aromatic amines after degradation, while aliphatic isocyanate-based PUs have better UV light stability, transparent, exterior durability and lower toxicity [75][76]. Aliphatic isocyanates-based PUs also produce rubbery materials with high elongation but low in tensile strength [77]. Besides, polymerisation processes can be in a lower temperature, easily

customisable process conditions and product properties have led to unique applications in this isocyanate-based PUs, specifically hexamethylene diisocyanate [176].

Reinforcement of PUs with cellulose had great attention for the improvement of the physical and mechanical properties of PUs composites. A recent study shows the tensile strength and Young`s modulus of PUs were enhanced by 287% and 900% with 1 wt % cellulose nanocrystals as compared to the neat PUs [141]. Meanwhile, Pei *et al*. [177] reported increased tensile strength and strain-to-failure of aromatic PUs with only 1 wt % of cellulose nanocrystals incorporated. The tensile strength were obtained at 61.5 MPa, strain-to-failure at 994.2% and Young's modulus at 42.4 Mpa. Besides, Zhang *et al*. [178] reported use of nanocrystalline cellulose could improve the anti-yellowing property of aromatic polyurethane, and the yellowing of the composite was decreased by 57.7% with 1.5% surface-modified of nanocrystalline cellulose. The PUs/cellulose nanocrystal nanocomposites are usually prepared by solvent casting and *in situ* polymerisation technique using dimethylformamide (DMF) as a solvent [58] [138]. However, due to the high boiling point (153 °C), nanocomposite entails difficulties for solvent removal later, time-consuming and hazardous effects of DMF [179].

Besides, the high content of cellulose fibre in the PUs polymer will cause a slightly poor adhesion between the fibre and matrix interface [22]. In order to avoid the agglomeration in PUs nanocomposites, the surface modification of cellulose needs to be done. Cellulose possesses a high hydrogen bond that makes it have hydrophilic properties in nature [27]. Without surface modification on the cellulose surface, its tendency to agglomeration in a PUs matrix and decreases the mechanical properties of composites material. The surface modification of cellulose, for

example, acetylation, esterification, silanisation, silylation, glyoxalization, grafting of glycidyl methacrylate, and maleic anhydride is an effective method for improving the interface compatibility between composites material [138][28].

Cellulose fibres attract much more interest and have been widely used as the polymer fillers to improve the mechanical properties due to their superior advantages including biodegradability, renewable resources, eco-friendly, good biocompatibility, and tailorable surface chemistry [84]. Comparing to cellulose fibre, cellulose nanofibre (CNF) is lighter in weight with high surface area to volume ratio, higher strength, stiffness and it can act as an excellent reinforcing agent for developing green bio-nano composites [20]. CNF has hydroxyl groups as reactive groups which can be functionalised to various surface properties [86]. However, CNF has some difficulties, such as poor compatibility between nanomaterials and PUs matrix, which is easy agglomeration and poor dispersion in a polymer matrix. Herein, to obtain advanced nanocomposites, a proper dispersion of the nanofiller in the matrix must be achieved.

PUs-based nanocomposites reinforced with cellulose nanomaterials is remains challenging due to the hydrophilicity of cellulose. In this study, CNF with different DP was treated with phosphoric acid and incorporated into PUs matrix in acetone solvent by *in situ* polymerisation. This our first approach used different DP of CNF in PUs composite. The PUs matrix consisted of PTMO and $H_{12}MDI$. This isocyanate-based PUs is low in tensile strength. Therefore, the final purpose is to develop high mechanical and thermal properties PUs with good biocompatibility by introducing a much stronger chemical bond between CNF and PUs. The morphological, chemical analysis and thermal degradation of PUs composite were investigated by comparing to PU with 1,4-butanediol

as control (PU BD). For mechanical properties, we were comparing treated and untreated CNF with different DP in PUs composite.

4.2 Experimental

4.2.1 Material

Poly(tetramethylene oxide) 2,000 (PTMO) M_w:1900-2120 obtained from Wako Pure Chemical Industries Ltd, Japan and dicyclohexylmethane 4,4'-diisocyanate (H$_{12}$MDI) M_w: 262.35 obtained from Tokyo Chemical Industry Co., Ltd. Dibutyltin (IV) dilaurate (DTBL) M_w: 631.56 as the polymerisation catalyst, acetone (99%) obtained from Wako Pure Chemical Industries Ltd, Japan and 1,4-butanediol M_w: 90.12 obtained from Tokyo Chemical Industry Co., Ltd used as a chain extender. Commercial of CNF was kindly provided by Sugino Machine Limited, Toyama Prefecture, Japan. This NFC was produced by a super high-pressure water jet system. Different degree of polymerization (DP) of CNF (5 wt % in water) were used which is CNF FMa-100 (DP 200), CNF WFo-100 (DP 650) and CNF IMa-100 (DP 800).

4.2.2 Surface modification of CNF by phosphoric acid.

Commercial CNF with different DP has undergone acid treatment, as described in Chapter 2 are listed in Table 4.1. CNF was treated by phosphoric acid under ultrasonic 40 Hz for 3 hours and continuously stirred for 4 hours at room temperature. Then, the product was washed with RO water and centrifuged at 8000 rpm for 10 minutes until it reached pH 6−7. In order to use in PUs polymerisation, modified CNF was solvent exchanged to acetone and stirred for 24 hours. After that, modified CNF was centrifuged at 8000 rpm for 10 minutes, and sediment was collected. These processes were repeated three times to ensure water is removed.

Table 4.1: Percentage and volume of acids used in the acid treatment of CNF

Sample Code Name	NFC aq. (5 wt %)	Acids	Acid volume (Total 100 mL)
FMa-P	10 g	Phosphoric acid (85% w/w)	30 mL
WFo-P	10 g	Phosphoric acid (85% w/w)	30 mL
IMa-P	10 g	Phosphoric acid (85% w/w)	30 mL

3.2.3 Synthesis of PUs/modified CNF in acetone solvent

PUs composite was synthesised *in situ* polymerisation in acetone solvent using three-neck bottle flask (500 mL) equipped with a reflux condenser, temperature indicator, and mechanical stirrer (Figure 4.1). Table 4.2 shows the composition of PUs composite with CNF, and Table 4.3 shows the composition of PUs composite with modified CNF used *in situ* polymerisation. Initially, CNF or modified CNF was dispersed in acetone solvent by sonication treatment for 5 minutes. After that, PTMO was added and continue mixed at 90 °C for 2 hours. The reflux condenser was used to avoid evaporation of the solvent. Then, H_{12}MDI and DBTL were added to the mixture, and the chemical reaction was carried out under a nitrogen condition at 90°C for 3 hours. After the polymerisation was completed, the composite was collected and washed with acetone solvent and filtered through a filter paper. The filtered product was dried in the vacuum oven at 70 °C to remove any remaining solvent.
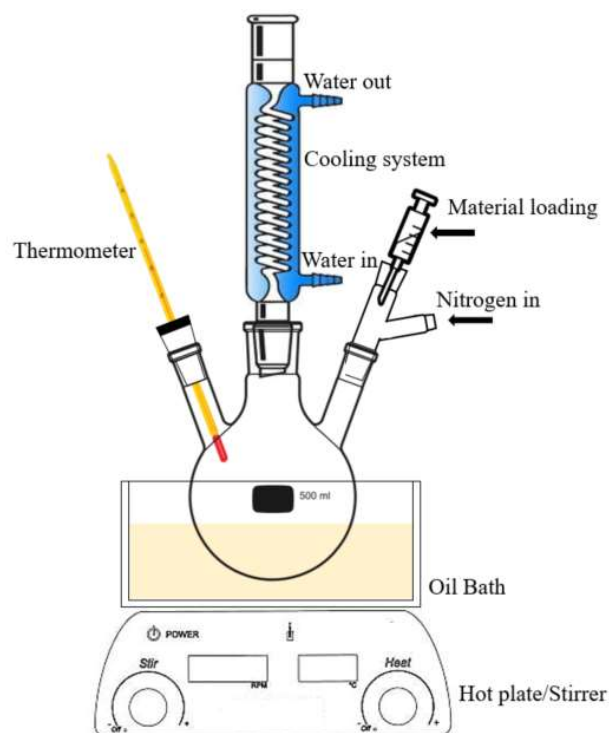
Figure 4.1: Schematic of the reflux process to synthesising PUs composite with CNF or modified CNF in acetone solvent.

Table 4.2: Chemical composition of PUs composite with CNF

	Composition (mmol)		BD (%)(w/w)	CNF (%)(w/w)
Sample Code	PTMO	H_{12}MDI/DBTL		
PU BD	0.6	3/0.05	30	-
PU FMa 10%	0.6	3/0.05	-	10
PU FMa 20%	0.6	3/0.05	-	20
PU FMa 30%	0.6	3/0.05	-	30
PU WFo 10%	0.6	3/0.05	-	10
PU WFo 20%	0.6	3/0.05	-	20
PU WFo 30%	0.6	3/0.05	-	30
PU IMa 10%	0.6	3/0.05	-	10
PU IMa 20%	0.6	3/0.05	-	20
PU IMa 30%	0.6	3/0.05	-	30

Table 4.3: Chemical composition of PUs composite with acid-modified CNF

Sample Code	Composition (mmol)		CNF-P (%)(w/w)
	PTMO	H_{12}MDI/DBTL	
PU FMa-P 10%	0.6	3/0.05	10
PU FMa-P 20%	0.6	3/0.05	20
PU FMa-P 30%	0.6	3/0.05	30
PU WFo-P 10%	0.6	3/0.05	10
PU WFo-P 20%	0.6	3/0.05	20
PU WFo-P 30%	0.6	3/0.05	30
PU IMa-P 10%	0.6	3/0.05	10
PU IMa-P 20%	0.6	3/0.05	20
PU IMa-P 30%	0.6	3/0.05	30

4.2.4   Preparation of PUs film

PUs composite films were formed using a hydraulic hot-press (IMC-180C, Imoto Machinery Co., Japan) at 120 °C for 15 min under a pressure of 30 MPa, and then the cold press was performed at 30 °C for 30 minutes.

4.3   Characterisation of PUs film

4.3.1   Scanning electron microscopy (SEM)

Surface morphologies of the fractured PUs composite films were observed by Scanning electron microscopy (SEM) (JCM-6000, JEOL, Japan) operated at 15 kV accelerating voltage. The composite samples were fractured under liquid nitrogen. Each sample was deposited on carbon tape and carbon-coated for 90 seconds before the observation.

4.3.2 Optical property

Optical property of the PUs composite was determined by UV–Vis spectra. A rectangular piece of each film sample (4 cm × 4cm) was directly mounted between the two spectrophotometer magnetic cell holders. The transmittance spectra of the PUs composite were measured at selected wavelength ranges from 190 to 1000 nm using a UV–Vis spectrophotometer (GENESYS 50, Thermo Fisher Scientific, USA). The optical properties of PU BD and PUs composite were characterized by the transmittance of visible (660 nm) regions

4.3.3 Chemical analysis

PUs composite was analysed using a microscopic Fourier Transform Infrared (FT-IR) spectroscope Nicolet iS5 using iD7 ATR (Thermo Fisher Scientific, Japan). The spectrum was recorded over the wavenumber ranging between 400 and 4,000 cm^{-1}. The spectra were the average of 16 scans at a spectral resolution of 4 cm^{-1}.

4.3.4 Mechanical properties

PUs composite was prepared as a dumbbell-shaped film with a size of 60 × 3 × 0.5 mm. The mechanical properties of composite PUs were determined by an IMC-18E0 model machine (Imoto Machinery Co. Ltd, Kyoto, Japan) at a rate of 10 mm/min crosshead speed at 23 °C. The measurement was carried out using five replicates.

4.3.5 Thermogravimetric analysis (TGA)

TGA and DTG were carried out using EXSTAR TG/DTA 7200 (SII Nanotechnology Inc., Japan) with a scan range from 30 to 550 °C at a constant heating rate of 10 °C /min under a continuous nitrogen flow rate of 100 mL/min. Initial degradation temperatures (T_{onset}) were determined at 5%

stage of mass loss, while the maximum degradation temperatures (T_{max}) were calculated from the first derivative of the TGA curves (DTG).

4.3.6   Wide Angle X-ray Diffraction (WAXD)

The WAXD measurement was performed using X-ray diffractometer (MiniFlex 600, Rigaku Co., Japan) at 30 kV and 15 mA operated at room temperature. The X-ray source used was Cu Kα radiation ($\lambda = 1.54$ Å). The diffraction angle was scanned from 3° to 70° at a rate of 1.4°/min.

4.3.7   Swelling behaviour

Swelling behaviour of the synthesised PUs composite was performed at room temperature. The solvent used is hexane, methanol, ethanol, dimethyl sulfoxide (DMSO), dimethylformamide (DMF), and chloroform. Test samples for swelling experiments were squares, cut from the films after the hot press method, weighing about 0.2 g. The PUs composite samples were immersed in a solvent in 24 hours, and the picture was taken start form 0 hours, 12 hours and 24 hours.

4.3.8   Ultraviolet (UV) Exposure Conditions.

UV exposure was carried out using a UV light source MUV-202 (Moritex Co., Tokyo, Japan) (λ=200-600nm). The samples were placed at a distance of 10 cm from a standard UV lamp that reproduces the solar spectrum and is exposed to light in a conditioned cabinet (40 ° C) for 8 days observation.

4.4   Results and Discussion

4.4.1   Synthesis and morphological characteristics of the composite PUs

Composite PUs were prepared *in situ* polymerisation method in acetone solvent. The advantage of acetone as a polymerisation solvent obtain a homogeneous mixture solution, a wide range of structure and emulsion, high quality and reliable reproducibility of end products [143]. In this synthesis, urethane groups are formed by reacting PTMO and H_{12}MDI with the presences of DTBL as a catalyst. Concurrently, the isocyanate group from H_{12}MDI reacted with the hydroxyl group from CNF to extend the urethane chain polymer. After polymerisation is completed, the successful synthesised product was precipitated in a white colour form. Figure 4.2a and Figure 4.2b are the PUs composite product after the hot press method. The image shows a good dispersion of the modified CNF was observed in PUs composite.
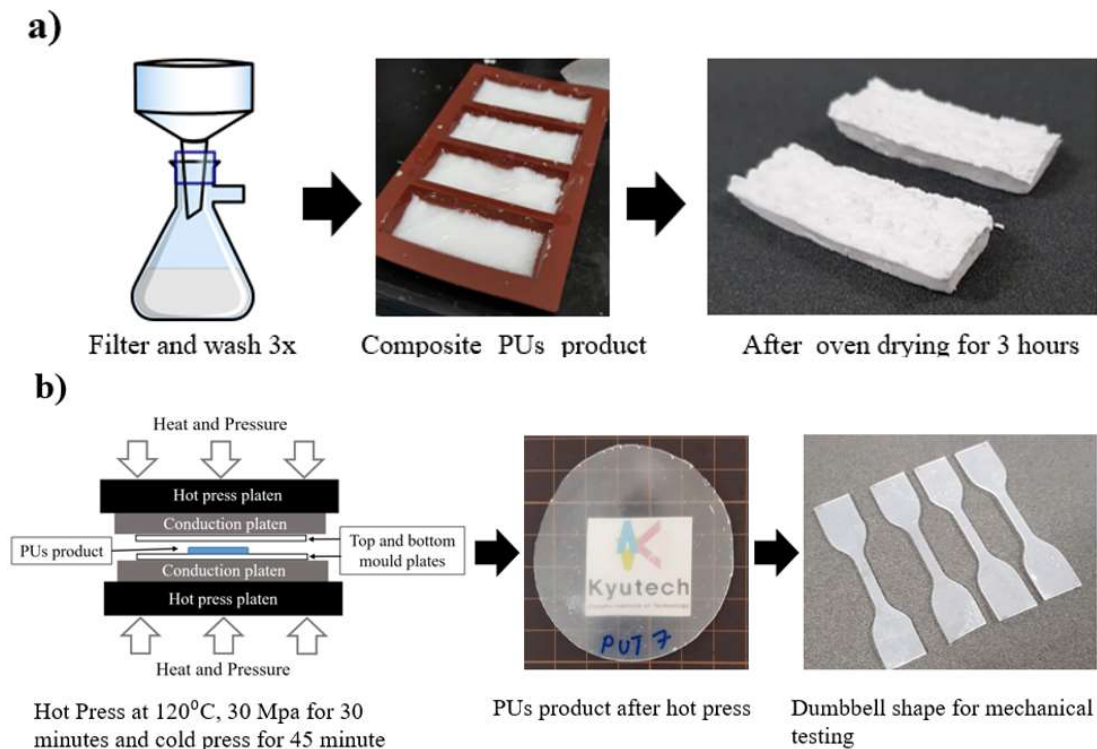
Figure 4.2: Flow diagram of composite PUs (a) the product after polymerisation process and drying in silicone mould using oven-dry (b) the product after hot press method for analysis.

Figure 4.3 shows the PUs composite product after hot press moulding. The PU BD (Figure 4.3a) showed the transparency and smooth surface of PUs film. The PUs composite (Figure 4.3b, 4.3c, and 4.3d) also showed the transparency and no aggregation of modified CNF indicated a good dispersibility of modified CNF in PUs composite. However, PU IMa-P 20% (Figure 4.3d) sample with a higher number of DP in modified CNF, were aggregation in some spots. The PUs composite prepared with untreated CNF showed some aggregation occur in the composite compared to PUs composite with modified CNF (Image not show).

Figure 4.3: Images of PUs film after hot press; (a) PU BD (b) PU FMa-P 20% (c) PU WFo-P 20% (d) PU IMa-P 20%.
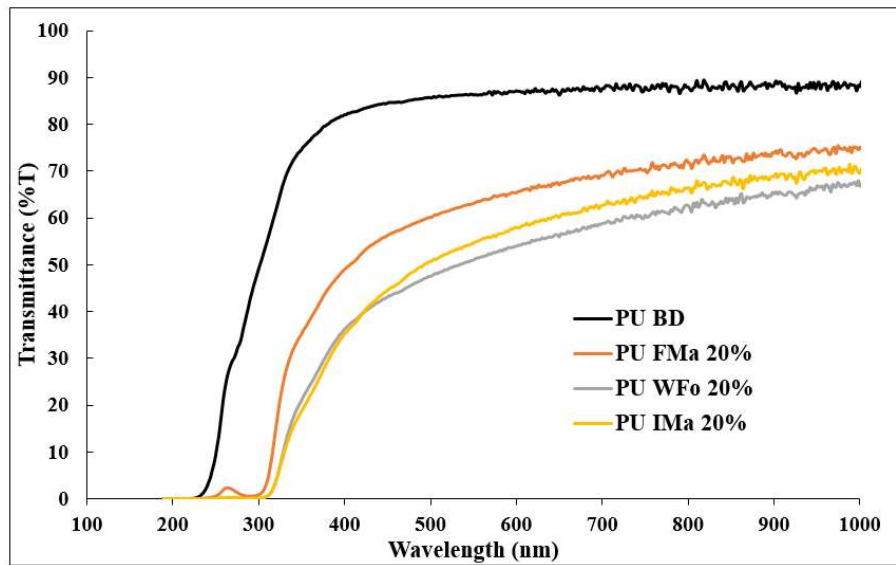
Figure 4.4: UV–vis transmittance spectra for PU BD and PUs composite

The UV-vis transmittance spectra of the PUs composite with different DP of treated CNF are shown in Figure 4.4. It shows that the transparency of all the PUs composites is good in the visible light range even when the treated CNF content is as high as 20 wt%. Table 4.4 (approximate thickness: 5 mm) show the optical properties of PUs composite in visible light transmission at 660 nm. All PUs composite with different DP of treated CNF possess good visible light transmittance and slightly decrease compared to the PU BD.

Table 4.4: Optical properties of PU BD and PUs composite

Sample	Thickness (mm)	%Transmittance (660 nm)
PU BD	0.433	87.7
PU FMa 20%	0.503	67.9
PU WFo 20%	0.504	57.1
PU IMa 20%	0.533	61.1

SEM images of the fractured PUs composite sample are shown in Figure 4.5. The PU BD fractures have a smooth surface, revealing the low resistance to the propagation of cracks. The PU FMa-P 20%, PU WFo-P 20% and PU IMa-P 20% observed similar trends and features. These samples presented fracture regions with a large amount of roughness with different profiles compared to PU BD, which is associated with modified CNF within the PUs Matrix (red circles). Better compatibilization between the modified CNF and the PUs matrix might be attributed to the enhanced tensile strength of PUs. This also allows stress to efficiently transfer from the matrix to the reinforcing phase, resulting in the better mechanical strength of the PUs [141].
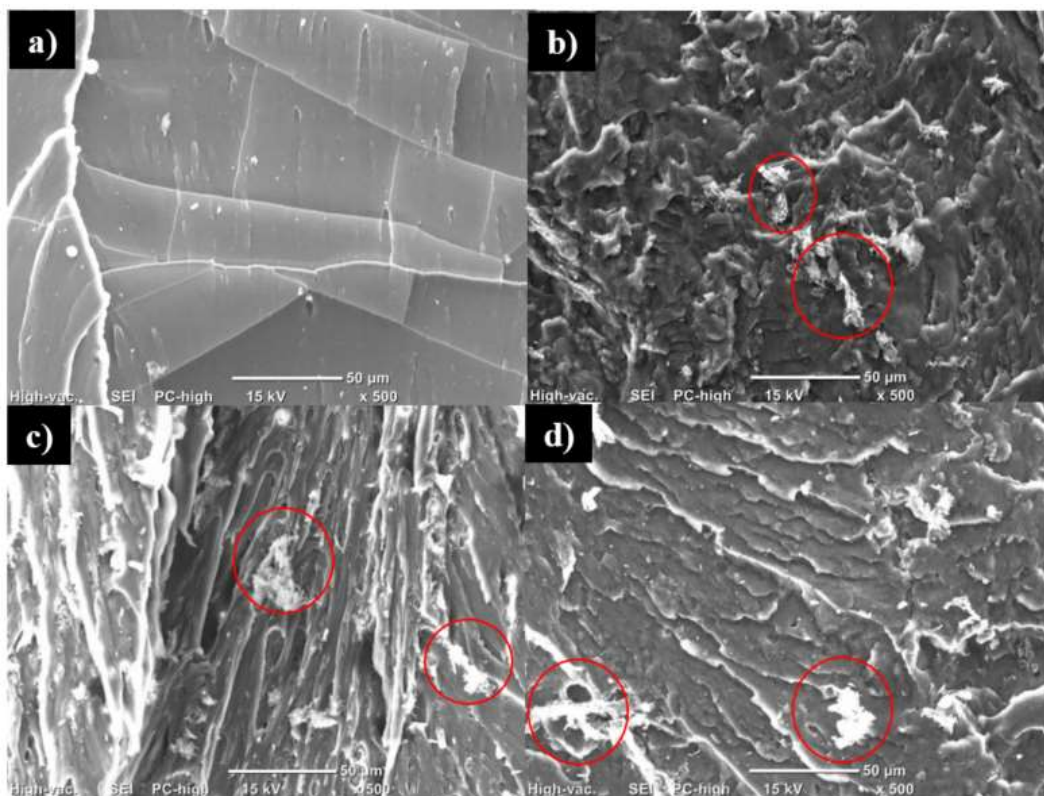
Figure 4.5: SEM images of the fractured surface of the PUs; (a) PU BD, (b) PU FMa-P 20%, (c) PU WFo-P 20%, and (d) PU IMa-P 20%

4.4.2 Chemical structures of the PUs composite

As shown in Figure 4.6a, 4.6b, and 4.6c, the chemical structures of PUs composite with different DP and percentage of modified CNF, and PU BD as reference have been investigated using FT-IR spectroscopy. The presence of urethane linkages was observed at 3330-3315 cm^{-1} of the NH stretching and bending vibration absorptions, indicating the polymerisation reaction occurred to form a urethane group, and a PUs successfully was obtained. The disappearance of isocyanate bond (-NCO) was observed at wavenumber approximately 2250 cm^{-1}, demonstrated that the diisocyanate was completely reacted with PTMO and modified CNF [151]. The characteristic absorptions peaks of the PUs series were observed at 2925-2850 cm^{-1} for CH$_2$ and CH$_3$ stretching [152][153]. The peak at 1100 cm^{-1} was C–O–C stretching vibration of PTMO [153]. Furthermore, C-H bond at 1524 cm^{-1} for PU BD [83] and shifted C-H bond was identified at 1550 cm^{-1} for all sample PUs composite which is PU FMa-P, PU WFo-P and PU IMa-P. The carbonyl C=O stretching peak of urethane appeared at approximately 1700 cm^{-1} for PU BD. The new C=O stretch peak arose from the urethane bonding was observed at 1630 cm^{-1} for all sample PU FMa-P, PU WFo-P and PU IMa-P. This C=O group is possibly a reaction of the hydroxyl group of modified CNF and isocyanate group in PUs composite [180]. The absorption peaks in the range 1094-1043 cm^{-1} are due to the C-O-C bond was observed in PU BD. However, all sample PU FMa-P, PU WFo-P and PU IMa-P is shifted C-O-C peak was observed at 1135cm^{-1}. The CH and CH$_2$ stretching band in PUs composite series were observed at peak 1375 and 1325 cm^{-1}, respectively [143].

a)
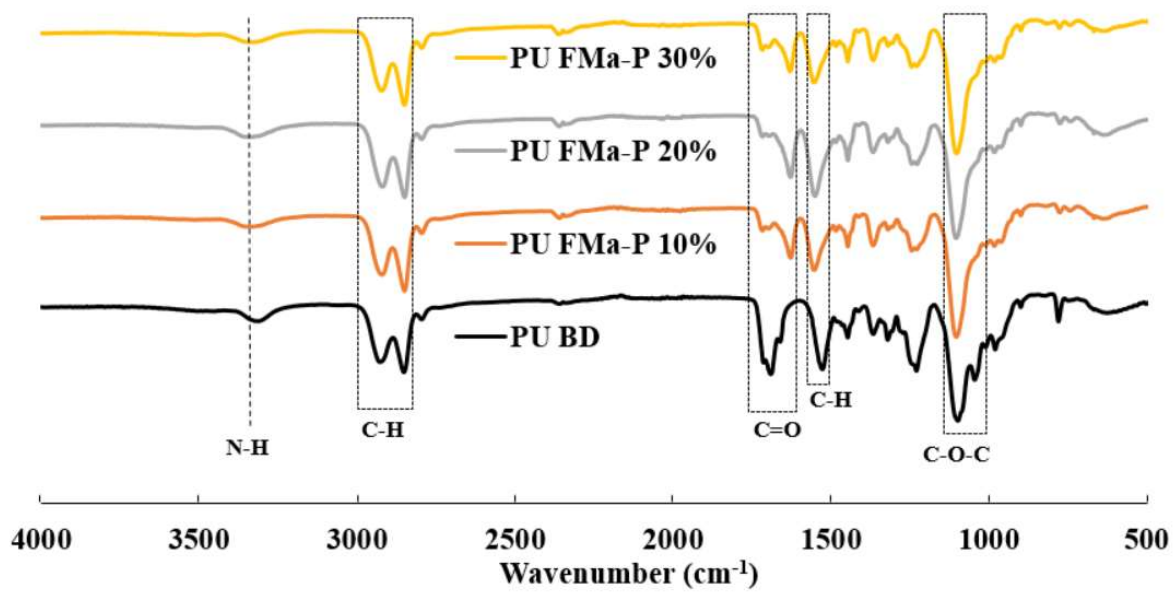
b)
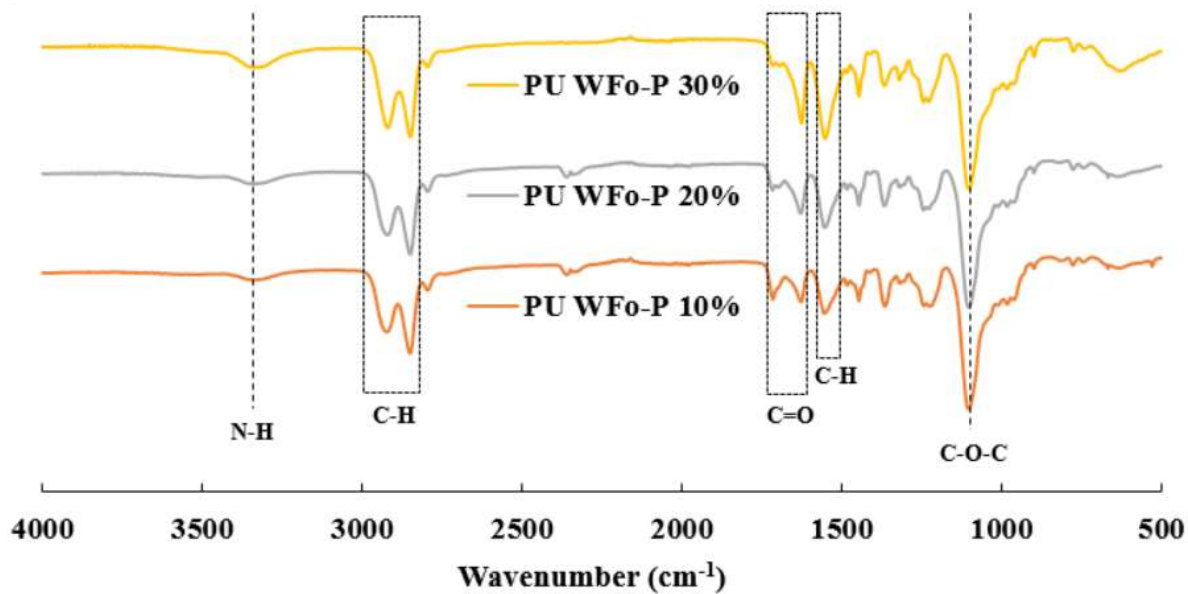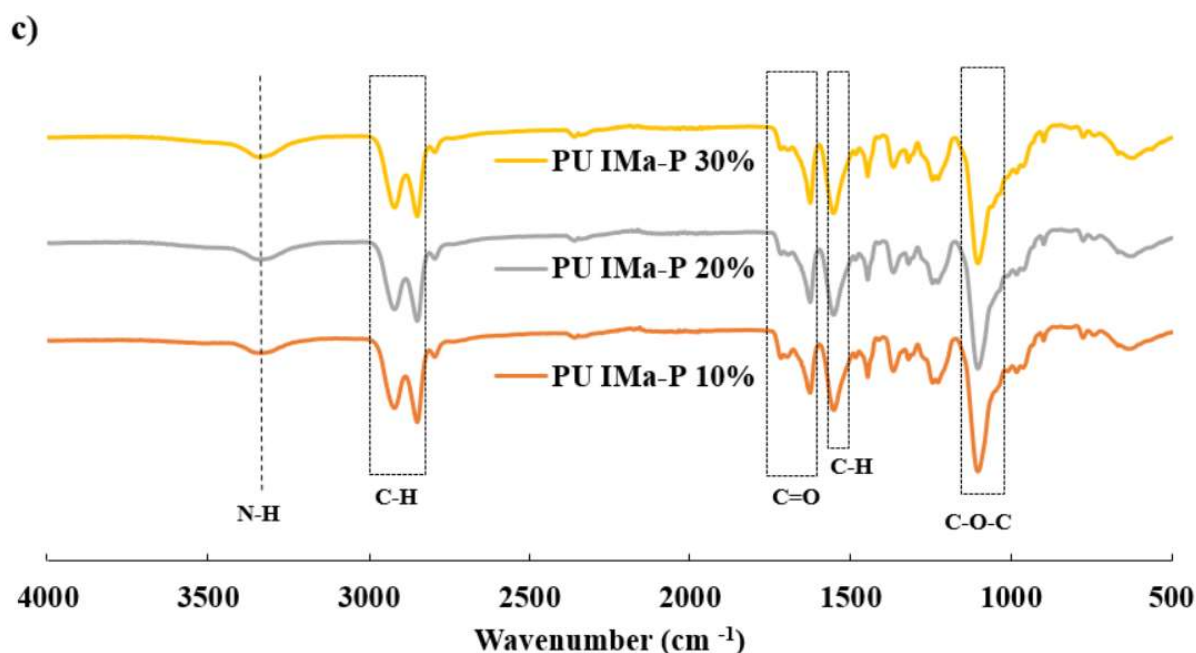
Figure 4.6: FT-IR spectra of PU BD and PUs composite with different DP and percentage of modified CNF; (a) PUs composite with modified FMa CNF, (b) PUs composite with modified WFo CNF, and (c) PUs composite with modified IMa CNF.

4.4.3   Mechanical properties of the PUs composite series

The enhancement of modified CNF on the property of PUs composite can be further demonstrated via tensile testing. The mechanical properties of PUs composite with modified CNF was compared with PUs composite with CNF (untreated), and PU BD is shown in Table 4.5 and Table 4.6. In general, the PU BD exhibited a weak and soft rubbery material with the ultimate tensile stress and elongation values of 5.76 MPa and 89.42%, respectively. Surface functionalisation has been applied to improve the wettability of the CNF surface, consequently increases the interfacial interaction between the PUs composite and CNF components and dispersion [181]. For PUs composite series with CNF, tensile strength is not significantly different from other CNF with

different DP, and the value is between 28.1-19.5 Mpa. CNF through surface modification using the phosphoric acid was shown to increases the tensile strength of the PUs composite. The highest value was achieved with 51.5 MPa for PU WFo-P 20% and followed by 48.8 MPa for PU WFo-P 30%, 40 MPa for PU FMa-P 10% and 37.2 MPa for PU IMa-P 10%. The PUs composite with modified CNF may have some cross-linkage points to assist the compatibility [175] since the composites showed high specific strength and tensile strength.

The Young`s modulus of the composite PUs is significantly improved with the modified CNF content embedded in the PUs composite (Table 4.5 and 4.6). PUs composite with pristine CNF, Young`s modulus is between 0.019-0.065 GPa. Meanwhile, for PUs composite with modified CNF, the value is around 0.049-0.165 GPa, and PU BD as a control PU shows the lowest, which is 0.020 GPa. The improvement in tensile strength and Young`s modulus indicates strong interfacial adhesion between filler and matrices. The elongation at break of the PUs composites increased with pristine NFC as similar to PU BD might be predominant to the backbone of PUs due to agglomeration occurred. The highest values were achieved with PU FMa 30% (697%) with pristine NFC. Contrary, the highest value of elongation at break of PUs composite with modified CNFs showed 363.9% with PU WFo-P 20%. Different DP of CNF was also influenced on the elongation of the PUs composite. As the concentration of the CNF increases to the maximum level, the PUs composite becomes more brittle because of surface adhesion reduced between filler and composite. For the strain energy, the highest value was indicated on PU FMa 30% which is 111.1 J/m^3 and followed with the composite PU WFo-P 20% which is 104.1 J/m^3.

Table 4.5: Mechanical properties of PU BD and PUs composite series with different DP and percentage of CNF.

Sample	Tensile strength (MPa)	Young`s Modulus (GPa)	Elongation (%)	Strain energy (J/m3)
PU BD	5.76	0.020	89.42	2.85
PU FMa 10%	28.1	0.042	317.4	56.1
PU FMa 20%	21.7	0.058	150.5	33.2
PU FMa 30%	27.2	0.025	697.3	111.1
PU WFo 10%	20.7	0.021	582.7	78.0
PU WFo 20%	25.2	0.046	515.6	84.3
PU WFo 30%	23.9	0.027	427.1	83.2
PU IMa 10%	19.5	0.042	455.6	60.4
PU IMa 20%	25.4	0.065	172.9	34.8
PU IMa 30%	10.0	0.043	68.8	12.5

Table 4.6: Mechanical properties of PUs composite series with different DP and percentage of modified CNF.

Sample	Tensile strength (MPa)	Young`s Modulus (GPa)	Elongation (%)	Strain energy (J/m^3)
PU FMa-P 10%	40.0	0.120	313.2	82.63
PU FMa-P 20%	28.7	0.165	175.9	34.93
PU FMa-P 30%	21.3	0.045	159.1	20.46
PU WFo-P 10%	33.4	0.034	344.4	72.54
PU WFo-P 20%	51.5	0.049	363.9	104.1
PU WFo-P 30%	48.8	0.122	239.2	100.0
PU IMa-P 10%	37.2	0.091	345.9	80.33
PU IMa-P 20%	30.7	0.121	127.9	25.08
PU IMa-P 30%	22.1	0.051	175.6	35.69

4.4.4 Thermal decomposition of the PUs composite

To investigate the thermal behaviour of PUs composite, TGA and DTG analysis was carried out, and their thermograms were shown in Figure 4.7. The thermal decomposition parameters determined from the thermograms were further summarised in Table 4.7. As can be seen, all samples exhibited two degradation stages, indicating that the diisocyanate polymerised with PTMO and modified CNF to form PUs. The first stage of the decomposition is attributed to the breakage of the urethane bonds. The decomposition leads to the formation of primary amine and olefin or the formation of secondary amine and carbon dioxide [157]. The second stage of weight loss has been associated with soft segment decomposition of ester groups [158]. Furthermore, it has been suggested that the amount of weight loss at each degradation stage may be used as a quantitative measurement of the hard and soft content in the PUs composite. The hard segments are less thermally stable, and that their degradation stage depending on the isocyanate properties [182]. Besides, incorporating modified CNF into PUs composite improves their thermal stability as the dispersed CNF layers hinder the permeability of volatile degradation products out of the materials. This enhancement can be observed on PUs composite series as compared to PU BD.
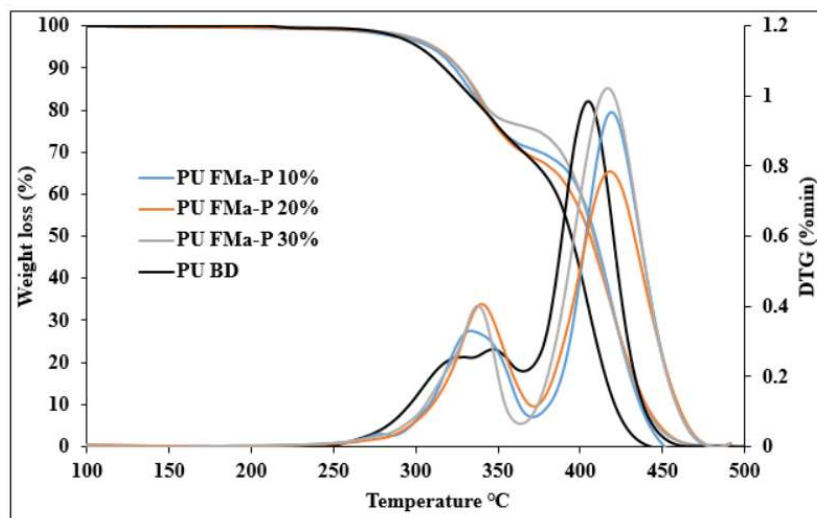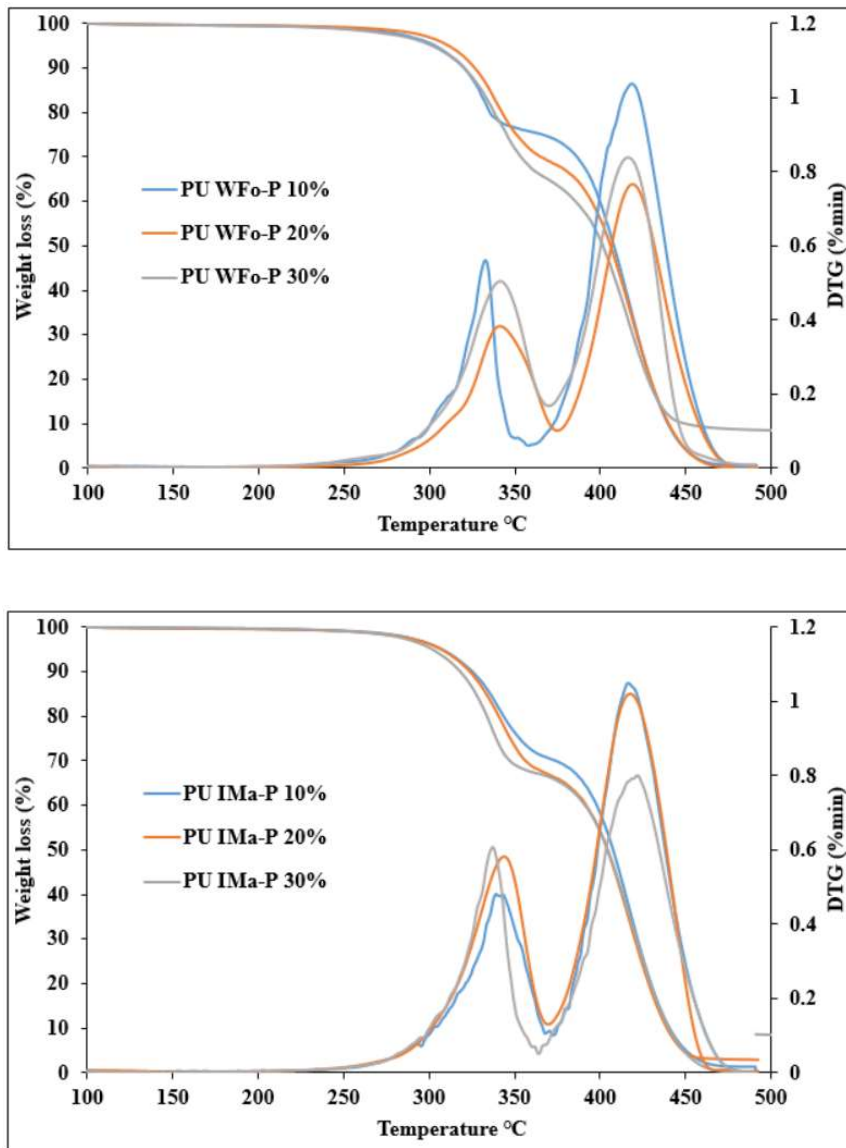
Figure 4.7: The TGA and DTG of PU BD, and PUs composite with different DP and percentage of modified CNF; (a) PUs composite with modified FMa CNF, (b) PUs composite with modified WFo CNF, and (c) PUs composite with modified IMa CNF

The initial temperature (T_{onset}) was calculated from DTG curves in Figure 4.7 to access the decomposition temperature and degradation dynamics. The decomposition process of PU BD occurred at 301.8 °C while all samples PUs composite series decomposition occurred at

around 303.3 °C - 311.2 °C (Table 4.7). The rate of weight loss was further analysed from the DTG curves to obtain the T_{max} values. The T_{max1} and T_{max2} of the PUs can be defined as the maximum temperature rate for the decomposition of PUs rigid segments and soft segments [161]. Based on the result in Table 4.7, the highest T_{max1} value was observed in PU BD, which is 351.1 °C. However, for PUs composite, T_{max1} value of PUs composite decreased with higher CNF loading. On the contrary, for PU WFo-P series with higher loading of CNF, T_{max1} value is horizontally increased. This might occur due to the presence of phosphorus atom on the surface of modified CNF (DP 650), and strong hydrogen bonding between modified CNF and urethane linkages. These results agreed with the mechanical properties, which is a higher density of urethane linkages, leading to more thermally stable PUs and higher mechanical properties [164][183]. On the other hand, higher loading of modified CNF may interrupt the crosslinked network in the hard segment of the PUs composite. The T_{max2} values for all the PUs composite were possessed almost similar decomposition temperature ranging from 420.3 °C to 422.9 °C as compared to PU BD (406.4 °C). Additionally, the weight residue at 500°C of the composite shows the highest on PU WFo-P 30% which is 8.49% followed by 2.9% residue of PU IMa-P 20% and 1.30% residue of PU IMa-P 10%.

Table 4.7: The decomposition temperature of PU BD, PUs composite series at 10 °C min^{-1} in nitrogen

Samples				Residue at 500 °C
	T_{onset} (°C)	T_{max1} (°C)	T_{max2} (°C)	(wt%)
PU BD	303.8	351.1	406.4	0.00
PU FMa-P 10%	308.6	334.8	423.3	0.00
PU FMa-P 20%	309.2	342.5	420.2	0.083
PU FMa-P 30%	310.9	338.4	422.3	0.29
PU WFo-P 10%	303.3	333.0	422.9	0.62
PU WFo-P 20%	311.2	343.3	421.1	0.08
PU WFo-P 30%	309.5	345.1	420.3	8.49
PU IMa-P 10%	307.6	339.5	422.7	1.30
PU IMa-P 20%	307.2	345.0	421.7	2.9
PU IMa-P 30%	304.0	338.2	422.2	0.14

4.4.5 Wide-angle X-ray diffraction (WAXD) analysis of the PUs composite

Wide-angle X-ray diffraction was carried out to identify the crystalline structure of PU BD and PUs composite. Generally, the phase separation between soft segments and hard segments in PUs occurred due to their relative material, structural regularity, and thermodynamic incompatibility [165], [166]. Figure 4.8 shows a different DP on the WAXD profiles of PU BD and PUs composite. The PU BD showed a sharp diffraction peak appearing at $2\theta = 20.64°$. Meanwhile, the peak for composite PU FMa-P 20%, PU WFo-P 20% and PU IMa-P 20% were also observed at $2\theta = 19.98°$, 19.46° and 19.56°, respectively.

Generally, the higher the intensity of the diffraction peaks, the higher the crystallinity in the polyurethane [171]. Therefore, the crystallinity of PUs composites was higher than the PU BD.

In this trend, low DP of modified CNF was induced higher crystallinity to PU composites. Since the reduction of the crystalline structure is due to the short-range ordering in the hard segment domains of PUs [169][167][168], The high DP of CNF causes a reduction of hydrogen bonding due to crosslinking with soft segments. The WAXD spectra profiles also corroborated the findings by Trovati *et al.* [158], which indicated that the PU BD and PUs composite series with modified CNF were soft PUs.
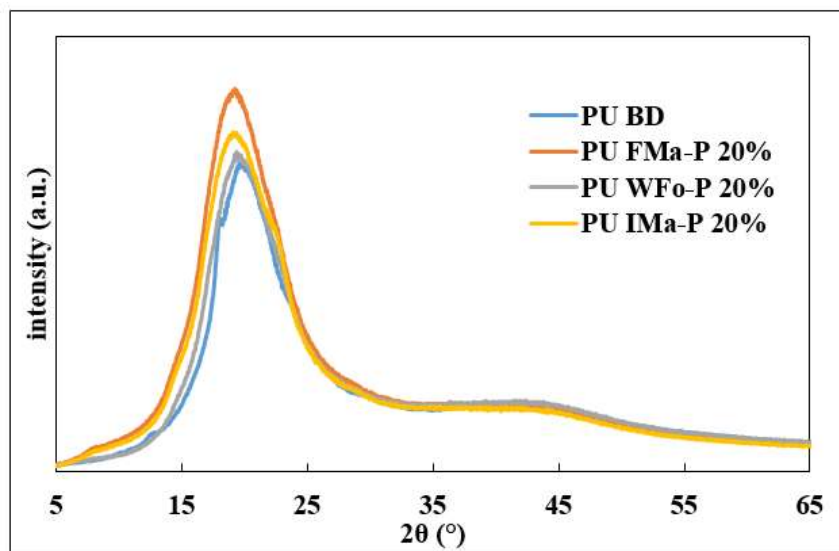
Figure 4.8: WAXD patterns of the PU BD and PUs composite series with different DP and percentage of modified CNF

4.4.6   Swelling behaviour of the PUs composite in a chemical solvent

Swelling behaviour of the PUs composite (PU WFo-20%) based on higher mechanical properties was investigated in a polar and non-polar solvent, which is methanol, ethanol, DMSO, DMF, hexane, and chloroform. The sample was immersed in dedicated solvents and was observed for 24 hours. Figure 4.9 shows the picture of PUs composite in various solvent was taken form 0 hours, 12 hours and 24 hours. Generally, polymers do not dissolve instantaneously, and dissolution is

controlled by either the disentanglement of the polymer chains or by the diffusion of the chains through a boundary layer adjacent to the polymer-solvent interface [184]. After 12 hours of observation, the PUs composite starts swelling in ethanol, methanol, and chloroform, but not in hexane, DMSO and DMF. When solvent diffuses into the PUs, a gel-like swollen layer is formed along with two separate interfaces, and this behaviour can be observed after 24 hours of composite PUs immersed in the dedicated solvent. The PUs composite is partially dissolved in ethanol and methanol but maintains swelling in the chloroform. However, PUs composite does not swell in hexane, DMSO and DMF after 24 hours immersed in the solvent.
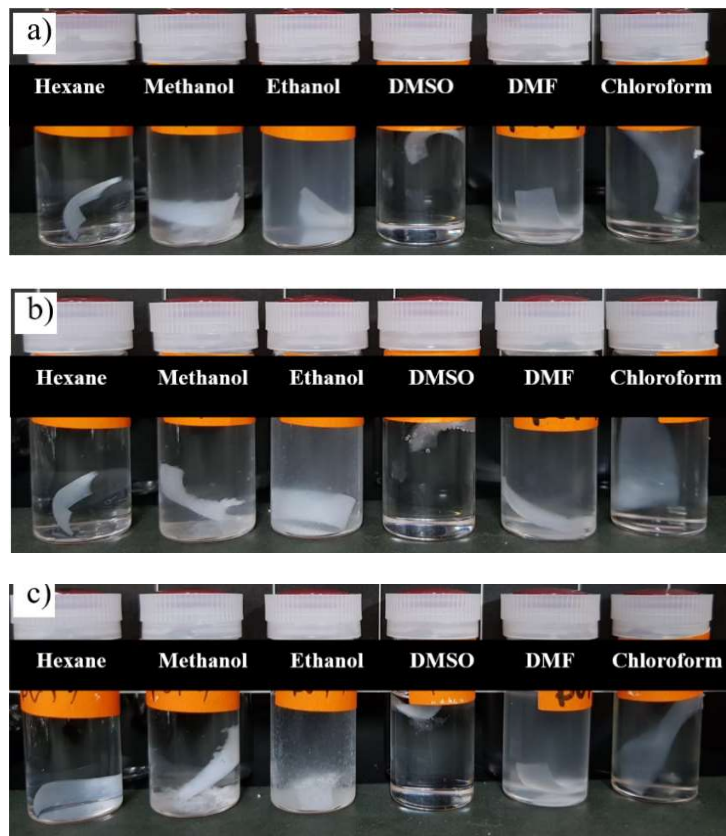
Figure 4.9: Image of swelling behaviour of PU WFo-P 20% in a various solvent; (a) 0 hours, (b) 12 hours, and (c) 24 hours

4.4.7   UV resistant of PUs composite

To evaluate the effect of the UV degradation of the PUs composite, the PU WFo-P 20% sample was exposed to well-controlled, accelerated UV environments and compared to PU BD and commercial aromatic based-PUs (Simpact™ 85A). Figure 4.10 shows the image of PU BD, PU WFo-P 20%, and Simpact™ 85A after 192 hours exposure to UV light. Aromatic based-PUs are more susceptible to UV degradation than aliphatic based-PUs [185]. The first indication is discolouration or yellowing on the surface when a PUs starts to degrade due to UV exposure. This behaviour can be observed on the commercial PUs in Figure 4.10c, which form yellowing after 48 hours exposure and continuing until 192 hours later. The yellowing is caused by the oxidation reaction in the backbone of the PUs. Irradiation affected the physical and chemical properties of the PUs surface and caused yellowish and degradation [186].
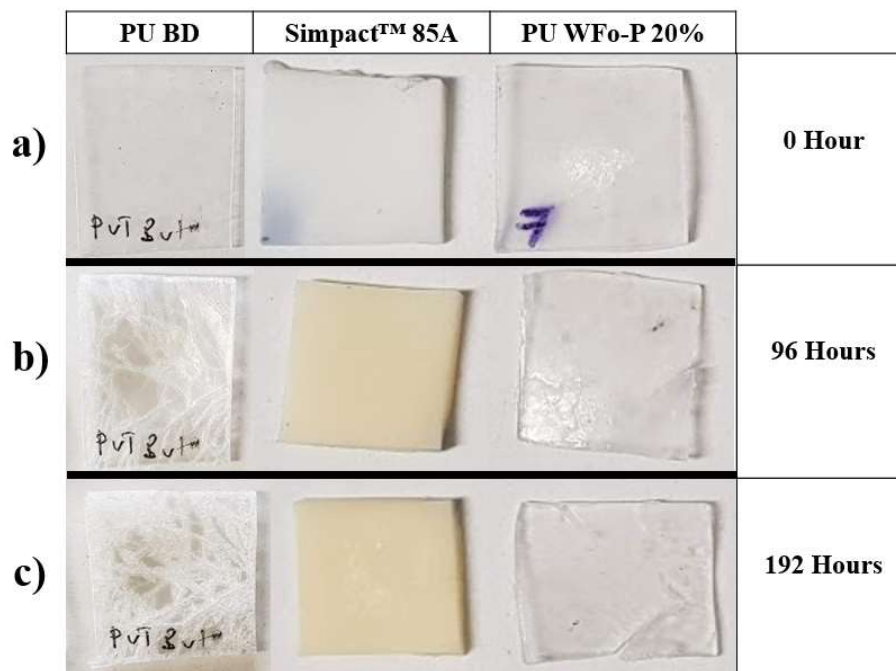
Figure 4.10: Images of PU BD, Simpact™ 85A, and PU WFo-P 20% samples before and after UV exposure. (a) 0 hour of UV exposure, (b) 96 Hours of UV exposure, and (c) 192 Hours of UV exposure

Comparing to commercial PUs, aliphatic based-PUs not yellowish after UV exposure. However, physical properties, such as colour, gloss, adhesion, are also affected negatively on sample PU BD and PU WFo-P 20% after 96 and 192 hours UV exposure (Figure 4.10b and 4.10c). The PUs becomes brittle, and cracks are formed at the sample surface. Influences of the modified CNF in the PUs composite (PU WFo-P 20%) improved the anti-yellowing property and inhibited the micro-crack formation of PUs as compared to the Simpact™ 85A and PU BD.
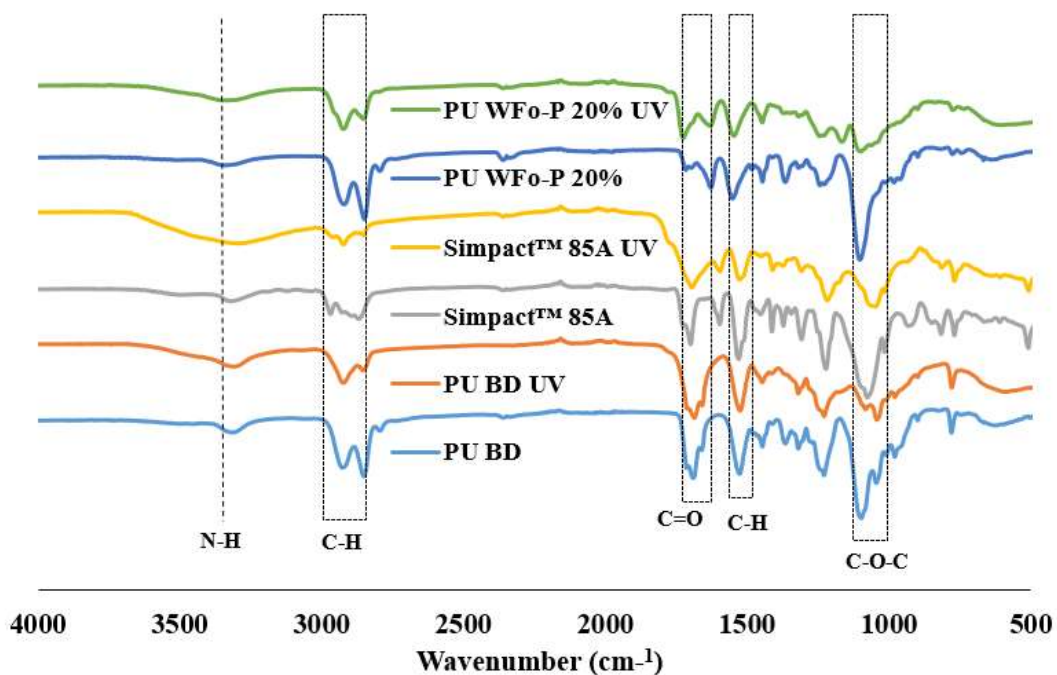
Figure 4.11: FT-IR spectra of PU BD, Simpact™ 85A and PU WFo-P 20% after and before UV exposure

The commercial PUs, PU BD and PU WFo-P 20% were further investigated using FT-IR spectroscopy to apprehend the effect changes in the chemical structure of PUs after UV exposure. As shown in Figure 4.11, FT-IR spectra are all the PUs before and after 8 days of UV exposure. The absence of the band at 2250 cm^{-1} is due to the complete consumption of isocyanate groups

and PUs were successfully obtained. The characteristic peaks of the PUs were observed at 2925-2850 cm^{-1} for CH$_2$ and CH$_3$ stretching, respectively [152][153]. The carbonyl group stretching vibrations related to the urethane and urea linkages, in the vibrational range 1625–1720 cm^{-1}. Furthermore, the urethane domains were also observed at peaks 3315 cm^{-1} attributed to the N-H stretching and bending vibration bands. After 8 days of UV exposure, PU BD UV and PU WFo-P 20% UV show the decreasing absorption C-O-C peaks at 1094 cm^{-1}, and 1100 cm^{-1}, respectively. These decreasing peaks have also been observed for sample Simpact™ 85A UV at 1047 cm^{-1}, and peak at 1522 cm^{-1} gradually decreases, which indicates a degradation of the urethane structure may occur. Besides, missing absorption peaks were observed at 2826 cm^{-1} after UV exposure revealed the photochemical decomposition of the PUs. Increasing absorption peaks carbonyl groups at 1723 cm^{-1} was observed on PU WFo-P 20% sample, due to hydroxyl groups of modified CNF is oxidized by the UV [178]. The degradation may occur in sample PU WFo-P 20% and become unstable and might reduce the performance of PUs. Modified CNF was confirm reduced the yellowish and micro crack formation in PUs composite compared to other reference PUs. However, the mechanical properties of the PUs composite may be affected.

4.5 Conclusion

Different DP of CNF was treated using phosphoric acid and was successfully incorporated in the polymerisation of PUs in acetone solvent. The morphological of PUs composite with modified CNF showed that a relatively good dispersion was achieved as no modified CNF aggregations were invisible, indicating that the modified CNF has good dispersibility in PUs composite. The FT-IR result shows chemical bonding between the hydroxyl group of modified CNF and isocyanate group in PUs composite. Modified CNF has confirmed the enhancement of the

mechanical properties in PUs composite as compared to untreated acid CNF and PU BD. From their thermal behaviour, PUs composite with modified CNF showed higher thermal stability than PU BD. Hence, modified CNF can be used to replace BD and further enhanced PUs performance in terms of their mechanical properties, thermal stability, and as the UV-resistance. As a result, the PUs composite prepared on this method is good on mechanical properties, and it can be a substitute for replacing aromatic PUs. It also a promising alternative material for outdoor and waterproof coating, thermal insulation film for glass windows, powder coatings, and biomedical applications.

CHAPTER 5

The Design of Dry CNF Filler by Hybridization with Silica Particle for Moulded Polypropylene Composite

Abstract

Silica/CNF as a hybrid filler was successfully prepared using ethanol/water mixed solvents at room temperature without a catalyst. The method was applied in this study is convenient, less energy required and time-saving. Polypropylene (PP) as a polymer matrix was melt blending using a twin-screw extruder to study the dispersion of filler in the composite. The morphology, chemical structure, mechanical properties and thermal stability of the prepared composites were investigated by scanning electron microscopy (SEM), Fourier transform infrared (FT-IR) spectroscope, tensile testing and thermogravimetric analysis (TGA). The image was obtained from SEM showed that the silica nanoparticles were deposited onto surface CNF fibres. All the PP composites sample showed good dispersion rate and strong adhesion between the filler and the PP matrix. The FT-IR shows the chemically bonding between the filler and PP composite. Incorporation of filler into the PP matrix significantly increase the mechanical properties on the composite. However, elongation sharply reduced due to the stiffening effect of filler. Silica as a filler also improves the thermal stability of the PP composite.

5.1 Introduction

Polymer composite is the material formed when the reinforcing materials are dispersed in the polymer matrix. Incorporating inorganic fillers into a polymer matrix can give unique composite properties, such as rigidity, high thermal stability and mechanical property, flexibility, and ductility [45]. The mechanical properties of polymers are regularly low, and fillers can provide overcoming this limitation. The most used nanoscale fillers include metal nanoparticles, polyhedral oligomeric silsesquioxane, carbon nanomaterials, graphite nanoplates, silica nanoparticles, and nanocellulose [187][188][189]. These fillers shape factor can be a particle, fibre, and sheet [190]. The reinforcing effect of filler is attributed to several factors, such as polymer properties, filler nature and type, polymer and filler concentration, particle size and distribution [45]. The fillers with particle sizes in the 1–100 nm range define as a nanofiller. These nanofillers incorporated into a polymer matrix can improve their mechanical properties, gas and solvents barrier properties, thermal degradation, and chemical resistance [191][192]. Traditional micro fillers can cause polymer embrittlement, loss of transparency and lightweight.

Natural fibres as a filler such as cellulose fibre produce composites that offer advantages, for example, superior mechanical properties, eco-friendly, processability, biodegradability, biocompatibility, low toxicity, cost-saving, and improved fuel efficiency [193][194]. The natural filler is difficult to disperse properly in hydrophobic polymer due to different surface properties. The strategy is using hybrid nanofillers with different surface properties such as silica nanoparticles is an effective way to achieve better mechanical and thermal properties of composites.

Researchers are trying to utilize more than one filler materials to explore the nanofillers synergistic effect on the final properties of polymer nanocomposites [49]. Anwer *et al.*[195] prepared nanocomposites using epoxy resin with carbon nanofibre (CNF), graphene nanoplatelets (GNP), and a hybrid combination of CNF/GNP as fillers. These composites were processed with and without the use of surfactants. It was proposed the GNP prevented agglomeration of the CNF during processing, leading to larger particle aspect ratios in the nanocomposite. Kwak *et al.*[196] successfully prevented the agglomeration of the CNF during dehydration using fish-derived gelatine. Both of these studies show combinations with other material is possible to prevent the agglomeration of CNF using physical modification without the use of surfactants. In a hybrid filler system, both fillers support the dispersion of one another and avoid the agglomeration on some level. Thomas *et al.* [197] study hybrid filler of carbon nanotube (CNT) and nano clay in nitrile rubber /natural rubber blends. The hybrid filler CNT/clay helps the dispersion of one another through synergism and prevents the agglomeration in the composite blend. Moreover, a hybrid filler system has reinforced mechanical properties such as tensile strength and tears resistance which are attributed to the large contact area between clay and CNT.

Few studies have been done to synthesized silica/cellulose as filler, and this hybrids filler usually were prepared by the sol-gel method application. Li *et al.* [198] synthesized cellulose nanocrystal/silica hybrids using TEOS as the silica precursor. This hybrids material was melt blending with ultrahigh molecular weight polyethylene (UHMWPE) polymer in the twin-screw extruder. The nanocomposite shows the improvement of flexural modulus, tensile and flexural strength. The sol-gel method is considered adequate to modify the surface of substrates or material. However, the limitation of this is method is energy demanding, costly chemical, and a time-

consuming cause needs days to obtain the product, volume shrinkage, and cracking during drying [190][199].

To obtain nanocomposite materials by an accessible, fast, and low-cost method, we attempted a new approach using ethanol/water mixed solvent method applied to silica particles/CNF without chemical modification. During this process, commercialized silica particles (SiP) and CNF will be dispersed in the mixed solvent, and SiP will be deposited onto the CNF surface. During the solvent evaporation process, it was expected that the property of the particle of this SiP could prevent the agglomeration of CNF. Before this method, it was impossible to incorporate cellulose particles into hydrophobic polymers without surfactants or chemical modifications [190].

In this study, polypropylene was used as a polymer matrix due to excellent properties as common applications [200]. Filler preparation using ethanol/water mixed solvents were investigated their morphological and structural properties. Subsequently, the composite preparation with polypropylene, fillers (SiP, CNF, or SiP/CNF) by melt blending in the twin-screw extruder. The effect of fillers on PP composites was investigated by morphological, chemical analysis, thermal degradation, and mechanical properties. Pulverized SiP and pulverized CNF as filler in PP composite have also investigated their performance on mechanical properties.

5.2 Experimental

5.2.1 Material

Polypropylene was used as the polymer matrix obtained from Japan Polypropylene Corporation, Japan. Cellulose nanofibre (5 wt% aqueous solutions, DP 650) was kindly provided from Sugino Machine Limited, Toyama Prefecture, Japan. This CNF was produced by a super high-pressure water jet system. SiP powders, Sylosphere 200 (SS, diameter 3.0μm), and Sylophobic 200 (SP, diameter 3.9μm) were obtained from Fuji Silysia Chemical, respectively. All other reagent-grade chemicals were purchased from Wako Pure Chemical Industries Ltd, Japan, and were used without further purification.

5.2.2 Filler preparation procedure

The prepared filler and hybrid filler samples in this study were coded, as demonstrated in Table 5.2. The required amount of SiP and CNF was added into the ethanol/water mixed solvents and stirred for one hour. The mixture was then evaporated by using a rotary evaporator (Eyela N-1110, Tokyo Rikakiki Co. Ltd., Tokyo, Japan). Subsequently, it was dried under vacuum overnight, before use.

5.2.2.1 Preparation of pulverized SiP and pulverized CNF

The pulverized SiP and pulverized CNF as reference filler were prepared by the wet-pulverizing using Star Burst Mini (Nozzle size: 0.10 mm, Sugino, Japan) using ethanol as a solvent. Then, the solvent was evaporated using a rotary evaporator and dried under vacuum overnight. Pulverized SiP and pulverized CNF and namely as pul.SS (Sylosphere 200), pul.SP (Sylophobic 200) and pul.CNF.

Table 5.1: Sample composition of PP and filler

Sample	PP (wt%)	Sylosphere (wt%)	Sylophobic (wt%)	CNF (wt%)
PP	100	-	-	-
PP-8.75 SS	91.25	8.75	-	-
PP-8.75 pul.SS	91.25	8.75	-	-
PP-10 SS	90	10	-	-
PP-1.25 CNF	98.75	-	-	1.25
PP-1.25 pul.CNF	98.75	-	-	1.25
PP-pul.SS/CNF	90	8.75	-	1.25
PP-pul(SS/CNF)	90	8.75	-	1.25
PP- SS/CNF	90	8.75	-	1.25
PP-8.75 SP	91.25	-	8.75	-
PP-8.75 pul.SP	91.25	-	8.75	-
PP-10 SP	90	-	10	-
PP-pul.SP/CNF	90	-	8.75	1.25
PP-pul(SP/CNF)	90	-	8.75	1.25
PP- SP/CNF	90	-	8.75	1.25

5.2.3   Composite preparation

5.2.3.1   Twin-screw extruder

The desired amount of filler, hybrid filler and polymer matrix were feds into the twin-screw extruder (IMC-1979, Imoto Machinery Co., Japan). The rotation speed, temperature, and residence time for melt mixing are controlled at 40 rpm, 180 °C, and 5 minutes, respectively.

5.2.3.2   Preparation of composites film

The films were prepared using a hydraulic hot-press (IMC-180C, Imoto Machinery Co., Japan) at 180 °C for 3 minutes under a pressure of 30MPa, and then cooled at room temperature.

5.3   Characterisation of PP composite

5.3.1   Morphological analysis

The surface morphologies of SiP were observed under a 3D laser scanning confocal microscope (LSCM) model VK-X 100 (Keyence Corporation, Osaka, Japan) under prescribed conditions of laser: red semiconductor laser, λ=658 nm, 0.95 mW, and pulse width of 1 ns using a depth composition procedure.

5.3.2   Scanning electron microscopy (SEM)

The morphology of the fractured composites and dispersion state of the filler in the PP matrix was observed by scanning electron microscopy (SEM) (JCM-6000, JEOL, Japan) operated at 15 kV accelerating voltage. The PP composite samples were fractured under liquid nitrogen. Each sample was deposited on carbon tape and carbon-coated for 90 seconds before the observation.

5.3.3   Optical property

Optical property of the composite films was determined by UV–Vis spectra. A rectangular piece of each film sample (4 cm × 4 cm) was directly mounted between the two spectrophotometer magnetic cell holders. The transmittance spectra of the PP films were measured at selected wavelength ranges from 190 to 1000 nm using a UV–Vis spectrophotometer (GENESYS 50, Thermo Fisher Scientific, USA). The optical properties of PP and PP composite films were characterized by the transmittance of visible (660 nm) regions.

5.3.4 Chemical analysis

The chemical analysis was carried out using the Fourier Transform Infrared (FT-IR) spectroscope Nicolet iD7 ATR (Thermo Fisher Scientific, Japan). Each sample recording consisted of 16 scans recorded from 400 to 4000 cm^{-1}.

5.3.5 Mechanical properties

The PP composite films were cut into a rectangular shape with $40 \times 5 \times 0.5$ mm. The mechanical properties of PP composite were determined by an IMC-18E0 model machine (Imoto Machinery Co. Ltd, Kyoto, Japan) at a rate of 10 mm/min crosshead speed at 23 °C. The measurement was carried out with five replicates.

5.3.6 Thermogravimetric analysis (TGA)

TGA was carried out using EXSTAR TG/DTA 7200 (SII Nanotechnology Inc., Japan) with a scan range from 30 to 550 °C at a constant heating rate of 10 °C /min under a continuous nitrogen flow rate of 100 mL/min.

5.4 Result and Discussion

5.4.1 Silica/CNF filler mechanism in PP polymer

Figure 5.1a and 5.1b show the schematic filler preparation in the ethanol/water mixed solvents and the possible mechanism of hybrid filler in the hydrophobic polymer. Hydrophilic CNF causes irreversible agglomeration during drying, and due to the formation of additional hydrogen bonds between particles, hydrophilic CNF induces aggregation in the non-polar matrix [201]. SiP powder was used to prevent the CNF aggregation from occurring when incorporated into the hydrophobic

polymer. SiP powders, which are Sylosphere 200 (SS) and Sylophobic 200 (SP) with different shapes and surface properties, were used. This two silica was compared and further used in hybrid filler preparation with CNF in ethanol/water mixed solvents. For hybrid filler preparation sample, namely PP-pul.SS/CNF and PP-pul.SP/CNF, SiP powder was prepared in ethanol/water mixed solvent and pulverized. After pulverized, the required amount of CNF was added into the solution and stirred for one hour. Then, the solvent was removed using a rotary evaporator.

Meanwhile, hybrid preparation sample for PP-pul(SS/CNF) and PP-pul(SP/CNF), SiP powder and CNF were prepared in ethanol/water mixed solvent and pulverized. After pulverized, the mixture was continued stirred for one hour. Then the solvent was removed using a rotary evaporator. The hybrid filler preparation for sample PP-SS/CNF and PP-SP/CNF, the required amount of SiP and CNF was added into the ethanol/water mixed solvents and stirred for one hour. The mixture was then evaporated by using a rotary evaporator. All the sample after evaporated was dried under vacuum overnight before use. This ethanol/water mix solvents promote the SiP to deposited onto the surface of the CNF fibre. When the SiP/CNF mixture solvent is evaporated, both fillers will prevent one or both from agglomerated.

As shown in Figure 5.1a, the SiP covered mostly localized at the intersection of the CNF fibres. Interaction between SiP and CNF may be caused by hydrogen bonds, due to the large surface areas and high amount of hydroxyl groups present in SiP [202][203] and figure 5.1b shows the dry CNF is agglomerated without silica. In further to understand the hypothesis mechanism, PP polymer as the polymer matrix was melt blending using a twin-screw extruder. After the composite was melt bending in a twin-screw extruder, the composite was hot press for further analysis. As a result, the

hybrid filler prevented the aggregation formation of CNF in PP composite, and a good dispersion rate and transparency were achieved (Figure 5.1c).
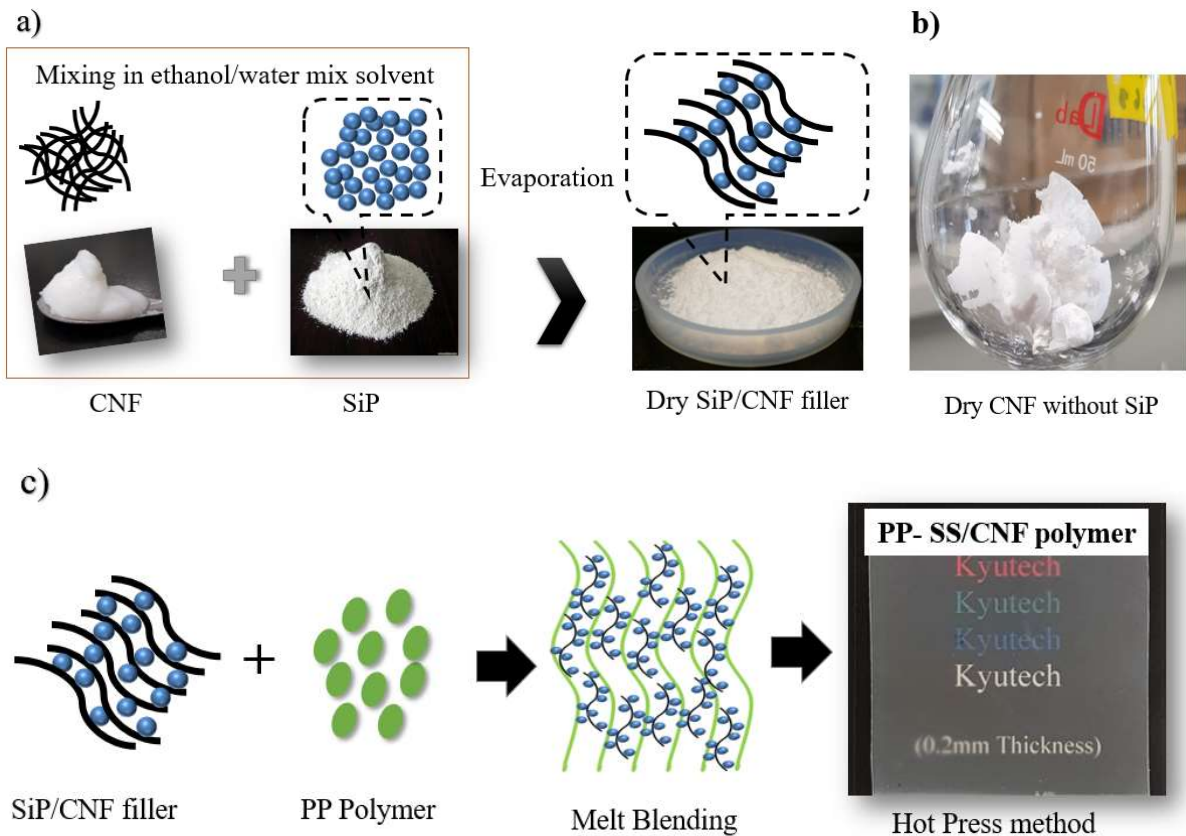
Figure 5.1: Schematic representation of SiP/CNF filler; (a) hybrid filler preparation, (b) agglomerated CNF without SiP and (c) hybrid filler mechanism in PP polymer

5.4.2 Morphological characteristics of the hybrid filler and PP composite

Figures 5.2a and 5.2c are a detailed microscopic view of SiP SS and SP under a laser microscope with 50x magnification. The view sample was done by using scotch tape techniques without using a solvent. SiP SS is single-distributed spherical silica particles and smooth surfaces with average size 3-4 μm giving the features such as high mobility and outstanding dispersivity. Meanwhile, SiP SP has a rough surface and irregular shape with an average size of 2-7 μm. According to the

manufacturer, SiP SP demonstrates completely hydrophobic properties by chemically replacing the silanol groups on the silica surface with organic silicone compounds.
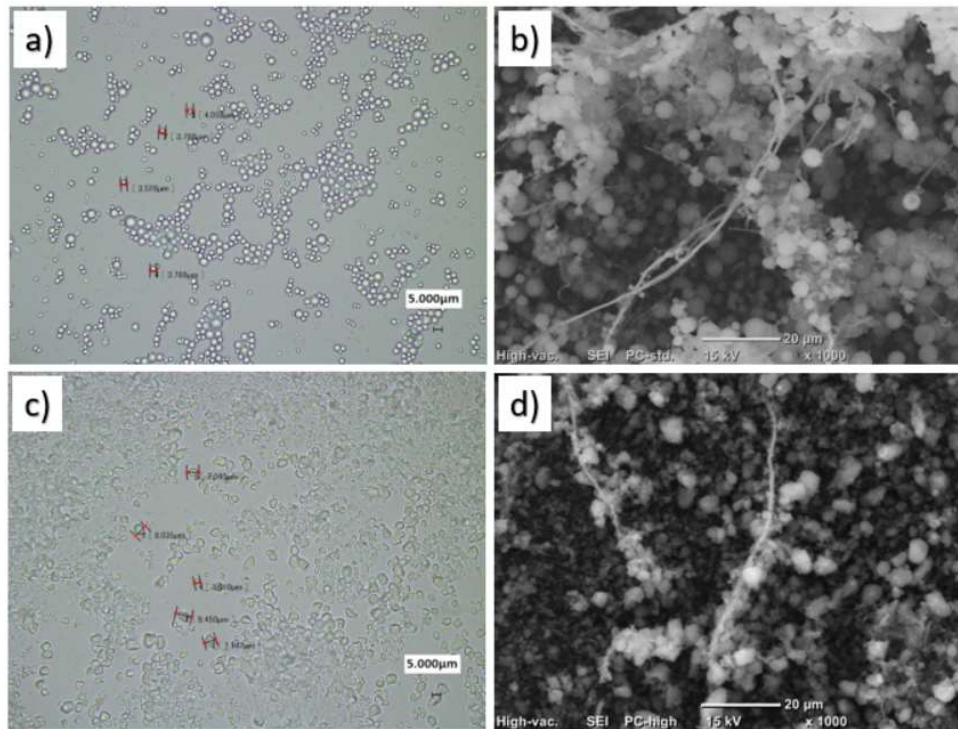
Figure 5.2: Morphological image of SiP particles; (a) SiP SS 50X, (c) SiP SB 50X, and SEM image of hybrid filler; (b) SS/CNF 1000X, (d) SP/CNF 1000X

The structures of both hybrid fillers can be directly observed by using SEM. The SEM images in Figures 5.2b and 5.2d (SS/CNF and SP/CNF) illustrate that the SiP were relatively homogeneously dispersed in the CNF matrix. It was verified that both SiP was deposited predominantly on the surface of CNF fibres and prevent the CNF agglomeration when drying. Both SiP SS and SP help the dispersion of CNF by way of synergism effect and avoid the agglomeration to some degree. This result also indicates that the hybrid filler particles play a very important role in preventing aggregation formation in the polymer matrix.

Figure 5.3: Morphological of PP composite (a) PP, (b) PP-8.75 pul.SS, (c) PP-8.75 pul.SP, (d) PP-1.25 pul.CNF, (e) PP- SS/CNF and (d) PP- SP/CNF

Successful the hybrid nanofiller preparation was further investigated in PP as a polymer matrix. The PP composite was melt blending through a twin-screw extruder. Figure 5.3 shows the PP composite after melt blending and hot press for analyses and mechanical properties study. Neat PP polymer is without SiP, and CNF (Figure 5.3a) was used as a reference. Figure 5.3b and 5.3c is PP composite with SiP SS, and SP as control and Figure 5.3d is PP composite with CNF without SiP. PP composite with SiP show excellent dispersibility, and no agglomeration was observed. However, PP composite with CNF, it clearly can see significant agglomeration or poor dispersion of CNF in PP composite, caused by different surface properties and the hydrophilicity nature of CNF nanofibers. With the right amount and percentage of SiP/CNF content, the PP composite shows the superior distribution of hybrid filler was observed in Figure 5.3e and 5.3f. Archiving

good dispersion of fillers and polymer matrix are the most critical factors to determine their resultant mechanical performances [204].
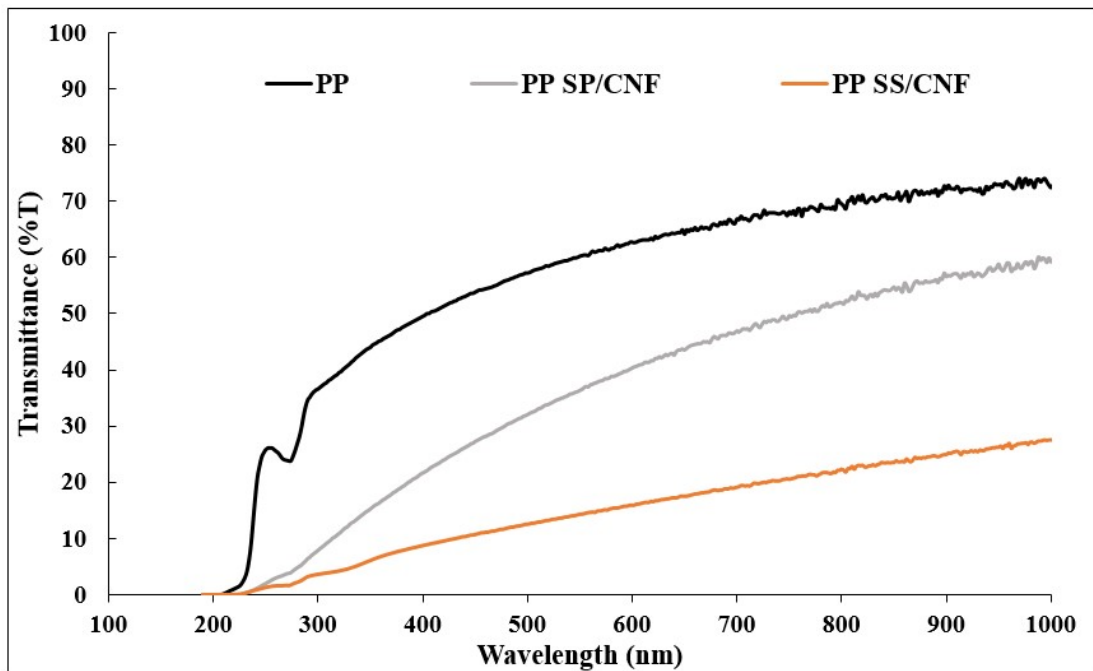
Figure 5.4: UV–vis transmittance spectra for PP and PP composite

Figure 5.4 show the UV-vis transmittance spectra of the PP composite with hybrid filler. The percentage of visible light transmittance values of the PP composite are summarized in Table 5.2. It should be noted that the see-through clarity, as determined by the naked eye, might be different from light transmission measured by an instrument. Based on data given in Table 2, it was found that the transmittance of PP polymer at 65.3 %T and after adding the hybrid filler, the transmittance value is reduced. The percentage transmittance values of the two composite revealed that the PP SP/CNF was higher than the PP SS/CNF, even provided the same hybrid filler loading level.

Table 5.2: Optical properties of PP and PP composite

Sample	Thickness (mm)	%T(Transmittance) (660 nm)
PP	0.255	65.3
PP SS/CNF	0.446	17.9
PP SP/CNF	0.356	44.6

5.4.3 Characterization of composite films

Chemical structures of PP composite were characterized using FT-IR spectroscope. Figure 5.5 depicts the typical FT-IR spectra of neat PP, SiP, CNF, and PP composite. The appearance of characteristic absorption bands of SiP at 1054 and 1048 cm^{-1} is assigned to the siloxane Si–O–Si bonds were observed for SiP SS and SP, respectively. Furthermore, adsorption bands at 794 and 797 cm^{-1} indicate the presence of hydroxyl groups on the surface [205]. The characteristic absorption bands of the CH$_3$ groups for polyalkyl siloxane on the SiP SP as hydrophobic surface treatments were observed at 2966, 2898 and 1392 cm^{-1} [206]. For the CNF, the broad peak was observed at 3400-3300 cm^{-1} was attributed to the stretching vibration of O-H bonding from absorbed water molecules of the cellulose chains. This peak also includes inter- and intra-molecular hydrogen bond vibrations in hydroxyl groups in cellulose I [107][108]. The peak at 2895 cm^{-1} was attributed to the CH stretching vibration of all hydrocarbon constituent in polysaccharides and the peak at 894 cm^{-1} attributed to the ß-glycosidic linkages of the cellulose chain [109].

As shown in Figure 5.5, the peaks at 2950–2835 cm^{-1} were contributed by C–H stretching vibrations in neat PP chains. The absorption peak observed at 2952 cm^{-1} is related to CH$_3$ asymmetric stretching vibration. The peaks found at 1450 and 1376 cm^{-1} were assigned to CH$_2$

and CH$_3$ bending vibration in neat PP [207]. Absorption peaks displayed at 972, 997, and 1165 cm^{-1} are assigned to CH$_3$ rocking vibration. Also, the absorption peak located at 840 cm^{-1} is assigned to C–CH$_3$ stretching vibration [208]. This peak is a typical characteristic of PP polymer. Influencing of the hybrid filler in the PP composites for sample PP SS/CNF and PP SP/CNF were observed at peak at 1087 and 1076 cm^{-1} of the asymmetric vibration of O-Si-O bonds. Besides, increasing the medium intensity were observed at 806 cm^{-1} is stretching vibrations of Si-O. However, The characteristic bonds of the C-O in CNF is not observed due to the overlapping with the O-Si-O band [209].
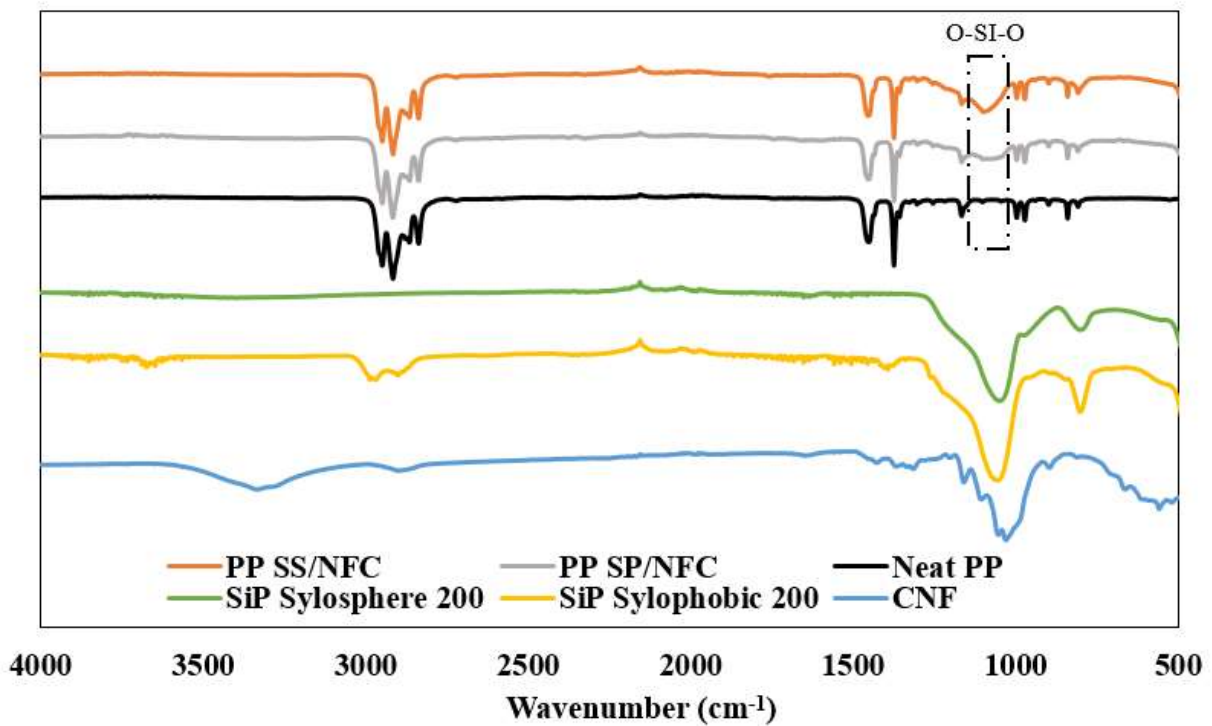
Figure 5.5: FTIR spectra of SiP Sylosphere 200, Sylophobic 200, CNF, and PP composites

5.4.4 Mechanical properties of PP composite

Mechanical properties, precisely tensile strength, and elongation are often used to measure the strength and elasticity of the composite film. Nanoparticles or fillers incorporated into composite films significantly affect their mechanical properties due to the specific surface area and dispersion of the filler. The improved mechanical properties can be achieved through an improved interface between the filler and polymer matrix [210].

Table 5.3 shows the effect of filler properties on the tensile strength of PP composites compares to neat PP. Incorporating the filler increased the tensile strength of PP composites corresponding to the neat PP polymer (21.2 Mpa). The values of the tensile strength of PP composite with SiP as a reference have also been observed. PP composite with SiP SS, PP-8.75 SS, PP-8.75 pul.SS, and PP-10 SS are 27.8, 21.8, and 23.5 MPa. This result shows that the pulverized SiP SS did not influence the tensile strength of the PP composite, and increasing the weight percentage up to 10% of filler also decreased the tensile strength. For Sample SiP SP as filler, pulverized SP also decreased the tensile strength, which is at 26.3 MPa, were observed on sample PP-8.75 pul.SP, as compare to PP-8.75 SP (29.5 MPa). However increasing the weight percentage of SiP SP (PP-10 SP), increased the tensile strength. Besides, the sample PP-1.25 CNF in the composites does not bring much change compared to PP-1.25 pul.CNF. It can be concluded that pulverized CNF in the PP composite does not affect the tensile strength.

The synergism of hybrid filler occurs due to the possibility of bonding between the functional groups of SiP and CNF. This functional group built the interfacial surface compatibility and increased the dispersibility between CNF and PP matrix. Furthermore, it improves system

homogeneity and matrix particle interaction, increasing the strength values were obtained. Compared to the neat PP (21.2MPa), the value of sample PP-SS/CNF and PP-SP/CNF shows tensile strength increment at 73.5% and 60.3%, respectively. The result obtained also shows the pulverized SiP on the CNF surface did not improve much on tensile strength. The pulverized process may destroy the spherical shape on the SiP SS and functional group present on the surface SiP SP, thus reducing the performance of SiP, which already optimize by the manufacturer.

The elongation at break of PP composites was sharply reduced by the addition of filler due to the stiffening effect of SiP and CNF on the PP composite [210]. Presence of a rigid interface between SiP and CNF fibres and PP matrix decreased the deformability of the PP matrix, which led to more rigid and stiffer composites [207][211]. Furthermore, the PP-8.75 SP (149.2%) composites with SiP SP exhibit higher elongation at break than other PP composites. The functional group that present in SiP SP enhanced the interfacial interaction between filler and PP matrix and generated a stronger interfacial bonding due to the hydrophobicity compatibility and suitable for molecular chain flexibility. Functional group present on SiP may destroy after the pulverized process, which can be observed on sample PP-8.75 pul.SP, the elongation is reduced to 16.2%. However, increasing the weight percentage up to 10% of SiP SP also reduces the elongation on the PP composite, which can be observed on sample PP-10 SP (47.4%).

Young's modulus is an essential parameter in engineering materials and can directly reflect polymers mechanical properties [212]. Rigid fillers such as SiP and CNF typically increase the polymer's stiffness, which can be measured with Young's modulus. Young's modulus for composites containing filler is also shown in Table 5.3, and the results show higher modulus values

at 1.44 GPa for sample PP-8.75 SS compare to neat PP (1.09 GPa). The inclusion of a rigid phase of filler increased the composite stiffness. However, a higher percentage of the filler reduces the Young' modulus value, and the lower Young's modulus value was observed on sample PP-1.25 CNF which 0.81 GPa. Relatively, the stiffness of the composite with SiP/CNF filler (PP-SS/CNF and PP-SS/CNF) is lower than the neat PP. In conclusion, interfacial stress transfer efficiency depends on the stiffness of the interphase, and with higher interfacial stiffness, it improved the modulus of the composite [213].

Table 5.3: Mechanical properties PP composites

Sample code	Tensile strength (MPa)	Young`s Modulus (GPa)	Elongation (%)
PP	21.2	1.09	260.5
PP-8.75 SS	27.8	1.44	7.30
PP-8.75 pul.SS	21.8	0.94	9.97
PP-10 SS	23.5	0.87	24.7
PP-1.25 CNF	24.5	0.81	12.1
PP-1.25 pul.CNF	24.8	1.07	18.1
PP-pul.SS/CNF	28.3	1.17	5.45
PP-pul.(SS/CNF)	25.7	1.13	8.80
PP- SS/CNF	36.8	0.93	20.8
PP-8.75 SP	29.5	0.91	149.2
PP-8.75 pul.SP	26.3	1.15	16.2
PP-10 SP	31.4	0.95	47.4
PP-pul.SP/CNF	24.3	0.92	24.7
PP-pul.(SP/CNF)	27.3	1.21	6.27
PP- SP/CNF	34.0	1.01	10.2

5.4.5 Morphology of the Fracture Surface of PP Composites

PP composites were further analysed with SEM to study fatigue crack propagation. The sample was freeze fractured in a liquid nitrogen bath. After freeze-fracture, the cross-section of the fracture surface was carbon-coated and view. Figure 5.6 depicts the SEM micrograph typical fracture surfaces of neat PP and PP composite samples. The rough surface was observed on neat PP (Figure 5.6a) indicated the typical characteristic of the elastic behaviour of PP [214].
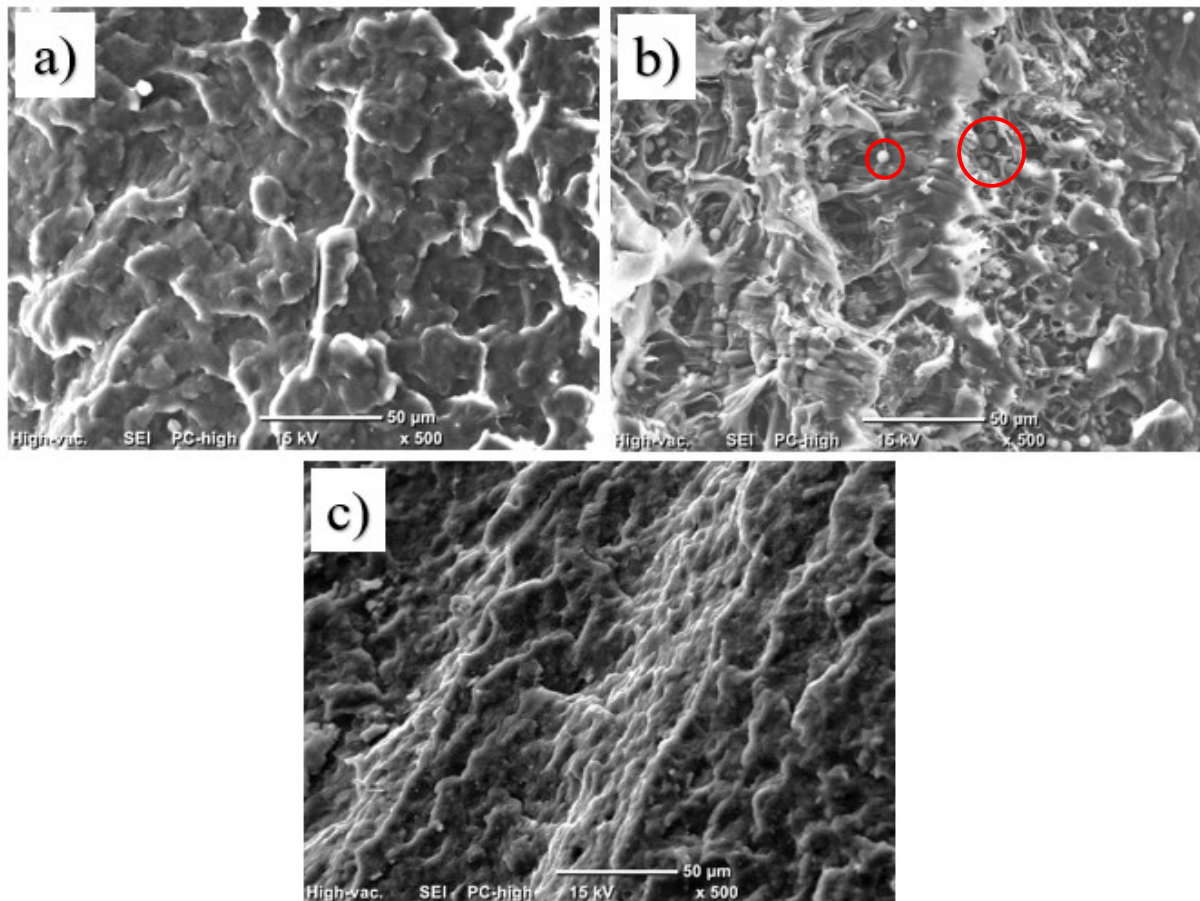
Figure 5.6: SEM micrographs of composites: (a) PP polymer, (b) PP SS/CNF and (c) PP SP/CNF

In Figures 5.6b and 5.6c, the SEM images show a uniform distribution of the fillers in a porous matrix surface in PP composite. Sample PP SS/CNF shows the particulate fillers with a spherical and fibrous shape with holes left (red circle) have been found in the composite, suggesting the applied stress effectively transferred to the filler from the polymer matrix by scattering the energy during crack propagation [90]. While on the sample PP SP/CNF, interconnected nanofibers are formed with rough surfaces in irregular shape were observed. SiP SP exhibit better interfacial bonding strength and filler dispersion in PP composite (Figure 5.6c). These results indicated a robust interfacial adhesion between the PP matrix and filler due to the hydrophobicity compatibility.

5.4.6 Thermogravimetric analysis (TGA) of PP composite

Figure 5.7 shows the thermal stability of the neat PP, SiP, CNF, and PP composite. The TGA result shows the neat PP and PP composite degradation in a single step degradation. SiP SP has a weight slightly loss at 420 °C may be attributed to the thermal decomposition of the functional group of polyalkyl siloxane. Form temperature above 450 °C, there is no weight loss observed for both SiP samples, indicating the left residual is SiP. Besides, SiP have high thermal stability temperatures up to 800 °C [215]. Moreover, for CNF sample, the weight loss was observed at 270 °C due to the thermal decomposition of the carboxyl groups [216].

The TGA result also shows the neat PP degrades completely without any char formation, with the residual of the original sample mass being only 1.3%. Compared to the neat PP, the decomposition temperature of PP composite was increased significantly with the addition of hybrid filler, indicated that SiP protected thermal decomposition of PP composite. Improvement of thermal

stability is related to the excellent dispersion of hybrid filler in the polymer matrix. As a result, it inhibited the distribution of volatile decomposition products out of the materials and the formation of carbonaceous-silicate char, which acts as a physical barrier [217]. Additionally, the weight residue at 500 °C of the PP composite shows the highest for sample PP SS/CNF, which at 10.28% residue, followed by CNF, which 9.54% residue and PP SP/CNF is 7.53% residue.
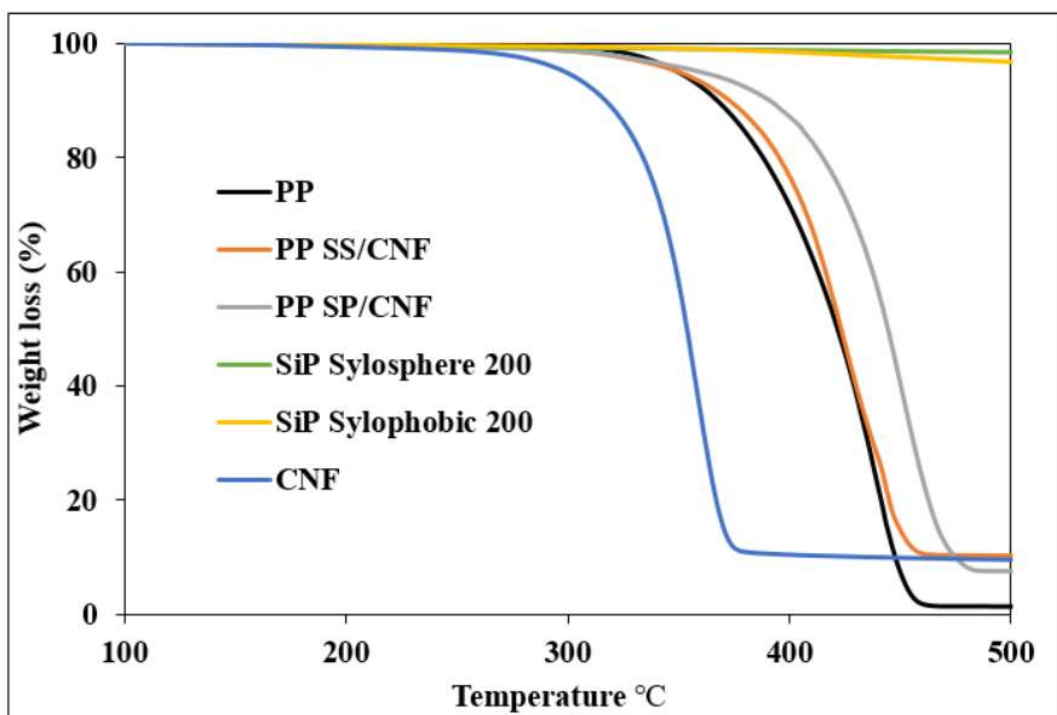
Figure 5.7: TGA curves of PP, SiP, CNF, PP SS/CNF, and PP SP/CNF

5.5   Conclusion

An environmentally friendly method using ethanol/water mixed solvent was successfully prepared on the SiP/CNF and used as a hybrid filler in the polymer matrix. This method applied in this work is very convenient, time-saving, less energy requires, and sidestepping chemical modification. It was noted that the synergistic effect of hybrid filler occurred at this composition by showing a

significant enhancement dispersion of CNF in the hydrophobic polymer. The morphologies result has confirmed the deposition of SiP onto the CNF surface, resulting in good dispersion of hybrid filler in the PP matrix, and no agglomeration was observed. The FT-IR results demonstrated existence of interfacial interactions between hybrid filler and the PP matrix. The incorporation of filler into the PP matrix significantly increases the mechanical properties of the composites. Sample PP-SS/CNF exhibit higher tensile strength at 36.8 Mpa, which increments 73.55% compared to the neat PP. However, the elongation sharply reduced due to the stiffening effect of filler. The thermal stability of PP composite was improved by the incorporation of filler acts as a physical barrier. The hybrid filler exhibited synergistic effects, especially for the tensile strength proved to be more effective than single filler systems. The simplicity of these methods can be applied to other fillers such as metal oxide and graphene oxide to prepare hybrid fillers for designing polymer composites, especially to improve mechanical properties and thermal stability.

CHAPTER 6

CONCLUSION AND RECOMMENDATIONS

6.1   Conclusion

Nanocellulose fibre focused as a sustainable biomaterial with exceptional physicochemical properties. Though it can be upgraded from inexpensive renewable cellulosic biomass, their utilization is limited for applications or exploitation due to original hydrophilicity. This study focuses on surface modification treatment on the CNF and its effects as filler in the hydrophobic polymer. In chapter 2, the surface modified of CNFs using acid treatment by introducing the functional group were successfully obtained. CNF can be used as a reinforced filler, which has confirmed the enhancement of the tensile strength in silicone/CNF composite. Therefore, the morphological of silicone/CNF composite showed relatively good dispersion to prevent CNF aggregations into polymer matrices. Among various cellulose derivatives, cellulose acetate (CA) possessed unique features such as excellent mechanical properties, good thermal stability, tailorable surface chemistry, and can be used as hydroxyl providers to enhance the properties of PUs.

In chapter 3, PUs with commercialized CA were prepared to PUs composite to investigate polymer composite potential with modified cellulose. CA in PUs composite as a thermosetting polymer can be obtained through modifying reaction conditions. Furthermore, the PUs with CA composite prepared transparent film after moulding and showed enhancement of its mechanical property compare to control PUs. Hence, CA can replace 1,4 butanediol (PU BD) as the chain extender to further enhance the PUs performance in terms of their transparency, thermal stability, and

mechanical properties. However, CNF has more hydroxyl groups as reactive moieties with isocyanate group comparing to CA. Chapter 4 investigate preparation reinforced PUs with modified CNF as a reinforcer. The different degree of polymerization (DP) of CNF was treated with phosphoric acid to prepare modified CNF and successfully obtained the PUs through *in situ* polymerization. The morphological of PUs composite with modified CNF showed a relatively good dispersion compared with that of pristine CNF. Furthermore, PUs with modified CNF showed various positive performance compare to PUs with pristine CNF such as mechanical properties, thermal stability, and UV resistant. The modified CNF to aliphatic-based PUs can be upgraded mechanical performance as similar to aromatic-based PUs.

However, these CNF have to use water solutions as emulsion due to prepare composites even though almost all polymer matrices are hydrophobic. In order to study the availability of handling CNF for the polymer moulding process to prepare polymer composite, preparation of dried CNF filler was prepared in Chapter 5. Commercial silica nanoparticles (SiP) and CNF were mixed in ethanol/water mixed solvent. This procedure is a revolutionary convenience to obtain fillers, such as time-saving, less energy, and sidestepping chemical modification. In this methodology, the interaction between CNF and SiP can prevent agglomeration and enhance the dispersion of CNF in the hydrophobic polymer, resulting in excellent mechanical performances and the dispersion of the hybrid filler in the PP matrix. The thermal stability of PP composite also improved.

In conclusion, the author accomplished to control the characterisation of CNF, which can be a broad application for potential polymer matrices. These findings expect to contribute widely to academia and industries.

6.2   Recommendations

This study has contributed to the surface modification of cellulose nanofiber (CNF) with enhanced dispersibility in hydrophobic polymer by changing the surface properties or reducing the hydroxyl group on the CNF surface. The method that was used is convenience, environmentally friendly, time-saving and low cost. Further investigations are recommended further to understand CNF surface properties after treatment and their interaction when reinforcing potential with other a hydrophobic polymer. Further development bio-based polyols and isocyanates for the production of bio-based PUs are also should be considered.

Based on the results obtained in the surface modification CNF via acid treatment, a more detailed investigation of surface chemistry and potential surface modification strategies for functionalized CNF is recommended.

Based on the results obtained from the polyurethane polymerization, an alternative method to incorporate NC into a PUs matrix can involve the use of:

I.   functionalized NC for enhancing chemical/covalent bonding between PUs and NC

II.   different type of cellulose to prepare PUs/cellulose nanocomposites

III.   different type of diisocyanate and compatibilizer for enhancing the surface wettability of PUs

REFERENCES

[1]   M. Rahimi Kord Sofla, R. J. Brown, T. Tsuzuki, and T. J. Rainey, "A comparison of cellulose nanocrystals and cellulose nanofibres extracted from bagasse using acid and ball milling methods," *Adv. Nat. Sci. Nanosci. Nanotechnol.*, vol. 7, no. 3, 2016.

[2]   A. D. French, "Glucose, not cellobiose, is the repeating unit of cellulose and why that is important," *Cellulose*, vol. 24, no. 11, pp. 4605–4609, 2017.

[3]   R. B. Chavan, S. Rathi, V. G. S. S. Jyothi, and N. R. Shastri, "Cellulose based polymers in development of amorphous solid dispersions," *Asian J. Pharm. Sci.*, vol. 14, no. 3, pp. 248–264, 2019.

[4]   O. A. Hisseine, A. F. Omran, and A. Tagnit-Hamou, "Influence of cellulose filaments on cement paste and concrete," *J. Mater. Civ. Eng.*, vol. 30, no. 6, pp. 1–14, 2018.

[5]   O. S. Manoukian *et al.*, "Biomaterials for Tissue Engineering and Regenerative Medicine," in *Encyclopedia of Biomedical Engineering*, vol. 1–3, Elsevier, 2019, pp. 462–482.

[6]   Z. T. Niyazbekova, G. Z. Nagmetova, and A. A. Kurmanbayev, "an Overview of Bacterial Cellulose Applications," *Biotechnol. Theory Pract.*, pp. 1–15, 2018.

[7]   H. M. C. Azeredo, H. Barud, C. S. Farinas, V. M. Vasconcellos, and A. M. Claro, "Bacterial Cellulose as a Raw Material for Food and Food Packaging Applications," *Front. Sustain. Food Syst.*, vol. 3, no. February, 2019.

[8]   T. Theivasanthi, F. L. Anne Christma, A. J. Toyin, S. C. B. Gopinath, and R. Ravichandran, "Synthesis and characterization of cotton fiber-based nanocellulose," *Int. J. Biol. Macromol.*, vol. 109, pp. 832–836, 2018.

[9]   M. Börjesson and G. Westman, "Crystalline Nanocellulose — Preparation, Modification, and Properties," *Cellul. - Fundam. Asp. Curr. Trends*, 2015.

[10]   P. Bajpai, "Structure and Properties of Cellulose and Nanocellulose," in *Pulp and Paper Industry*, Elsevier, 2017, pp. 27–40.

[11]   M. M. Mahmud *et al.*, "Preparation of different polymorphs of cellulose from different acid hydrolysis medium," *Int. J. Biol. Macromol.*, vol. 130, pp. 969–976, 2019.

[12]   Y. Nishiyama, J. Sugiyama, H. Chanzy, and P. Langan, "Crystal Structure and Hydrogen Bonding System in Cellulose Iα from Synchrotron X-ray and Neutron Fiber Diffraction," *J. Am. Chem. Soc.*, vol. 125, no. 47, pp. 14300–14306, 2003.

[13]   O. A. El Seoud, M. Kostag, K. Jedvert, and N. I. Malek, "Cellulose in ionic liquids and alkaline solutions: Advances in the mechanisms of biopolymer dissolution and regeneration," *Polymers (Basel).*, vol. 11, no. 12, pp. 1–28, 2019.

[14]   R. Abouzeid, "Advanced cellulose composites ; preparation and properties Ragab Abouzeid To cite this version :," 2017.

[15] M. T. Holtzapple, "Encyclopedia of Food Sciences and Nutrition," *Encycl. Food Sci. Nutr.*, pp. 998–1007, 2003.

[16] R. J. Hickey and A. E. Pelling, "Cellulose biomaterials for tissue engineering," *Front. Bioeng. Biotechnol.*, vol. 7, no. MAR, pp. 1–15, 2019.

[17] T. Cui, J. Li, Z. Yan, M. Yu, and S. Li, "The correlation between the enzymatic saccharification and the multidimensional structure of cellulose changed by different pretreatments," *Biotechnol. Biofuels*, vol. 7, no. 1, pp. 1–10, 2014.

[18] K. Igarashi, M. Wada, and M. Samejima, "Activation of crystalline cellulose to cellulose IIII results in efficient hydrolysis by cellobiohydrolase," *FEBS J.*, vol. 274, no. 7, pp. 1785–1792, 2007.

[19] M. Wada, L. Heux, and J. Sugiyama, "Polymorphism of cellulose I family: Reinvestigation of cellulose IVl," *Biomacromolecules*, vol. 5, no. 4, pp. 1385–1391, 2004.

[20] A. Sharma, M. Thakur, M. Bhattacharya, T. Mandal, and S. Goswami, "Commercial application of cellulose nano-composites – A review," *Biotechnol. Reports*, vol. 21, no. 2018, p. e00316, 2019.

[21] A. Solikhin, Y. S. Hadi, M. Y. Massijaya, and S. Nikmatin, "Morphological, Chemical, and Thermal Characteristics of Nanofibrillated Cellulose Isolated Using Chemo-mechanical Methods," *Makara J. Sci.*, vol. 21, no. 2, pp. 59–68, 2017.

[22] K. Plermjai, K. Boonyarattanakalin, W. Mekprasart, S. Pavasupree, W. Phoohinkong, and W. Pecharapa, "Extraction and characterization of nanocellulose from sugarcane bagasse by ball-milling-assisted acid hydrolysis," *AIP Conf. Proc.*, vol. 2010, no. September, 2018.

[23] Y. Watanabe *et al.*, "Application of a water jet system to the pretreatment of cellulose," *Biopolymers*, vol. 95, no. 12, pp. 833–839, 2011.

[24] B. Thomas *et al.*, "Nanocellulose, a Versatile Green Platform: From Biosources to Materials and Their Applications," *Chem. Rev.*, vol. 118, no. 24, pp. 11575–11625, 2018.

[25] N. K. Luneva and T. I. Ezovitova, "Cellulose phosphorylation with a mixture of orthophosphoric acid and ammonium polyphosphate in urea medium," *Russ. J. Appl. Chem.*, vol. 87, no. 10, pp. 1558–1565, 2014.

[26] A. Chakrabarty and Y. Teramoto, "Recent advances in nanocellulose composites with polymers: A guide for choosing partners and how to incorporate them," *Polymers (Basel).*, vol. 10, no. 5, 2018.

[27] M. N. A. M. Taib, W. A. Yehye, N. M. Julkapli, and S. B. O. A. A. Hamid, "Influence of Hydrophobicity of Acetylated Nanocellulose on the Mechanical Performance of Nitrile Butadiene Rubber (NBR) Composites," *Fibers Polym.*, vol. 19, no. 2, pp. 383–392, 2018.

[28] W. Lin *et al.*, "Hydrophobic modification of nanocellulose via a two-step silanation method," *Polymers (Basel).*, vol. 10, no. 9, 2018.

[29] D. Miyashiro, R. Hamano, and K. Umemura, "A review of applications using mixed

materials of cellulose, nanocellulose and carbon nanotubes," *Nanomaterials*, vol. 10, no. 2, pp. 1–23, 2020.

[30] N. Halib *et al.*, "Potential applications of nanocellulose-containing materials in the biomedical field," *Materials (Basel).*, vol. 10, no. 8, pp. 1–31, 2017.

[31] W. Im, S. Lee, A. Rajabi Abhari, H. J. Youn, and H. L. Lee, "Optimization of carboxymethylation reaction as a pretreatment for production of cellulose nanofibrils," *Cellulose*, vol. 25, no. 7, pp. 3873–3883, 2018.

[32] X. J. Shen, P. L. Huang, J. H. Chen, Y. Y. Wu, Q. Y. Liu, and R. C. Sun, "Comparison of acid-hydrolyzed and TEMPO-oxidized nanocellulose for reinforcing alginate fibers," *BioResources*, vol. 12, no. 4, pp. 8180–8198, 2017.

[33] A. Isogai, T. Saito, and H. Fukuzumi, "TEMPO-oxidized cellulose nanofibers," *Nanoscale*, vol. 3, no. 1, pp. 71–85, 2011.

[34] N. Lin and A. Dufresne, "Surface chemistry, morphological analysis and properties of cellulose nanocrystals with gradiented sulfation degrees," *Nanoscale*, vol. 6, no. 10, pp. 5384–5393, 2014.

[35] C. Ruiz-Palomero, M. L. Soriano, and M. Valcárcel, "Sulfonated nanocellulose for the efficient dispersive micro solid-phase extraction and determination of silver nanoparticles in food products," *J. Chromatogr. A*, vol. 1428, pp. 352–358, 2016.

[36] Y. Wang, X. Wang, Y. Xie, and K. Zhang, "Functional nanomaterials through esterification of cellulose: a review of chemistry and application," *Cellulose*, vol. 25, no. 7, pp. 3703–3731, 2018.

[37] X. Zhou *et al.*, "Effect of the degree of substitution on the hydrophobicity of acetylated cellulose for production of liquid marbles," *Cellulose*, vol. 23, no. 1, pp. 811–821, 2016.

[38] J. B. Daud and K.-Y. Lee, "Surface Modification of Nanocellulose," *Handb. Nanocellulose Cellul. Nanocomposites*, no. May 2011, pp. 101–122, 2017.

[39] Z. Zhang, P. Tingaut, D. Rentsch, T. Zimmermann, and G. Sèbe, "Controlled Silylation of Nanofibrillated Cellulose in Water: Reinforcement of a Model Polydimethylsiloxane Network," *ChemSusChem*, vol. 8, no. 16, pp. 2681–2690, 2015.

[40] V. M. Gun'ko, "Polymer Composites With Functionalized Silica," in *Polymer Composites with Functionalized Nanoparticles*, Elsevier, 2019, pp. 119–148.

[41] A. H. Bhat, Y. K. Dasan, I. Khan, H. Soleimani, and A. Usmani, *Application of nanocrystalline cellulose: Processing and biomedical applications*. Elsevier Ltd, 2017.

[42] C. M. Hussain, "Polymer nanocomposites-An intro," *New Polym. Nanocomposites Environ. Remediat.*, pp. xxi–xxv, 2018.

[43] M. Bhattacharya, "Polymer nanocomposites-A comparison between carbon nanotubes, graphene, and clay as nanofillers," *Materials (Basel).*, vol. 9, no. 4, pp. 1–35, 2016.

[44] K. Müller *et al.*, "Review on the processing and properties of polymer nanocomposites and nanocoatings and their applications in the packaging, automotive and solar energy

fields," *Nanomaterials*, vol. 7, no. 4, 2017.

[45]   A. Dantas de Oliveira and C. Augusto Gonçalves Beatrice, "Polymer Nanocomposites with Different Types of Nanofiller," *Nanocomposites - Recent Evol.*, 2019.

[46]   A. Bouty *et al.*, "Nanofiller structure and reinforcement in model silica/rubber composites: A quantitative correlation driven by interfacial agents," *Macromolecules*, vol. 47, no. 15, pp. 5365–5378, 2014.

[47]   D. Olmos, G. González-Gaitano, and J. González-Benito, "Effect of a silica nanofiller on the structure, dynamics and thermostability of LDPE in LDPE/silica nanocomposites," *RSC Adv.*, vol. 5, no. 44, pp. 34979–34984, 2015.

[48]   S. Z. Al Sheheri, Z. M. Al-Amshany, Q. A. Al Sulami, N. Y. Tashkandi, M. A. Hussein, and R. M. El-Shishtawy, "The preparation of carbon nanofillers and their role on the performance of variable polymer nanocomposites," *Des. Monomers Polym.*, vol. 22, no. 1, pp. 8–53, 2019.

[49]   M. Nuruddin, M. Hosur, R. Gupta, G. Hosur, A. Tcherbi-Narteh, and S. Jeelani, "Cellulose nanofibers-graphene nanoplatelets hybrids nanofillers as high-performance multifunctional reinforcements in epoxy composites," *Polym. Polym. Compos.*, vol. 25, no. 4, pp. 273–283, 2017.

[50]   S. C. Tjong, "Polymer composites with graphene nanofillers: Electrical properties and applications," *J. Nanosci. Nanotechnol.*, vol. 14, no. 2, pp. 1154–1168, 2014.

[51]   S. Sim *et al.*, "Development of Organo-Dispersible Graphene Oxide via Pseudo-Surface Modification for Thermally Conductive Green Polymer Composites," *ACS Omega*, vol. 3, no. 12, pp. 18124–18131, 2018.

[52]   D. K. Patel, S. D. Dutta, and K. T. Lim, "Nanocellulose-based polymer hybrids and their emerging applications in biomedical engineering and water purification," *RSC Adv.*, vol. 9, no. 33, pp. 19143–19162, 2019.

[53]   T. E. Motaung and L. Z. Linganiso, *Critical review on agrowaste cellulose applications for biopolymers*, vol. 22, no. 2. Springer India, 2018.

[54]   F. A. dos Santos, G. C. V. Iulianelli, and M. I. B. Tavares, "The Use of Cellulose Nanofillers in Obtaining Polymer Nanocomposites: Properties, Processing, and Applications," *Mater. Sci. Appl.*, vol. 07, no. 05, pp. 257–294, 2016.

[55]   E. Jamróz, P. Kulawik, and P. Kopel, "The effect of nanofillers on the functional properties of biopolymer-based films: A review," *Polymers (Basel).*, vol. 11, no. 4, pp. 1–43, 2019.

[56]   O. Manero and A. Sanchez-Solis, "Polymer Nanocomposites," *Handb. Polym. Synth. Charact. Process.*, pp. 585–604, 2013.

[57]   S. Paszkiewicz and A. Szymczyk, *Graphene-Based Nanomaterials and Their Polymer Nanocomposites*. Elsevier Inc., 2018.

[58]   L. Rueda *et al.*, "In situ polymerization and characterization of elastomeric polyurethane-

cellulose nanocrystal nanocomposites. Cell response evaluation," *Cellulose*, 2013.

[59] L. C. Tang, L. Zhao, F. Qiang, Q. Wu, L. X. Gong, and J. P. Peng, *Mechanical properties of rubber nanocomposites containing carbon nanofillers*. Elsevier Inc., 2019.

[60] K. D. Nelson, *Absorbable, drug-loaded, extruded fiber for implantation*. Elsevier Ltd., 2015.

[61] S. A. Ashter, "Extrusion of Biopolymers," *Introd. to Bioplastics Eng.*, pp. 211–225, 2016.

[62] M. N. F. Norrrahim, H. Ariffin, T. A. T. Yasim-Anuar, M. A. Hassan, H. Nishida, and T. Tsukegi, "One-pot nanofibrillation of cellulose and nanocomposite production in a twin-screw extruder," *IOP Conf. Ser. Mater. Sci. Eng.*, vol. 368, no. 1, 2018.

[63] Y. Yanping, "The development of polyurethane," *Mater. Sci. Mater. Rev.*, vol. 1, no. 1, pp. 1–8, 2018.

[64] F. H. Ikhwan, S. Ilmiati, H. Kurnia Adi, R. Arumsari, and M. Chalid, "Novel route of synthesis for cellulose fiber-based hybrid polyurethane," *IOP Conf. Ser. Mater. Sci. Eng.*, vol. 223, no. 1, 2017.

[65] M. A. Alaa, K. Yusoh, and S. F. Hasany, "PURE POLYURETHANE AND CASTOR OIL BASED POLYURETHANE: SYNTHESIS AND CHARACTERIZATION," *J. Mech. Eng. Sci.*, vol. 8, no. June, pp. 1507–1515, 2015.

[66] M. M. Rahman, M. M. Rabbani, and J. K. Saha, "Polyurethane and Its Derivatives," 2019, pp. 225–240.

[67] A. S. Dutta, "Polyurethane Foam Chemistry," in *Recycling of Polyurethane Foams*, Elsevier, 2018, pp. 17–27.

[68] K. Dimitrov, D. Todorova, S. Nenkova, and M. Herzog, "Polycarbonate diols to produce elastic polyurethane foams - A method of immobilization of carbon dioxide into a polymer structure," *J. Chem. Technol. Metall.*, vol. 52, no. 1, pp. 28–40, 2017.

[69] J. O. Akindoyo, M. D. H. Beg, S. Ghazali, M. R. Islam, N. Jeyaratnam, and A. R. Yuvaraj, "Polyurethane types, synthesis and applications-a review," *RSC Adv.*, vol. 6, no. 115, pp. 114453–114482, 2016.

[70] E. Sharmin and F. Zafar, "Polyurethane: An Introduction," in *Polyurethane*, InTech, 2012.

[71] T. F. Garrison and M. R. Kessler, "Plant Oil-Based Polyurethanes," in *Bio-Based Plant Oil Polymers and Composites*, Elsevier, 2016, pp. 37–54.

[72] C. Saha, T. K. Chaki, and N. K. Singha, "Synthesis and characterization of elastomeric polyurethane and PU/clay nanocomposites based on an aliphatic diisocyanate," *J. Appl. Polym. Sci.*, vol. 130, no. 5, pp. 3328–3334, 2013.

[73] T. J. Touchet and E. M. Cosgriff-Hernandez, *Hierarchal Structure-Property Relationships of Segmented Polyurethanes*. Elsevier Ltd, 2016.

[74] L. Bengtström, M. Salden, and A. A. Stec, "The role of isocyanates in fire toxicity," *Fire Sci. Rev.*, vol. 5, no. 1, 2016.

[75] K. C. Hung, C. S. Tseng, and S. H. Hsu, *3D Printing of Polyurethane Biomaterials*. Elsevier Ltd, 2016.

[76] L. W. McKeen, "Elastomers and Rubbers," in *The Effect of Long Term Thermal Exposure on Plastics and Elastomers*, Elsevier, 2014, pp. 239–271.

[77] I. Javni, W. Zhang, and Z. S. Petrović, "Effect of different isocyanates on the properties of soy-based polyurethanes," *J. Appl. Polym. Sci.*, vol. 88, no. 13, pp. 2912–2916, 2003.

[78] H. Abushammala and J. Mao, "A review of the surface modification of cellulose and nanocellulose using aliphatic and aromatic mono- And di-isocyanates," *Molecules*, vol. 24, no. 15, pp. 1–18, 2019.

[79] L. Rueda *et al.*, "Isocyanate-rich cellulose nanocrystals and their selective insertion in elastomeric polyurethane," *Compos. Sci. Technol.*, vol. 71, no. 16, pp. 1953–1960, 2011.

[80] N. M. Girouard, S. Xu, G. T. Schueneman, M. L. Shofner, and J. C. Meredith, "Site-Selective Modification of Cellulose Nanocrystals with Isophorone Diisocyanate and Formation of Polyurethane-CNC Composites," *ACS Appl. Mater. Interfaces*, vol. 8, no. 2, pp. 1458–1467, 2016.

[81] C. Prisacariu and E. Scortanu, "Influence of the type of chain extender and urethane group content on the mechanical properties of polyurethane elastomers with flexible hard segments," *High Perform. Polym.*, vol. 23, no. 4, pp. 308–313, 2011.

[82] A. D. Padsalgikar, "Speciality Plastics in Cardiovascular Applications," in *Plastics in Medical Devices for Cardiovascular Applications*, Elsevier, 2017, pp. 53–82.

[83] Y. C. Chung, N. D. Khiem, J. W. Choi, and B. C. Chun, "Covalent incorporation of cellulose derivative into polyurethane copolymers and the effect on crosslinking and water vapor permeability," *J. Macromol. Sci. Part A Pure Appl. Chem.*, vol. 51, no. 4, pp. 339–349, 2014.

[84] C. Vilela, R. J. B. Pinto, S. Pinto, P. A. A. P. Marques, A. J. D. Silvestre, and C. S. R. Freire, "Polysaccharide based hybrid materials," p. 136, 2018.

[85] M. Hassanzadeh, R. Sabo, A. Rudie, R. Reiner, R. Gleisner, and G. S. Oporto, "Nanofibrillated Cellulose from Appalachian Hardwoods Logging Residues as Template for Antimicrobial Copper," *J. Nanomater.*, vol. 2017, 2017.

[86] P. Phanthong, P. Reubroycharoen, X. Hao, G. Xu, A. Abudula, and G. Guan, "Nanocellulose: Extraction and application," *Carbon Resour. Convers.*, 2018.

[87] H. P. S. Abdul Khalil *et al.*, "Production and modification of nanofibrillated cellulose using various mechanical processes: A review," *Carbohydr. Polym.*, vol. 99, pp. 649–665, 2014.

[88] A. Leszczyńska, P. Radzik, E. Szefer, M. Mičušík, M. Omastová, and K. Pielichowski, "Surface modification of cellulose nanocrystals with succinic anhydride," *Polymers (Basel).*, vol. 11, no. 5, 2019.

[89] Y. He, J. Zhu, W. Wang, and H. Ni, "Surface modification of cellulose nanocrystals with

different acid anhydrides for improved dispersion in poly(butylene succinate)," *RSC Adv.*, vol. 8, no. 67, pp. 38305–38314, 2018.

[90] S. Y. Fu, X. Q. Feng, B. Lauke, and Y. W. Mai, "Effects of particle size, particle/matrix interface adhesion and particle loading on mechanical properties of particulate-polymer composites," *Compos. Part B Eng.*, vol. 39, no. 6, pp. 933–961, 2008.

[91] H. P. S. Abdul Khalil *et al.*, *Nanofibrillated cellulose reinforcement in thermoset polymer composites*. Elsevier Ltd, 2017.

[92] M. Andriot *et al.*, "Silicones in Industrial Applications," *Inorg. Polym.*, vol. 84, no. January, pp. 61–161, 2009.

[93] P. Hron, "Hydrophilisation of silicone rubber for medical applications," *Polym. Int.*, vol. 52, no. 9, pp. 1531–1539, 2003.

[94] A. Rahimi and A. Mashak, "Review on rubbers in medicine: Natural, silicone and polyurethane rubbers," *Plast. Rubber Compos.*, vol. 42, no. 6, pp. 223–230, 2013.

[95] E.-S. Park, "Mechanical Properties and Processibilty of Glass-Fiber-, Wollastonite-, and Fluoro-Rubber-Reinforced Silicone Rubber Composites," *J. Appl. Polym. Sci.*, vol. 116, no. 5, pp. 2658–2667, 2007.

[96] J. C. Almeida, A. Wacha, P. S. Gomes, M. H. R. Fernandes, M. H. V. Fernandes, and I. M. M. Salvado, "PDMS-SiO2-TiO2-CaO hybrid materials - Cytocompatibility and nanoscale surface features," *Mater. Sci. Eng. C*, vol. 64, pp. 74–86, 2016.

[97] D. R. Paul and J. E. Mark, "Fillers for polysiloxane ('silicone') elastomers," *Prog. Polym. Sci.*, vol. 35, no. 7, pp. 893–901, 2010.

[98] S. N. L. Mamauod, N. A. N. A. Rahim, N. R. Mohamed, and A. Z. Romli, "Synergistic effect of hybrid nanofiller (nano-calcium carbonate/nano-silicone dioxide) on the tensile and impact properties of modified epoxy resin (EP/CTBN) composites," *AIP Conf. Proc.*, vol. 1985, no. August, 2018.

[99] X. Xu, Y. Song, and G. H. Qiang Zheng, "Influence of Incorporating CaCO3 into Room Temperatureon vulcanized silicone sealant on Its Mechanical and Dynamic Rheological Properties," *J. Appl. Polym. Sci.*, vol. 110, pp. 2017–2035, 2007.

[100] A. Colas and J. Curtis, "Silicones," *Handb. Polym. Appl. Med. Med. Devices*, pp. 131–143, 2013.

[101] V. JANKAUSKAITĖ *et al.*, "Silicone Rubber and Microcrystalline Cellulose Composites with Antimicrobial Properties," *Mater. Sci.*, vol. 20, no. 1, 2014.

[102] A. Isogai, "Emerging Nanocellulose Technologies: Recent Developments," *Adv. Mater.*, pp. 1–10, 2020.

[103] K. Missoum, M. N. Belgacem, and J. Bras, "Nanofibrillated cellulose surface modification: A review," *Materials (Basel).*, vol. 6, no. 5, pp. 1745–1766, 2013.

[104] J. Shojaeiarani, D. Bajwa, and G. Holt, "Sonication amplitude and processing time influence the cellulose nanocrystals morphology and dispersion," *Nanocomposites*, vol. 0,

no. 0, pp. 1–6, 2020.

[105] M. Szymańska-Chargot *et al.*, "Effect of ultrasonication on physicochemical properties of apple based nanocellulose-calcium carbonate composites," *Cellulose*, vol. 25, no. 8, pp. 4603–4621, 2018.

[106] S. P. S. Chundawat and U. P. Agarwal, "Swelling by Hydrochloric Acid Partially Retains Cellulose-I Type Allomorphic Ultrastructure But Enhances Susceptibility toward Cellulase Hydrolysis Such as Highly Amorphous Cellulose," in *ACS Symposium Series*, vol. 1338, American Chemical Society, 2019, pp. 69–88.

[107] Y. Hishikawa, E. Togawa, and T. Kondo, "Characterization of Individual Hydrogen Bonds in Crystalline Regenerated Cellulose Using Resolved Polarized FTIR Spectra," *ACS Omega*, vol. 2, no. 4, pp. 1469–1476, 2017.

[108] K. Sahlin, L. Forsgren, T. Moberg, D. Bernin, M. Rigdahl, and G. Westman, "Surface treatment of cellulose nanocrystals (CNC): effects on dispersion rheology," *Cellulose*, vol. 25, no. 1, pp. 331–345, 2018.

[109] J. Lamaming, R. Hashim, O. Sulaiman, C. P. Leh, T. Sugimoto, and N. A. Nordin, "Cellulose nanocrystals isolated from oil palm trunk," *Carbohydr. Polym.*, vol. 127, pp. 202–208, 2015.

[110] G. A. Giffin *et al.*, "A vibrational spectroscopic and modeling study of poly(2,5-benzimidazole) (ABPBI) - Phosphoric acid interactions in high temperature PEFC membranes," *Int. J. Hydrogen Energy*, vol. 39, no. 6, pp. 2776–2784, 2014.

[111] Z. N. Siddiqui and T. Khan, "An efficient synthesis of novel bis-chalcones and bis-pyrazolines in the presence of cellulose sulfuric acid as biodegradable catalyst under solvent-free conditions," *J. Braz. Chem. Soc.*, vol. 25, no. 6, pp. 1002–1011, 2014.

[112] S. Ebnesajjad, *Surface and Material Characterization Techniques*. 2014.

[113] W. R. W. Daud, M. H. M. Kassim, and A. Seeni, "Cellulose phosphate from oil palm biomass as potential biomaterials," *BioResources*, vol. 6, no. 2, pp. 1719–1740, 2011.

[114] P. L. Hariani, F. Riyanti, and A. Kurniaty, "Modification of cellulose with acetic acid to removal of methylene blue dye," *J. Phys. Conf. Ser.*, vol. 1282, no. 1, 2019.

[115] J. A. F. Gamelas *et al.*, "On the morphology of cellulose nanofibrils obtained by TEMPO-mediated oxidation and mechanical treatment," *Micron*, vol. 72, pp. 28–33, 2015.

[116] P. Phanthong, P. Reubroycharoen, X. Hao, G. Xu, A. Abudula, and G. Guan, "Nanocellulose: Extraction and application," *Carbon Resour. Convers.*, vol. 1, no. 1, pp. 32–43, 2018.

[117] S. F. M. Hanafiah *et al.*, "Extraction and characterization of microfibrillated and nanofibrillated cellulose from office paper waste," *Malaysian J. Anal. Sci.*, vol. 23, no. 5, pp. 901–913, 2019.

[118] Z. Tang *et al.*, "TEMPO-Oxidized cellulose with high degree of oxidation," *Polymers (Basel).*, vol. 9, no. 9, pp. 3–4, 2017.

[119] K. Missoum, J. Bras, and M. N. Belgacem, "Water redispersible dried nanofibrillated cellulose by adding sodium chloride," *Biomacromolecules*, vol. 13, no. 12, pp. 4118–4125, 2012.

[120] Y. Chu, Y. Sun, W. Wu, and H. Xiao, "Dispersion Properties of Nanocellulose: A Review," *Carbohydr. Polym.*, vol. 250, no. June, p. 116892, 2020.

[121] K. P. Y. Shak, Y. L. Pang, and S. K. Mah, "Nanocellulose: Recent advances and its prospects in environmental remediation," *Beilstein J. Nanotechnol.*, vol. 9, no. 1, pp. 2479–2498, 2018.

[122] M. B. Agustin, F. Nakatsubo, and H. Yano, "The thermal stability of nanocellulose and its acetates with different degree of polymerization," *Cellulose*, vol. 23, no. 1, pp. 451–464, 2016.

[123] L. Du, J. Wang, Y. Zhang, C. Qi, M. P. Wolcott, and Z. Yu, "Preparation and characterization of cellulose nanocrystals from the bio-ethanol residuals," *Nanomaterials*, vol. 7, no. 3, pp. 1–12, 2017.

[124] X. Jia *et al.*, "Preparation and characterization of cellulose regenerated from phosphoric acid," *J. Agric. Food Chem.*, vol. 61, no. 50, pp. 12405–12414, 2013.

[125] K. Lichtenstein and N. Lavoine, "Toward a deeper understanding of the thermal degradation mechanism of nanocellulose," *Polym. Degrad. Stab.*, vol. 146, pp. 53–60, 2017.

[126] S. Cichosz, A. Masek, and A. Rylski, "Cellulose modification for improved compatibility with the polymer matrix: Mechanical characterization of the composite material," *Materials (Basel).*, vol. 13, no. 23, pp. 1–18, 2020.

[127] T. Noguchi, M. Endo, K. Niihara, H. Jinnai, and A. Isogai, "Cellulose nanofiber / elastomer composites with high tensile strength , modulus , toughness , and thermal stability," *Compos. Sci. Technol.*, p. 108005, 2020.

[128] B. Zhang *et al.*, "Eects of cellulose nanocrystals and cellulose nanofibers on the structure and properties of polyhydroxybutyrate nanocomposites," *Polymers (Basel).*, vol. 11, no. 12, 2019.

[129] P. M. T. and Nur Sharmila Sharip, Hidayah Ariffin, Yoshito Andou, Yuki Shirosaki, Ezyana Kamal Bahrin, Mohammad Jawaid and N. A. Ibrahim, "Process Optimization of Ultra-High Molecular Weight Polyethylene / Cellulose Nanofiber Bionanocomposites in Triple Screw Kneading Extruder by Response," vol. 25, 2020.

[130] S. Mania and M. Cie, "polymers The Synergistic Microbiological E ff ects of Industrial Produced Packaging Polyethylene Films Incorporated with Zinc Nanoparticles," pp. 1–15.

[131] N. V. Gama, A. Ferreira, and A. Barros-Timmons, "Polyurethane foams: Past, present, and future," *Materials (Basel).*, vol. 11, no. 10, 2018.

[132] S. Pina *et al.*, "Scaffolding strategies for tissue engineering and regenerative medicine applications," *Materials (Basel).*, vol. 12, no. 11, 2019.

[133] F. Rafiemanzelat, A. Fathollahi Zonouz, and G. Emtiazi, "Synthesis of new poly(ether-urethane-urea)s based on amino acid cyclopeptide and PEG: Study of their environmental degradation," *Amino Acids*, vol. 44, no. 2, pp. 449–459, 2013.

[134] M. Alinejad *et al.*, "Lignin-based polyurethanes: Opportunities for bio-based foams, elastomers, coatings and adhesives," *Polymers (Basel).*, vol. 11, no. 7, 2019.

[135] G. T. Howard, "Biodegradation of polyurethane: a review," *Int. Biodeterior. Biodegradation*, vol. 49, no. 4, pp. 245–252, 2002.

[136] S. Demiroğlu, F. Erdoğan, E. Akin, H. A. Karavana, and M. Ö. Seydibeyoğlu, "Natural fiber reinforced polyurethane rigid foam," *Gazi Univ. J. Sci.*, vol. 30, no. 2, pp. 97–109, 2017.

[137] R. Shi *et al.*, "Recent advances in synthetic bioelastomers," *Int. J. Mol. Sci.*, vol. 10, no. 10, pp. 4223–4256, 2009.

[138] V. Kupka *et al.*, "Well-dispersed polyurethane/cellulose nanocrystal nanocomposites synthesized by a solvent-free procedure in bulk," *Polym. Compos.*, vol. 40, pp. E456–E465, 2019.

[139] P. Khadivi, M. Salami-Kalajahi, H. Roghani-Mamaqani, and R. Lotfi Mayan Sofla, "Fabrication of microphase-separated polyurethane/cellulose nanocrystal nanocomposites with irregular mechanical and shape memory properties," *Appl. Phys. A*, vol. 125, no. 11, p. 779, 2019.

[140] S. Vlad *et al.*, "New polyetherurethanes based on cellulose derivative for biomedical applications," *Optoelectron. Adv. Mater. Rapid Commun.*, vol. 4, no. 3, pp. 407–414, 2010.

[141] K. Yuwawech, J. Wootthikanokkhan, S. Wanwong, and S. Tanpichai, "Polyurethane/esterified cellulose nanocrystal composites as a transparent moisture barrier coating for encapsulation of dye sensitized solar cells," *Journal of Applied Polymer Science*, vol. 134, no. 45. 2017.

[142] A. Hadjadj *et al.*, "Effects of cellulose fiber content on physical properties of polyurethane based composites," *Compos. Struct.*, vol. 135, pp. 217–223, 2016.

[143] S. Choi, M. Lee, and E. Shin, "One-Pot Processing of Regenerated Cellulose Nanoparticles/Waterborne Polyurethane Nanocomposite for Eco-friendly Polyurethane Matrix," *Polymers (Basel).*, vol. 11, no. 2, p. 356, 2019.

[144] E. N. Bifari, S. Bahadar Khan, K. A. Alamry, A. M. Asiri, and K. Akhtar, "Cellulose Acetate Based Nanocomposites for Biomedical Applications: A Review," *Curr. Pharm. Des.*, vol. 22, no. 20, pp. 3007–3019, 2016.

[145] M. Sivakumar, R. Malaisamy, C. J. Sajitha, D. Mohan, V. Mohan, and R. Rangarajan, "Preparation and performance of cellulose acetate-polyurethane blend membranes and their applications - II," *J. Memb. Sci.*, vol. 169, no. 2, pp. 215–228, 2000.

[146] T. Riaz *et al.*, "Synthesis and characterization of polyurethane-cellulose acetate blend membrane for chromium (VI) removal," *Carbohydr. Polym.*, vol. 153, pp. 582–591, 2016.

[147] A. R. Unnithan, G. Gnanasekaran, Y. Sathishkumar, Y. S. Lee, and C. S. Kim, "Electrospun antibacterial polyurethane-cellulose acetate-zein composite mats for wound dressing," *Carbohydr. Polym.*, vol. 102, no. 1, pp. 884–892, 2014.

[148] H. L. Chunyi Tang, Pingping Chen, "Cocontinuous Cellulose Acetate/Polyurethane Composite Nanofiber Fabricated Through Electrospinning," *Society*, 2008.

[149] M. M. Ali, N. Pakkang, S. Taira, K. Koda, K. Itoyama, and Y. Uraki, "Direct Electrospinning of Cellulose Acetate onto Polyurethane Sheet and Effect of Its Saponification on Mechanical Properties," *J. Wood Chem. Technol.*, vol. 39, no. 4, pp. 282–295, 2019.

[150] K. P. Somani, N. K. Patel, S. S. Kansara, and A. K. Rakshit, "Effect of chain length of Polyethylene glyeol and crosslink density (NCO/OH) on properties of castor oil based polyurethane elastomers," *J. Macromol. Sci. - Pure Appl. Chem.*, vol. 43, no. 4–5, pp. 797–811, 2006.

[151] C. S. Wong and K. H. Badri, "Chemical Analyses of Palm Kernel Oil-Based Polyurethane Prepolymer," *Mater. Sci. Appl.*, vol. 03, no. 02, pp. 78–86, 2012.

[152] K. C. Pradhan and P. L. Nayak, "Synthesis and Characterization of Polyurethane Nanocomposite from Castor Oil-Hexamethylene Diisocyanate (HMDI)," *Pelagia Res. Libr. Adv. Appl. Sci. Res.*, vol. 3, no. 5, pp. 3045–3052, 2012, [Online]. Available: www.pelagiaresearchlibrary.com.

[153] H. Zhao *et al.*, "Preparation and characterization of polyurethanes with cross-linked siloxane in the side chain by sol-gel reactions," *Materials (Basel).*, vol. 10, no. 3, 2017.

[154] H.-N. Kim, D.-W. Lee, H. Ryu, G.-S. Song, and D.-S. Lee, "Preparation and Characterization of Isosorbide-Based Self-Healable Polyurethane Elastomers with Thermally Reversible Bonds," *Molecules*, vol. 24, no. 6, p. 1061, 2019.

[155] J. Kujawa *et al.*, "Preparation and characterization of cellulose acetate propionate films functionalized with reactive ionic liquids," *Polymers (Basel).*, vol. 11, no. 7, 2019.

[156] M. De Carvalho Eufrásio Pinto *et al.*, "Film based on magnesium impregnated biochar/cellulose acetate for phosphorus adsorption from aqueous solution," *RSC Adv.*, vol. 9, no. 10, pp. 5620–5627, 2019.

[157] H. Bakhshi, H. Yeganeh, A. Yari, and S. K. Nezhad, "Castor oil-based polyurethane coatings containing benzyl triethanol ammonium chloride: Synthesis, characterization, and biological properties," *J. Mater. Sci.*, vol. 49, no. 15, pp. 5365–5377, 2014.

[158] G. O. C. Graziella Trovati, Edgar Ap Sanches, Salvador Claro Neto, Yvonne P. Mascarenhas, "Characterization of Polyurethane Resins by FTIR, TGA, and XRD," *J. Appl. Polym. Sci.*, vol. 115, pp. 263–268, 2010.

[159] A. M. Das, A. A. Ali, and M. P. Hazarika, "Synthesis and characterization of cellulose acetate from rice husk: Eco-friendly condition," *Carbohydr. Polym.*, vol. 112, pp. 342–349, 2014.

[160] H. Kamal, F. M. Abd-Elrahim, and S. Lotfy, "Characterization and some properties of

cellulose acetate-co-polyethylene oxide blends prepared by the use of gamma irradiation," *J. Radiat. Res. Appl. Sci.*, vol. 7, no. 2, pp. 146–153, 2014.

[161] A. Wolska, M. Goździkiewicz, and J. Ryszkowska, "Thermal and mechanical behaviour of flexible polyurethane foams modified with graphite and phosphorous fillers," *J. Mater. Sci.*, vol. 47, no. 15, pp. 5627–5634, 2012.

[162] S. Oprea, "The effect of chain extenders structure on properties of new polyurethane elastomers," *Polym. Bull.*, vol. 65, no. 8, pp. 753–766, 2010.

[163] T. Calvo-Correas, M. D. Martin, A. Retegi, N. Gabilondo, M. A. Corcuera, and A. Eceiza, "Synthesis and Characterization of Polyurethanes with High Renewable Carbon Content and Tailored Properties," *ACS Sustain. Chem. Eng.*, vol. 4, no. 10, pp. 5684–5692, 2016.

[164] A. Tenorio-Alfonso, M. C. Sánchez, and J. M. Franco, "Preparation, characterization and mechanical properties of bio-based polyurethane adhesives from isocyanate-functionalized cellulose acetate and castor oil for bonding wood," *Polymers (Basel).*, vol. 9, no. 4, pp. 1–14, 2017.

[165] M. Moghanizadeh-Ashkezari, P. Shokrollahi, M. Zandi, and F. Shokrolahi, "Polyurethanes with separately tunable biodegradation behavior and mechanical properties for tissue engineering," *Polym. Adv. Technol.*, vol. 29, no. 1, pp. 528–540, 2018.

[166] D. B. Klinedinst, I. Yilgör, E. Yilgör, M. Zhang, and G. L. Wilkes, "The effect of varying soft and hard segment length on the structure-property relationships of segmented polyurethanes based on a linear symmetric diisocyanate, 1,4-butanediol and PTMO soft segments," *Polymer (Guildf).*, vol. 53, no. 23, pp. 5358–5366, 2012.

[167] T. Fattahi Meyabadi, G. Mir Mohamad Sadeghi, F. Dadashian, and H. Ebrahimi Zanjani Asl, "From cellulosic waste to nanocomposites. Part 2: Synthesis and characterization of polyurethane/cellulose nanocomposites," *J. Mater. Sci.*, vol. 48, no. 20, pp. 7283–7293, 2013.

[168] V. R, S. T, and V. T, "Characterization of Polyurethane Coated Aerospace Aluminium Alloy (7075) By DSC, XRD and Adhesion Test," *J. Appl. Mech. Eng.*, vol. 06, no. 06, 2017.

[169] C. Wang, C. Ma, C. Mu, and W. Lin, "Tailor-made zwitterionic polyurethane coatings: microstructure, mechanical property and their antimicrobial performance," *RSC Adv.*, vol. 7, no. 44, pp. 27522–27529, 2017.

[170] T. Arunkumar and S. Ramachandran, "Surface coating and characterisation of polyurea for liquid storage," *Int. J. Ambient Energy*, vol. 38, no. 8, pp. 781–787, 2017.

[171] Y. Wang and L. Jin, "Preparation and characterization of self-colored waterborne polyurethane and its application in eco-friendly manufacturing of microfiber synthetic leather base," *Polymers (Basel).*, vol. 10, no. 3, 2018.

[172] W. Lei *et al.*, "Thermal properties of polyurethane elastomer with different flexible molecular chain based on para-phenylene diisocyanate," *J. Mater. Sci. Technol.*, vol. 33, no. 11, pp. 1424–1432, 2017.

[173] M. Stanzione *et al.*, "Tuning of polyurethane foam mechanical and thermal properties using ball-milled cellulose," *Carbohydr. Polym.*, vol. 231, no. December 2019, p. 115772, 2020.

[174] T. E. Youssef, H. Al-Turaif, and A. A. Wazzan, "Investigations on the Structural and Mechanical Properties of Polyurethane Resins Based on Cu(II)phthalocyanines," *Int. J. Polym. Sci.*, vol. 2015, 2015.

[175] L. Kong *et al.*, "Nanocellulose-reinforced polyurethane for waterborne wood coating," *Molecules*, vol. 24, no. 17, pp. 1–13, 2019.

[176] S. Li, R. Vatanparast, and H. Lemmetyinen, "Cross-linking kinetics and swelling behaviour of aliphatic polyurethane," *Polymer (Guildf).*, vol. 41, no. 15, pp. 5571–5576, 2000.

[177] A. Pei, J. M. Malho, J. Ruokolainen, Q. Zhou, and L. A. Berglund, "Strong nanocomposite reinforcement effects in polyurethane elastomer with low volume fraction of cellulose nanocrystals," *Macromolecules*, 2011.

[178] H. Zhang, H. Chen, Y. She, X. Zheng, and J. Pu, "Anti-yellowing property of polyurethane improved by the use of surface-modified nanocrystalline cellulose," *BioResources*, vol. 9, no. 1, pp. 673–684, 2014.

[179] T. H. Kim and S. G. Kim, "Clinical outcomes of occupational exposure to N,N-dimethylformamide: Perspectives from experimental toxicology," *Saf. Health Work*, vol. 2, no. 2, pp. 97–104, 2011.

[180] A. Pei, J. M. Malho, J. Ruokolainen, Q. Zhou, and L. A. Berglund, "Strong nanocomposite reinforcement effects in polyurethane elastomer with low volume fraction of cellulose nanocrystals," *Macromolecules*, vol. 44, no. 11, pp. 4422–4427, 2011.

[181] E. S. Abdul Rashid, N. Muhd Julkapli, and W. A. Yehye, "Nanocellulose reinforced as green agent in polymer matrix composites applications," *Polym. Adv. Technol.*, vol. 29, no. 6, pp. 1531–1546, 2018.

[182] Z. Yang, H. Peng, W. Wang, and T. Liu, "Crystallization behavior of poly(ε-caprolactone)/layered double hydroxide nanocomposites," *J. Appl. Polym. Sci.*, vol. 116, no. 5, pp. 2658–2667, 2010.

[183] M. Asensio, V. Costa, A. Nohales, O. Bianchi, and C. M. Gómez, "Tunable structure and properties of segmented thermoplastic polyurethanes as a function offlexible segment," *Polymers (Basel).*, vol. 11, no. 12, 2019.

[184] B. A. Miller-Chou and J. L. Koenig, "A review of polymer dissolution," *Prog. Polym. Sci.*, vol. 28, no. 8, pp. 1223–1270, 2003.

[185] M. Rashvand and Z. Ranjbar, "Degradation and stabilization of an aromatic polyurethane coating during an artificial aging test via FTIR spectroscopy," *Mater. Corros.*, vol. 65, no. 1, pp. 76–81, 2014.

[186] D. Rosu, L. Rosu, and C. N. Cascaval, "IR-change and yellowing of polyurethane as a result of UV irradiation," *Polym. Degrad. Stab.*, vol. 94, no. 4, pp. 591–596, 2009.

[187] R. Scaffaro and L. Botta, "Nanofilled Thermoplastic–Thermoplastic Polymer Blends," in *Nanostructured Polymer Blends*, Elsevier, 2014, pp. 133–160.

[188] M. Ajorloo, M. Fasihi, and H. Khoramishad, "The role of nanofiller size and polymer chain configuration on the properties of polypropylene/graphite nanoplates composites," *J. Taiwan Inst. Chem. Eng.*, vol. 108, pp. 82–91, 2020.

[189] L. Vasquez-Zacarias, P. Ponce-Peña, T. Pérez-López, E. A. Franco-Urquiza, G. Ramirez-Galicia, and M. Poisot, "Hybrid Cellulose-Silica Materials from Renewable Secondary Raw Resources: An Eco-friendly Method," *Glob. Challenges*, vol. 2, no. 7, p. 1700119, 2018.

[190] M. C. Rodríguez-Robledo *et al.*, "Cellulose-silica nanocomposites of high reinforcing content with fungi decay resistance by one-pot synthesis," *Materials (Basel).*, vol. 11, no. 4, pp. 1–13, 2018.

[191] R. Rothon, "Polymers and Polymeric Composites: A Reference Series," *Polym. Polym. Compos. A Ref. Ser.*, 2017.

[192] A. Dorigato, Y. Dzenis, and A. Pegoretti, "Nanofiller aggregation as reinforcing mechanism in nanocomposites," *Procedia Eng.*, vol. 10, no. September 2015, pp. 894–899, 2011.

[193] J. K. Pandey, H. Takagi, A. N. Nakagaito, and H. J. Kim, "Handbook of polymer nanocomposites. Processing, performance and application: Volume C: Polymer nanocomposites of cellulose nanoparticles," *Handb. Polym. Nanocomposites. Process. Perform. Appl. Vol. C Polym. Nanocomposites Cellul. Nanoparticles*, vol. C, pp. 1–511, 2015.

[194] Q. T. H. Shubhra, A. K. M. M. Alam, and M. A. Quaiyyum, "Mechanical properties of polypropylene composites: A review," *J. Thermoplast. Compos. Mater.*, vol. 26, no. 3, pp. 362–391, 2013.

[195] M. A. S. Anwer, J. Wang, and H. E. Naguib, "1D/2D CNF/GNP Hybrid Nanofillers: Evaluation of the Effect of Surfactant on the Morphological, Mechanical, Fracture, and Thermal Characteristics of Their Nanocomposites with Epoxy Resin," *Ind. Eng. Chem. Res.*, vol. 58, no. 19, pp. 8131–8139, 2019.

[196] H. W. Kwak, J. You, M. E. Lee, and H. J. Jin, "Prevention of cellulose nanofibril agglomeration during dehydration and enhancement of redispersibility by hydrophilic gelatin," *Cellulose*, vol. 26, no. 7, pp. 4357–4369, 2019.

[197] S. Thomas, J. Abraham, S. C. George, and S. Thomas, "Role of CNT/clay hybrid on the mechanical, electrical and transport properties of NBR/NR blends," *Polym. Bull.*, vol. 77, no. 1, pp. 1–16, 2020.

[198] Y. Li, H. He, B. Huang, L. Zhou, P. Yu, and Z. Lv, "In situ fabrication of cellulose nanocrystal-silica hybrids and its application in UHMWPE: Rheological, thermal, and wear resistance properties," *Polym. Compos.*, vol. 39, pp. E1701–E1713, 2018.

[199] C. B. Carter, M. G. Norton, C. B. Carter, and M. G. Norton, "Sols, Gels, and Organic Chemistry," *Ceram. Mater.*, pp. 411–422, 2013.

[200] L. Zu, R. Li, L. Jin, H. Lian, Y. Liu, and X. Cui, "Preparation and characterization of polypropylene/silica composite particle with interpenetrating network via hot emulsion sol-gel approach," *Prog. Nat. Sci. Mater. Int.*, vol. 24, no. 1, pp. 42–49, 2014.

[201] A. Dufresne, "Nanocellulose: a new ageless bionanomaterial," *Mater. Today*, vol. 16, no. 6, pp. 220–227, 2013.

[202] F. Abbate Dos Santos and M. I. Bruno Tavares, "Development of biopolymer/cellulose/silica nanostructured hybrid materials and their characterization by NMR relaxometry," *Polym. Test.*, vol. 47, pp. 92–100, 2015.

[203] P. Pouresmaeel-Selakjani, M. Jahanshahi, and M. Peyravi, "Synthesis of cellulose/silica nanocomposite through electrostatic interaction to reinforce polysulfone membranes," *Cellulose*, vol. 24, no. 3, pp. 1333–1353, 2017.

[204] X. Wen, "One-pot route to graft long-chain polymer onto silica nanoparticles and its application for high-performance poly(l-lactide) nanocomposites," *RSC Adv.*, vol. 9, no. 24, pp. 13908–13915, 2019.

[205] B. Gieseking *et al.*, "Effect of the Modified Silica Nanofiller on the Mechanical Properties of Unsaturated Polyester Resins Based on Recycled Polyethylene Terephthalate," *Adv. Energy Mater.*, vol. 2, no. 12, pp. 1477–1482, 2012.

[206] S. Deniz and B. Arikan, "Effect of silica type on superhydrophobic properties of PDMS-silica nanocomposite coatings," *Int. J. Eng. Appl. Sci.*, vol. 8, no. 01, pp. 19–27, 2016.

[207] K. S. Chun, S. Husseinsyah, and H. Osman, "Utilization of cocoa pod husk as filler in polypropylene biocomposites: Effect of maleated polypropylene," *J. Thermoplast. Compos. Mater.*, vol. 28, no. 11, pp. 1507–1521, 2015.

[208] A. Gopanna, R. N. Mandapati, S. P. Thomas, K. Rajan, and M. Chavali, "Fourier transform infrared spectroscopy (FTIR), Raman spectroscopy and wide-angle X-ray scattering (WAXS) of polypropylene (PP)/cyclic olefin copolymer (COC) blends for qualitative and quantitative analysis," *Polym. Bull.*, vol. 76, no. 8, pp. 4259–4274, 2019.

[209] N. Jia, S. M. Li, M. G. Ma, J. F. Zhu, and R. C. Sun, "Synthesis and characterization of cellulose-silica composite fiber in ethanol/water mixed solvents," *BioResources*, vol. 6, no. 2, pp. 1186–1195, 2011.

[210] S. Islam, R. Masoodi, and H. Rostami, "275037," *J. Nanosci.*, vol. 2013, 2013.

[211] K. Singh, A. Ohlan, P. Saini, and S. K. Dhawan, "composite – super paramagnetic behavior and variable range hopping 1D conduction mechanism – synthesis and characterization," *Polym. Adv. Technol.*, no. November 2007, pp. 229–236, 2008.

[212] J. Li, Z. Zhu, T. Li, X. Peng, S. Jiang, and L. S. Turng, "Quantification of the Young's modulus for polypropylene: Influence of initial crystallinity and service temperature," *J. Appl. Polym. Sci.*, vol. 137, no. 16, pp. 1–7, 2020.

[213] C. L. Wu, M. Q. Zhang, M. Z. Rong, and K. Friedrich, "Silica nanoparticles filled polypropylene: Effects of particle surface treatment, matrix ductility and particle species on mechanical performance of the composites," *Compos. Sci. Technol.*, vol. 65, no. 3–4,

pp. 635–645, 2005.

[214] I. Z. Luna, K. C. Dam, A. M. S. Chowdhury, M. A. Gafur, N. Khan, and R. A. Khan, "Physical and thermal characterization of alkali treated rice husk reinforced polypropylene composites," *Adv. Mater. Sci. Eng.*, vol. 2015, no. July, 2015.

[215] B. Lin and S. Zhou, "Poly(ethylene glycol)-grafted silica nanoparticles for highly hydrophilic acrylic-based polyurethane coatings," *Prog. Org. Coatings*, vol. 106, no. September, pp. 145–154, 2017.

[216] E. A. Hassan and M. L. Hassan, "Rice straw nanofibrillated cellulose films with antimicrobial properties via supramolecular route," *Ind. Crops Prod.*, vol. 93, pp. 142–151, 2016.

[217] M. H. Alaei *et al.*, "Effect of particle size on thermomechanical properties of particulate polymer composite," *Iran. Polym. J. (English Ed.*, vol. 22, no. 11, pp. 853–863, 2013.

PUBLICATION, PATENT AND CONFERENCES ATTENDED

PUBLICATION

1. **Safarul MUSTAPHA** and Yoshito ANDOU. Tailored higher performance silicone elastomer with nanofibrillated cellulose (NFC) through acidic treatment. Published in **Polymer Composites. Impact Factor 2.26**

2. **Safarul MUSTAPHA** and Yoshito ANDOU. Enhancing Mechanical Properties of Polyurethane with Cellulose Acetate as Chain Extender. Published in **Fibers and Polymers. Impact Factor 1.88**

3. **Safarul MUSTAPHA** and Yoshito ANDOU. Covalent Incorporation of Nanofibrillated Cellulose (NFC) Into Polyurethane Elastomer and the Effect of Mechanical Properties. (Manuscript Draft)

4. **Safarul MUSTAPHA,** Kubra Eksiler, Sim Siew Teng and Yoshito ANDOU. The Design of Dry CNF Filler by Hybridization with Silica Particle for Moulded Polypropylene Composite. (Manuscript Draft)

PATENT

1. Yoshito ANDOU and **Safarul MUSTAPHA.** Polyurethanes Composition and Its Manufacturing Method. **Japanese Patent Application: 2020-067026**

CONFERENCES

1. **Safarul MUSTAPHA** and Yoshito ANDOU (2018). Effect of Acid Treatment on Nanocellulose as Reinforcing Agent in Silicone Elastomers. *6th International Symposium on Applied Engineering and Sciences (SAES2018)*, Kyushu Institute of Technology, Japan, 15th – 16th Dec 2018

2. **Safarul MUSTAPHA** and Yoshito ANDOU (2019). Effect of Acid Treatment on Nanocellulose as Reinforcing Agent in Silicone Elastomers. *56th Kyushu Branch Chemical Society Meeting*, Kitakyushu International Conference Center, Kokura, Kitakyushu, 13th July, 2019

3. **Safarul MUSTAPHA** and Yoshito ANDOU (2019). Effect of Acid Treatment on Nanocellulose as Reinforcing Agent in Silicone Elastomers. *68th Symposium on Macromolecules,* Bunkyo Campus, Fukui University. September 25th-27th, 2019

4. **Safarul MUSTAPHA** and Yoshito ANDOU (2019). Synthesis of Polyurethane with Cellulose Acetate (CA L-30. *7th International Symposium on Applied Engineering and Sciences (SAES2019).* Universiti Putra Malaysia (UPM), Serdang, Selangor, Malaysia. 11th–12th November 2019

5. **Safarul MUSTAPHA** and Yoshito ANDOU (2019). Synthesis of Polyurethane with Cellulose Acetate (CA L-30). *18th Asian Chemical Congress (18th ACC) and the 20th General Assembly of the Federation of Asian Chemical Societies (FACS),* Taipei International Convention Center, Taiwan. December 8th-12th, 2019

6. **Safarul MUSTAPHA** and Yoshito ANDOU (2020). The Design of Dry CNF Filler by Hybridization with Silica particle for Moulded Polypropylene Composite. *8th International Symposium on Applied Engineering and Sciences (SAES 2020) Virtual Conference / December 12th – 19th 2020.*